408 972

N-63-14-2

Fifth Quarterly Technical Progress Report

on Investigation of the

Monocapillary Thermionic Emitter as a

Dual Source of Ions and Electrons

(for the Period 15 February—15 May 1963)

Allison EDR 3390

15 June 1963

Aero-Propulsion Laboratory
Aeronautical Systems Division
Air Force Systems Command
Wright-Patterson Air Force Base, Ohio

Project No. 8173, Task No. 817305

Fifth Quarterly Technical Progress Report
on Investigation of the
Monocapillary Thermionic Emitter as a
Dual Source of Ions and Electrons
(for the Period 15 February — 15 May 1963)

Allison EDR 3390

15 June 1963

MANAGEMENT APPROVAL:

(signature)

D. L. Dresser
Project Manager

(signature)

T. F. Nagey
Director of Research

(signature)

J. D. Dunlop
Research Scientist

(signature)

H. D. Wilsted
Chief of Engineering Research

(signature)

R. T. Schneider
Research Scientist

FOREWORD

This report was prepared by the Research Department of the Allison Division of General Motors Corporation—the work reported was accomplished on Air Force Contract AF33(616)-8299, Task No. 817305, Project No. 8173. The work was administered under the direction of the Aero-Propulsion Laboratory, Aeronautical Systems Division. Mr. G. H. Miller is the task engineer from ASD.

The work began 5 May 1961 on a basic contract to investigate the feasibility and practicality of a capillary emitter serving the dual role of a cathode surface and a cesium dispenser. Under the basic contract the theory of the capillary was to be formulated, and experiments were to be performed on a monocapillary geometry. A supplementary agreement was reached on 15 November 1961 extending the work to include the design, fabrication, and test of two multi-capillary converters. In the revised project schedule, Allison agreed to include a summary of the theoretical and experimental work on the monocapillary in the First Quarterly Technical Progress Report—delivered 15 February 1962 as Allison EDR 2617. The Second Quarterly Technical Progress Report—EDR 2791—covered the report period from 15 February to 15 May 1962. The Third Quarterly Technical Progress Report—EDR 2978—covered the report period from 15 May to 15 August 1962. The Fourth Quarterly Technical Progress Report—EDR 3207—covered the report period from 15 August 1962 to 15 February 1963. In the meantime Allison obtained a no-cost extension to pursue the capillary study further. The Fifth Quarterly Technical Progress Report covers the report period from 15 February to 15 May 1963.

The capillary emitter project is managed by D. L. Dresser, Section Head, Thermionic Conversion. Mr. Dresser, Mr. J. D. Dunlop, and Dr. R. T. Schneider are co-authors of this report. Mr. Dunlop conducted the testing on Converter G with assistance from H. Fuquay and D. R. Zimmerman. Mr. Dunlop and Dr. Schneider conducted the spectrographic studies with assistance from W. Woerner. Converter G was fabricated by the Centre de Physique Electronique et Corpusculaire (CEPEC), Compagnie generale de telegraphie Sans Fil (CSF) of France on a subcontract. Dr. H. Huber, assisted by Mr. Freytay and LeBihan, were responsible for the fabrication of the device. Management direction at Allison includes Mr. T. F. Nagey, Director of Research, and Mr. H. D. Wilsted, Manager of Applied Research.

ABSTRACT

Experimental data is reported on a multicapillary converter, Converter G, which operated for over 300 hours. Several types of data were obtained including:

1. Current-voltage characteristics for the temperature range from 1800 to 2100°K
2. High frequency oscillations
3. Ion current measurements
4. Spectroscopic data

It is shown that the data in the temperature range from 1800 to 2100°K agrees with the random current model of the capillary emitter. For operation at 2000 and 2100°K the data indicates several competitive advantages over conventional converters, including wider electrode spacings, higher converter voltage, and lower cesium bath temperature. The high frequency oscillation data shows that the peak current-voltage points form an arc mode characteristic. The ion currents at high collector temperature appear to be due to cesium atoms evaporating from the collector and impinging on the emitter surface. Spectrographic data indicate elevated electron temperatures in the arc mode. When high frequency oscillations are present in the passive mode, the line intensities of lower energy excited states are increased.

TABLE OF CONTENTS

LIST OF ILLUSTRATIONS

LIST OF TABLES

LIST OF SYMBOLS

Symbol	Definition
d	Distance
e	Charge on electron
f	Fractional ionization
I_o	Saturation current
I_+	Random ion current
I_-	Random electron current
I_w	Saturation current for tungsten surface
J	Current density
k	Boltzmann constant
K	Net cesium flow through capillaries
m	Mass of cesium atom
m_+	Mass of cesium ion
n	Incremental volume
N	Cesium atom number density at temperature T_E
N_+	Cesium ion number density
N_{Cs}	Cesium atom number density at temperature T_{Cs}
P	Power
T_{Cs}	Cesium temperature
T_C	Collector temperature
$\bar{v}$	Average kinetic velocity
V	Voltage
V_i	Ionization potential
V_T	Voltage equivalent of temperature (kT/e)
T_E	Emitter temperature
W	Probability factor
λ	Mean free path
ν	Arrival rate at capillary entrance
ϕ_E	Work function of emittance
ϕ_o	Plasma potential

I. INTRODUCTION

This is the Fifth Quarterly Technical Progress Report on Contract AF33(616)-8299 covering the period from 15 February to 15 May 1963. The material presented describes the theoretical and experimental results obtained on the investigation of a capillary emitter serving as a dual source of ions and electrons in a thermionic converter. This is a continuation of the project described in four earlier reports:

- First Quarterly Technical Progress Report—Allison EDR 2617
- Second Quarterly Technical Progress Report—Allison EDR 2791
- Third Quarterly Technical Progress Report—Allison EDR 2978
- Fourth Quarterly Technical Progress Report—Allison EDR 3207

In EDR 2617 various solutions of the flow equations describing the transport of cesium along the capillary were given. Detailed experimental results were discussed as obtained from two monocapillary test devices---one of tantalum and another of molybdenum. Experimental data from the tantalum monocapillary indicated an increase of a factor of ten in current density over a plane tantalum surface. In EDR 2791 the design and fabrication of a multicapillary converter was described---the emitter was made by stacking, alternately, corrugated and flat 10-micron thick tantalum foils. Also, an improved theoretical model was presented along with some work on circulating cesium by means of an electromagnetic (EM) pump. In EDR 2978 continued work on the capillary theoretical model is reported along with some experimental data obtained on two multicapillary converters. EDR 3207 describes a theoretical model of the capillary known as the random current model. Data from three more converters is summarized. The random current model agreed quite well with observed electron currents---the pressure in the inter-electrode space was shown not to be negligible for practical operation up to 1800°K.

The work reported herein includes:

1. Power density measurements at 2000 and 2100°K which are of interest for practical devices---special advantages of wide spacing and high converter voltage are demonstrated.

2. A multicapillary converter operated for 300 hours under various test conditions.

3. Data on high frequency oscillations.

4. A summary of spectrographic data taken in various modes of converter operation.

The final technical report will include experimental results on a porous tungsten emitter, and other results on some new studies initiated by Allison and CSF.

II. CONCLUSIONS

In the Fourth Quarterly Report it was concluded that, based upon the random current theory, a hollow cathode structure might offer advantages in the emitter temperature range from 1800 to 2200°K. During this report period data were obtained on a multicapillary converter operating in this temperature range. Typical performance obtained is given in Table I.

TABLE I

Typical Converter Performance Data

T_E (°K)	d (mm)	V (v)	P (w/cm^2)
2000	0.3	1.35	9.35
2000	1.0	1.50	6.6
2100	0.3	1.25	14.1
2100	1.0	1.50	10.0

Advantages due to wide spacing and high voltage were present. It does not appear that operation is dependent upon the circulation of cesium through the emitter.

It is concluded that a hollow cathode structure appears to offer significant advantages in the temperature range of 2000 to 2100°K.

III. MULTICAPILLARY CONVERTER TESTS

CONVERTER DESIGN

During this report period Converter G was tested. The basic design of Converter G was similar to Converter C, as described in the Fourth Quarterly Technical Progress Report, Allison EDR 3207. However, the emitter for Converter G was tungsten as compared to tantalum for Converter C. A layout diagram of Converter G is shown in Figure 1.

TEST PROCEDURE

The test set up for the multicapillary converter is shown in Figure 2. A block diagram of the electrical circuit used to measure the current-voltage characteristic curves is shown in Figure 3. These curves were plotted on an x-y recorder.

The voltage was measured directly across the terminals of the diode to eliminate the voltage drop in current carrying leads. Current was determined by measuring the voltage drop across a precision resistor. A transistorized regulated power supply was used to obtain the characteristic curves over the desired range. For observations of high frequency oscillations a non-inductive resistive load was used. However, because of the rapid rise-time or cut-off characteristic of the oscillations it was difficult to completely eliminate inductance from the circuit. Even with a No. 8 wire directly shorting the converter some ringing effects were observed with the scope.

A description of the spectrographic experimental set up is presented in Section V.

FAILURE AND ANALYSIS

Converter G was on the vacuum pumps from February 6 to June 6, 1963. During this period over 300 hours of test data were obtained.

The exact cause of failure is not known. However, the parts of the converter were examined. The tantalum tube joining the capillary was melted, fusing closed the capillary entrance (Figure 4). The melting point of tantalum is 2996°C. One possible explanation would be that a small leak developed where the tantalum tube from the cesium reservoir was electron beam welded to the capillary emitter. Such a leak would result in an arc discharge between the filament and the spot where the leak started. A localized arc discharge would explain the high temperature required to melt the tantalum, 2996°C.

5

Figure 1. Layout Diagram for Converter G
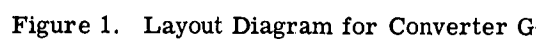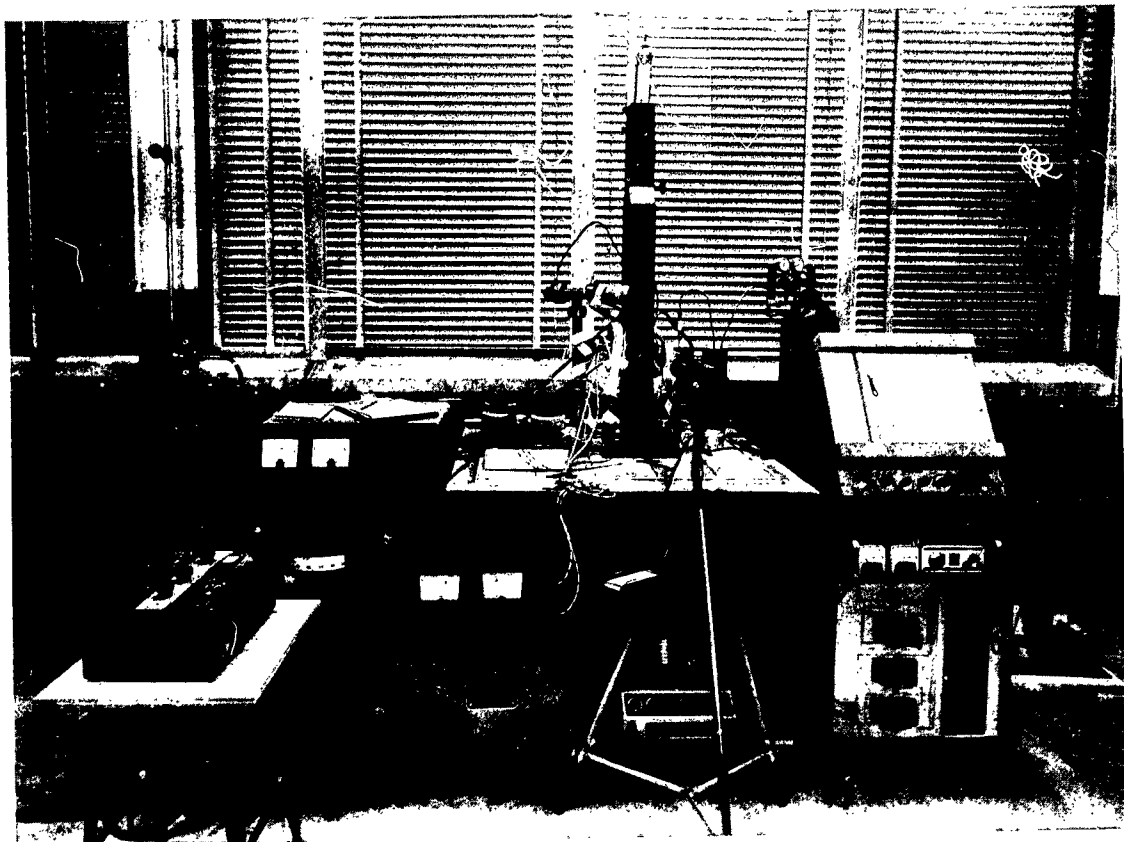
Figure 2. Test Arrangement for Converter G

Parts from Converter G are shown in Figure 5. Figure 6 shows two views of the emitter surface.

In the close-up of the capillary surface and tantalum membrane the capillary structure appears to be in good condition. The collector with the adjustable spacing mechanism is shown in Figure 7.
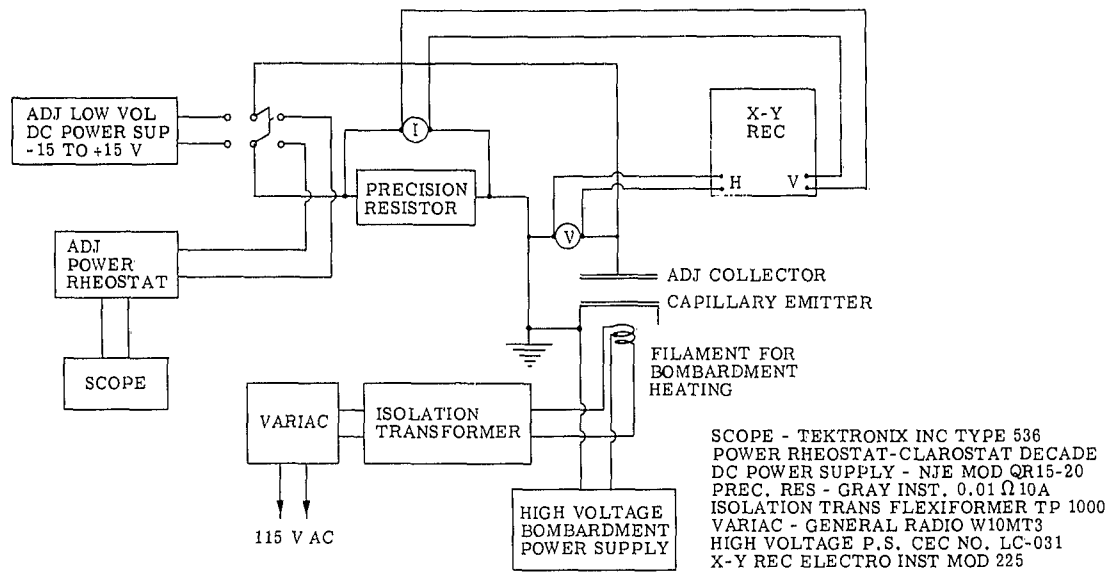
Figure 3. Converter Measurement Circuit
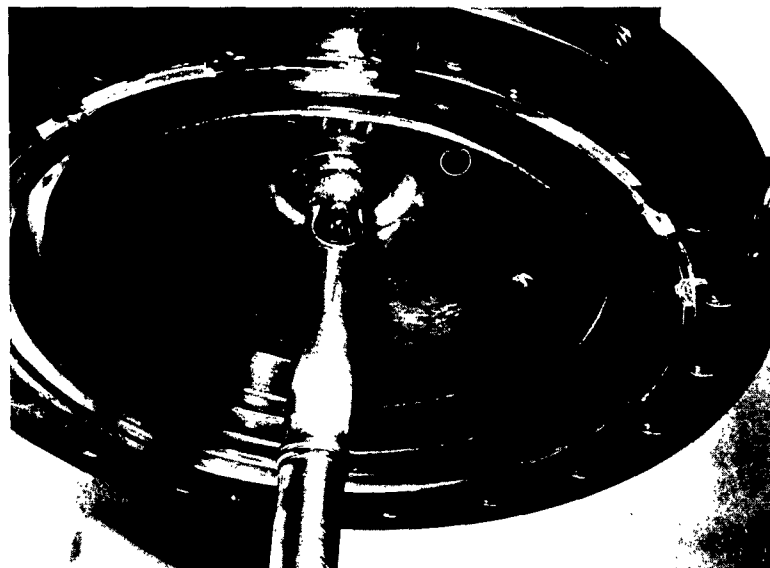
Figure 4. Close-up of Emitter Structure
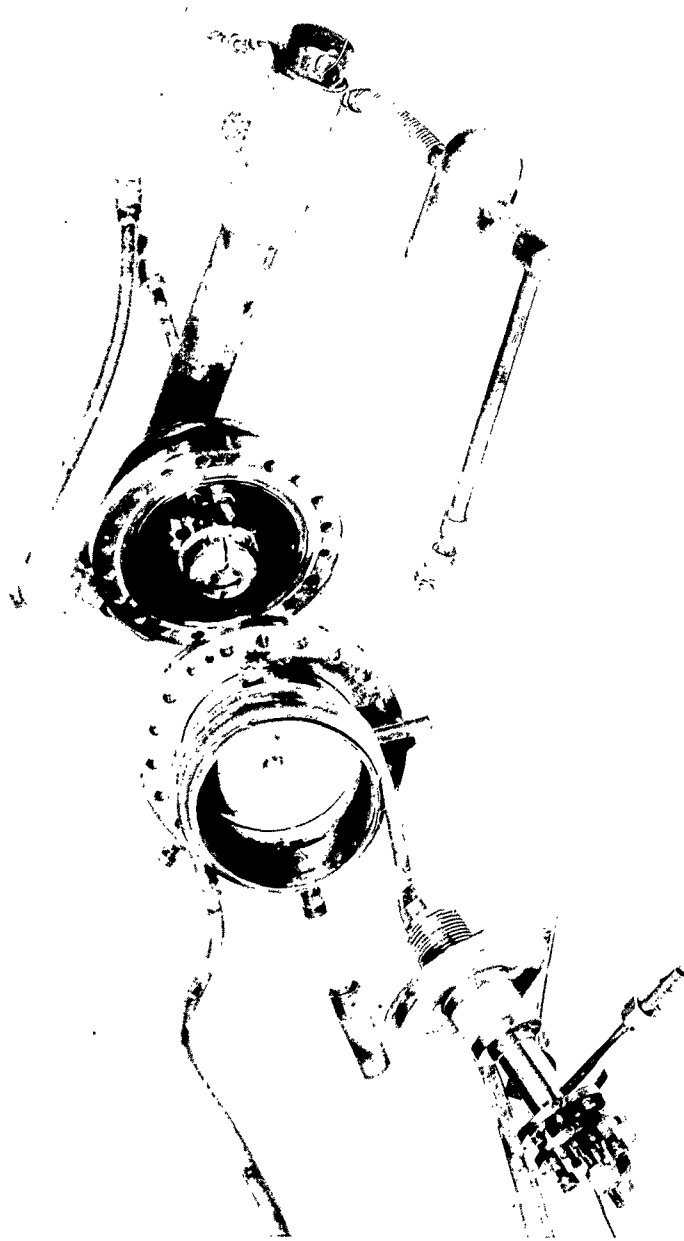
Figure 5. Parts from Converter G
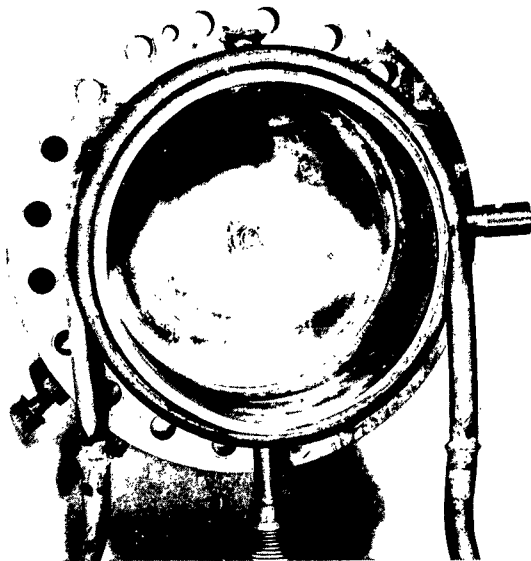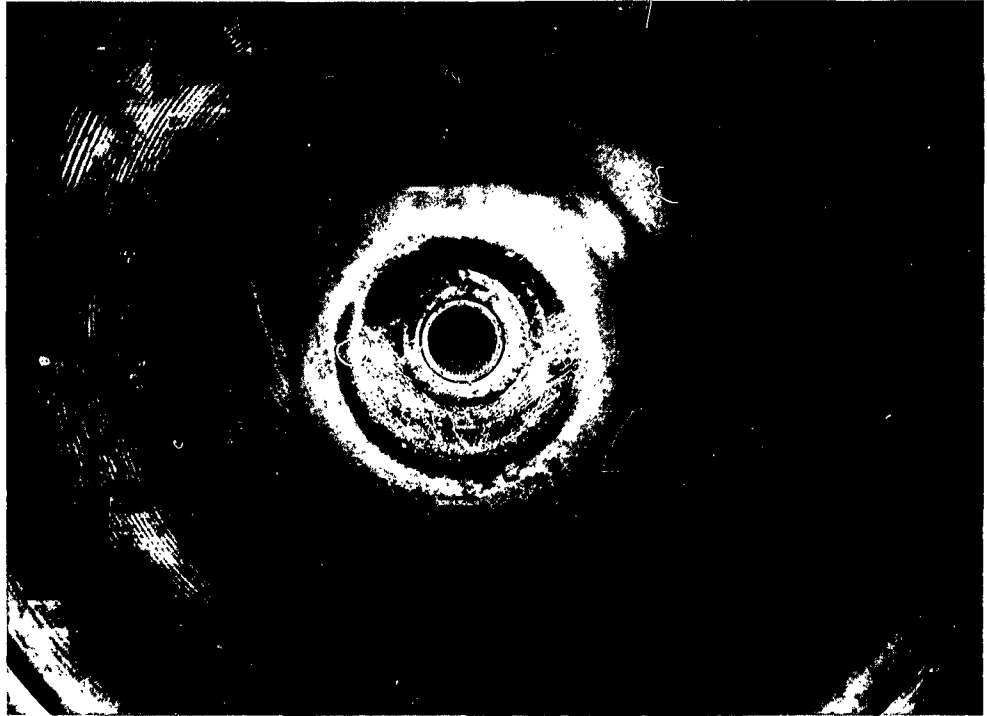
Figure 6.   Emitter Surface
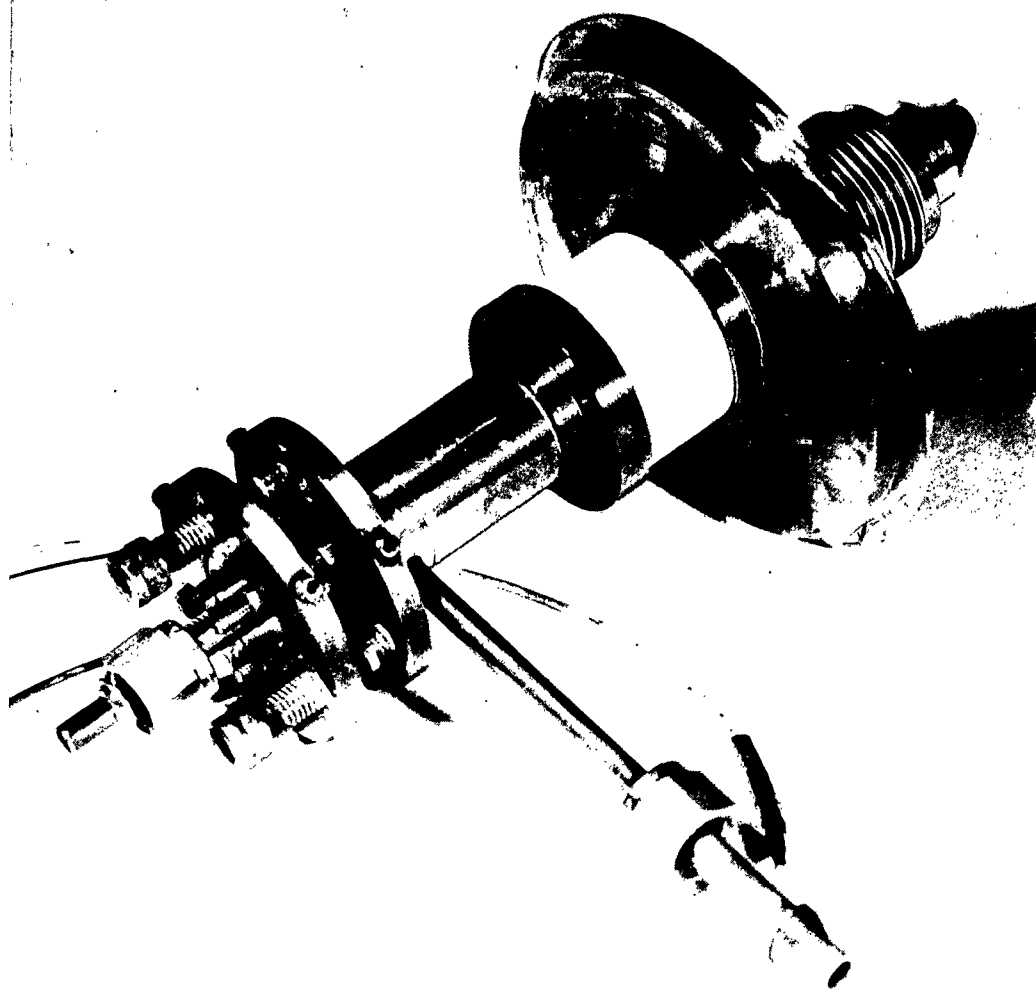
Figure 7. Collector and Spacing Mechanism

IV. DATA AND ANALYSIS

MAXIMUM POWER

Maximum power measurements were made in the emitter temperature range from 1400 to 1800°K in order to compare with data reported in the Fourth Quarterly Report—Allison EDR 3207. Figure 8 shows the results for several electrode spacings with notations on the optimum cesium temperature, and the current and voltage at maximum power. These results are quite comparable with the data reported previously (see Figures 48 and 49 in EDR 3207).
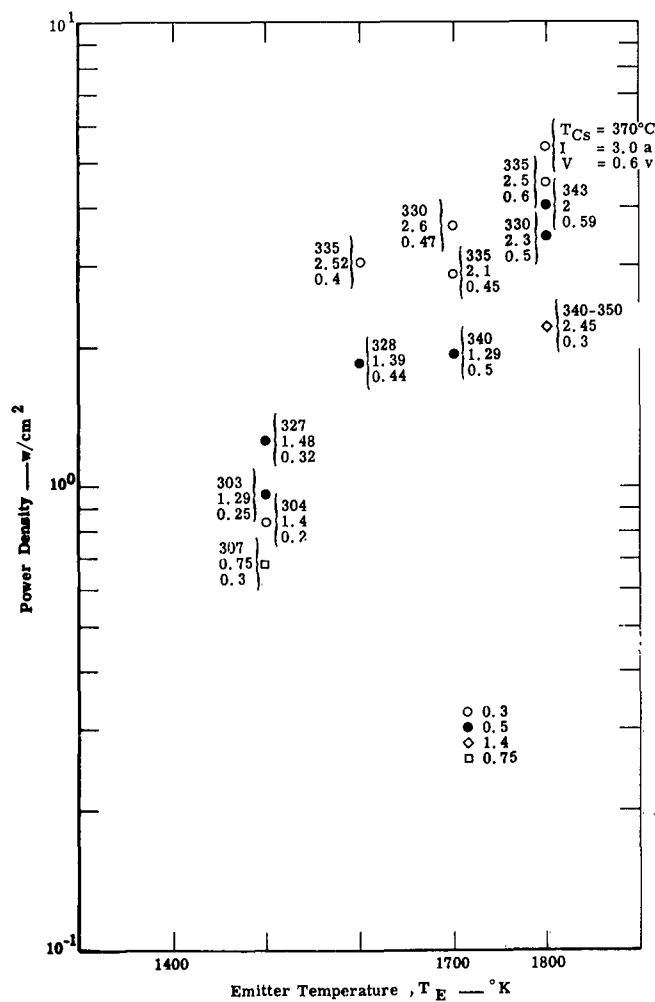
Figure 8. Maximum Power for Range Between 1400 and 1800°K

Conclusion 2 in EDR 3207 states:

"Based on the theory of the random current cathode as exposed in this report, it appears that a hollow cathode structure may offer advantages in the emitter temperature range from 1800 to 2200°K. This emitter would not require a circulating cesium system."

Converter G was operated at 1900, 2000, and 2100°K in order to determine the validity of this conclusion. Figures B1 through B21 in Appendix B show the original data taken during this study; data taken at 1800°K is included for completeness. The collector temperature was maintained at 673°K for all of this data.

Several interesting features in the I-V characteristics are worthy of comment. First, the three modes of operation suggested by R. Brietwieser appear to be present in the curves.* For example, in Figure B11, the I-V curves for spacings of 1.4, 1.0, 0.8, and 0.5 mm contain a passive mode region, a region of high frequency oscillation, and finally a saturation which could be interpreted as the ignited mode. The ignited mode identification seems reasonable because the saturation level does not appear to be a smooth, continuous extension of the initial passive mode curve. The I-V characteristic for a spacing of 0.3 mm contains very little oscillation and appears to consist of a passive mode and an arc mode. Hence, the I-V curves have all three modes as defined by Brietwieser—passive, ignited, and arc. A second feature of interest is the appearance of arc mode operation at comparatively wide spacing, which radically reduces the potential of the converter. Figure B12 is a good example of this behavior. The curve for 1.4 mm is completely devoid of passive mode. On the other hand, the curve for 1.0 mm is composed of passive mode from open circuit to about 1.25 volts, and then arc mode for the remainder. The curve is nearly reproducible for decreasing voltage as shown in the figure. Finally, in the passive mode the current is available at voltages between 1.25 and 1.5 volts.

From a power output standpoint the performance demonstrates some very desirable characteristics for a practical converter. Figure 9 shows the maximum power at a 0.3-mm spacing as a function of cesium temperature. Power in the passive mode is plotted below 290°C, while above 290°C the power in the arc mode is shown. At the lower emitter temperatures of 1800 and 1900°K the power in the arc mode is much higher than in the passive mode. However, at 2000°K there is not much difference between the two regions of operation. Figures 10 and 11

---

*R. Brietwieser, "Cesium Diode Operation in Three Modes," Proceedings of the 23rd Annual MIT Conference on Physical Electronics. March 20-22, 1963.

show the variation in passive mode power with T_{Cs} and d for the emitter temperatures of 2000 and 2100°K. Some pertinent values are summarized in Table II.

TABLE II

Variation in Passive Mode Power With T_{Cs} and d

T_E (°K)	T_{Cs}(°K)	d (mm)	V (v)	J (a/cm^2)	P (w/cm^2)
2000	523	0.3	1.25	7.5	9.35
2000	523	1.0	1.50	4.4	6.6
2100	523	0.3	1.25	11.25	14.1
2100	523	1.0	1.50	6.7	10.0
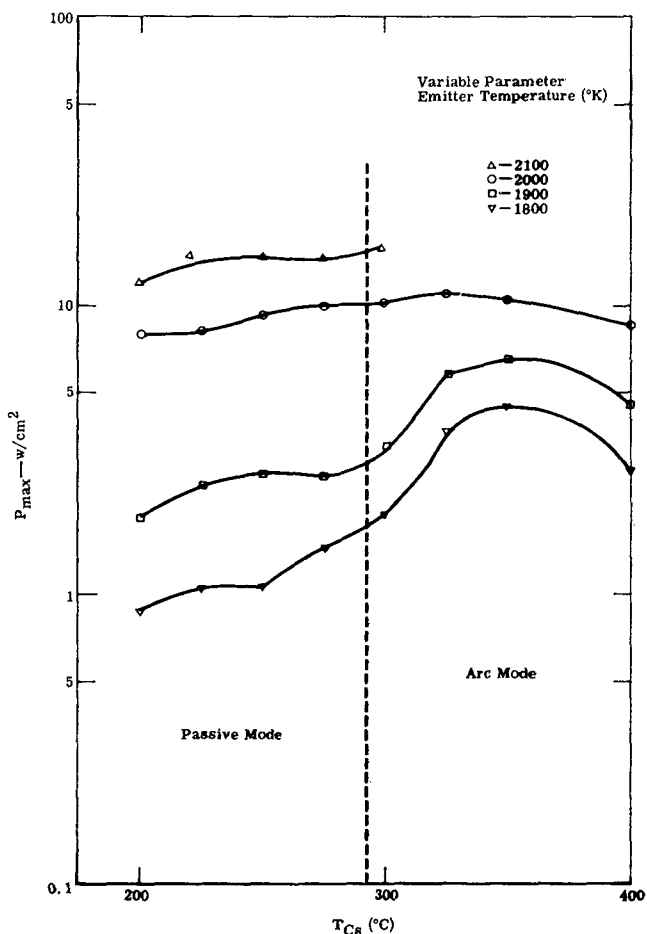
Figure 9.

Maximum Power at 0.3 mm for

Several T_{Cs} Values
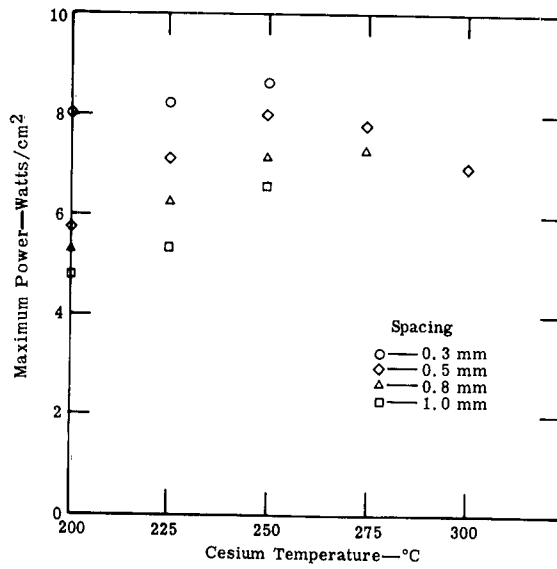
Figure 10.

Passive Mode Power at 2000°K

Figure 11.

Passive Mode Power at 2100°K

16
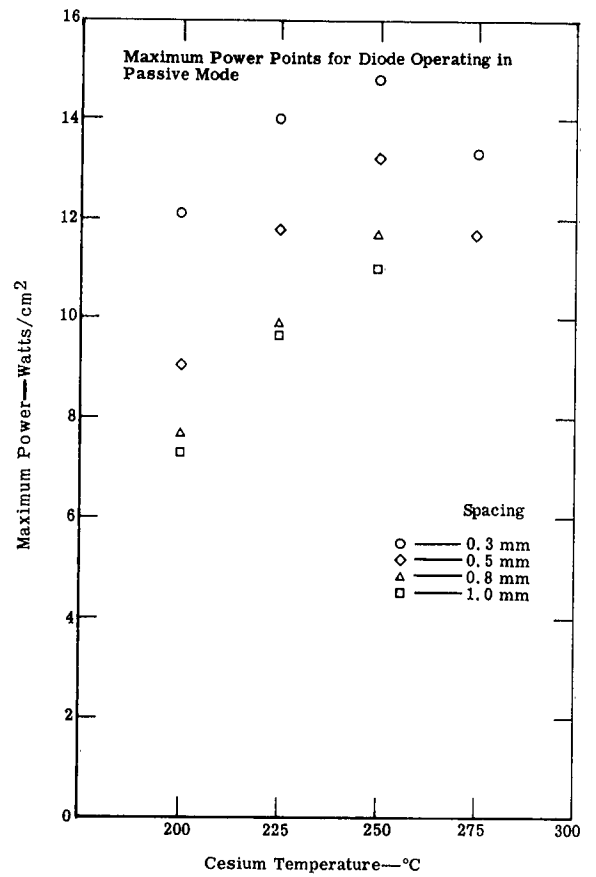
As can be seen in Table II, the converter has several features which would contribute to the reliability and utility of a practical device—these are:

1. Comparatively wide electrode spacing

2. Low cesium pressure to reduce the possibility of ceramic-metal seal failure

3. High converter voltage to ease the problems of generator design and improve the efficiency of the power conditioning process

As noted before, the maximum power in the arc mode is only slightly higher than in the passive mode for the temperatures of 2000 and 2100°K. For example, at 2100°K:

T_{Cs}(°K)	d (mm)	V (v)	J (a/cm^2)	P (w/cm^2)
573	0.3	1.04	15.4	16.2
573	1.0	0.65	6.6	4.28

These data are typical of arc mode operation in which the power is extremely sensitive to spacing, and operation is characterized by voltages of about one volt or less.

Passive mode saturation currents are compared with the random current theory in Figures 12, 13, 14, and 15. Random current curves for several density ratios (number density of cesium atoms at the exit to the number density at the entrance) are shown in each figure. These data show the following trends:

1. The closer the spacing the higher the current at a given T_{Cs} and T_E

2. At a constant d the density ratio decreases as T_{Cs} increases

3. At a given d and T_{Cs} the density ratio increases as T_E increases

According to the results reported in EDR 3207 the density at the exit should increase as the spacing is decreased for a given T_E and T_{Cs}. This is verified by the data in Figures 12, 13, 14, and 15. However, there are two trends in the data which are not explained by the theory.
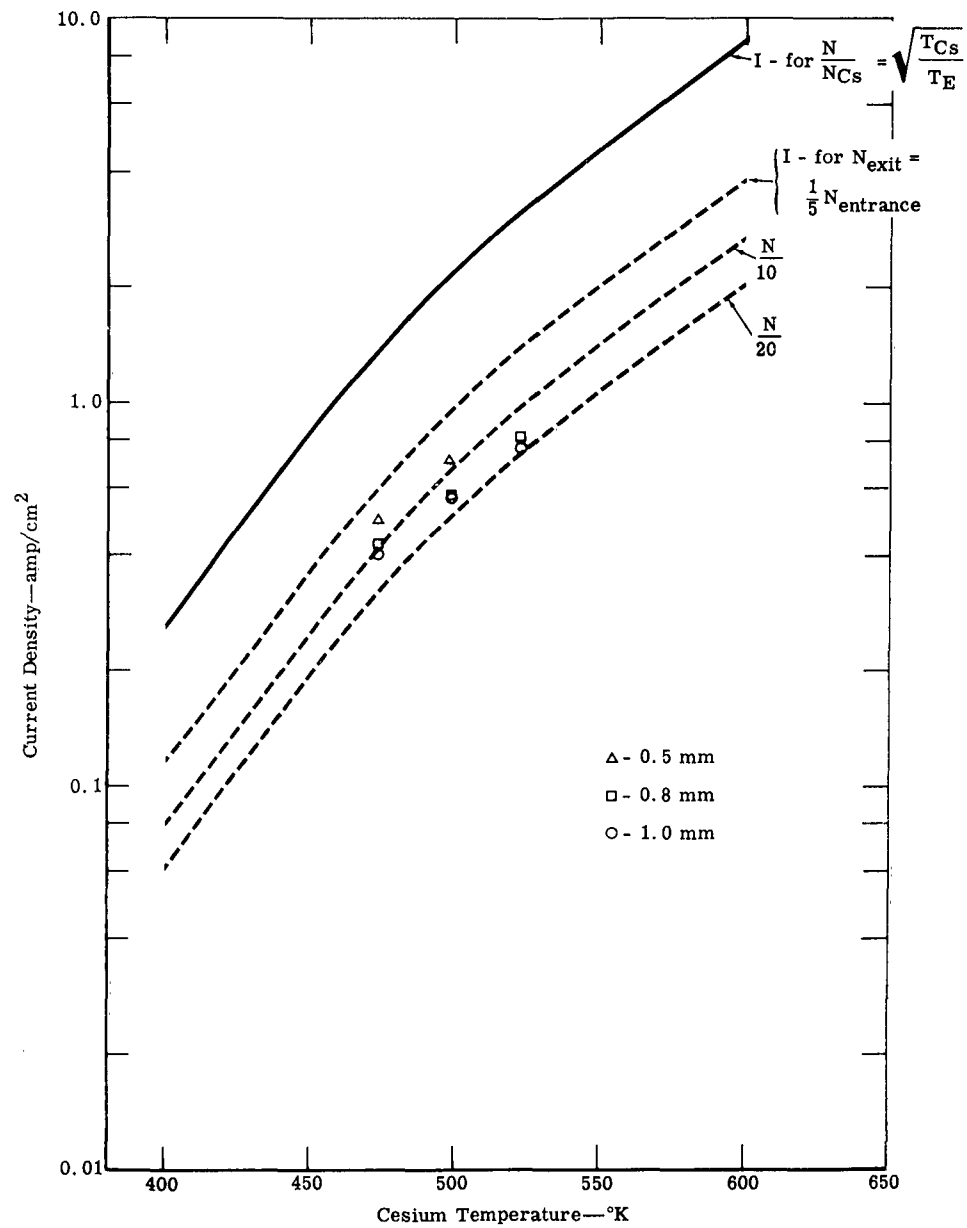
Figure 12. Comparison to Random Current Model at 1800°K
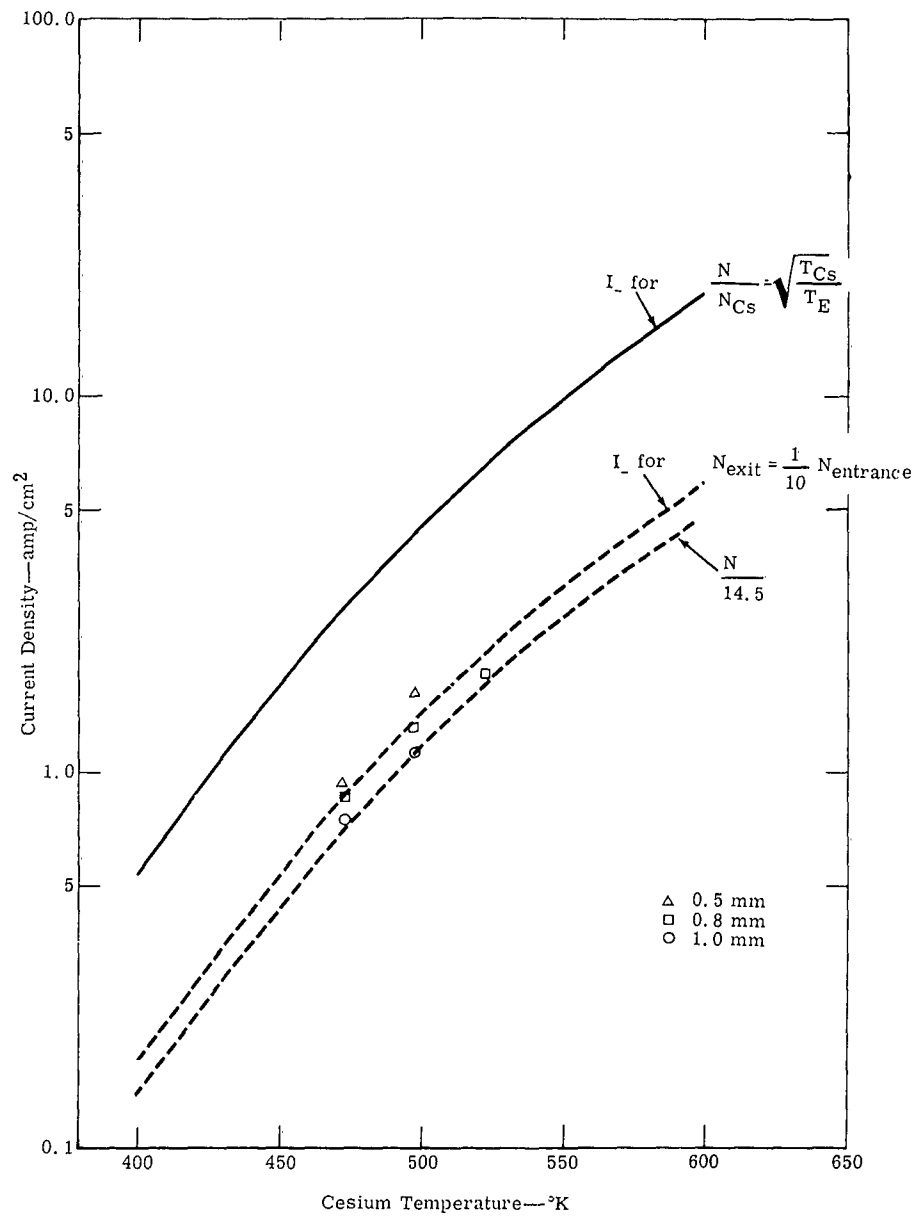
Figure 13. Comparison to Random Current Model at 1900°K
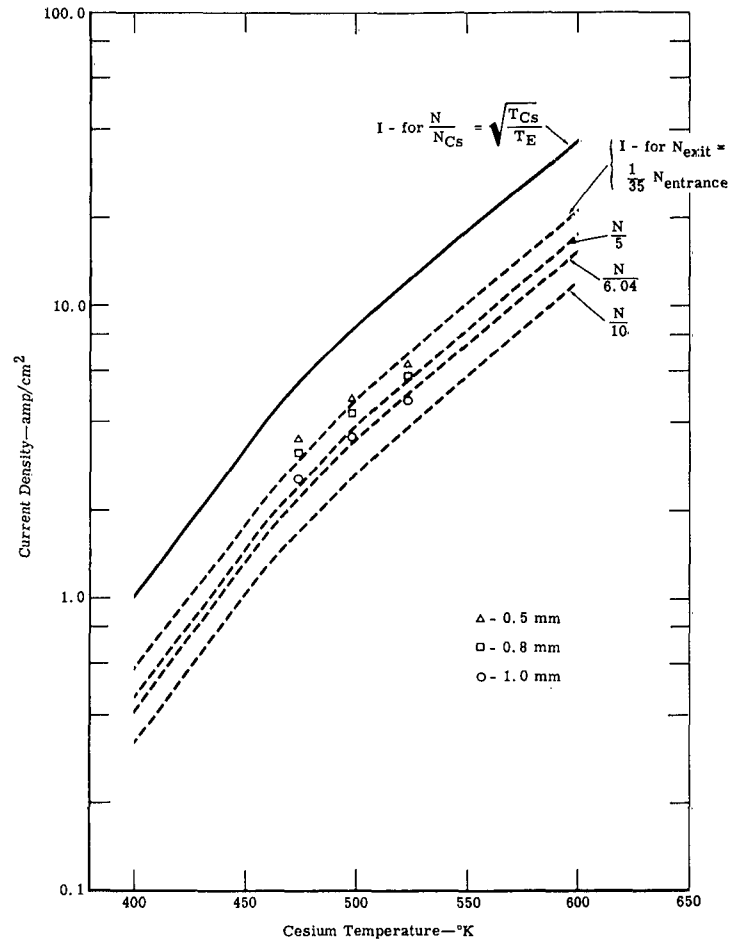
Figure 14. Comparison to Random Current Model at 2000°K

First, there is no reason to expect that, at constant d, the density ratio should decrease as T_{Cs} increases. Second, for a given d and T_{Cs} the density ratio should not change greatly as T_E increases. The trend of the data as a function of T_{Cs} suggests that space charge effects may be limiting the current. In the case of the behavior as a function of T_E, one possibility would be that other ionization processes besides thermal are becoming important. For example, volume ionization by electrons emitted from the inside wall of the capillary and accelerated through the ion sheath at the wall.

20
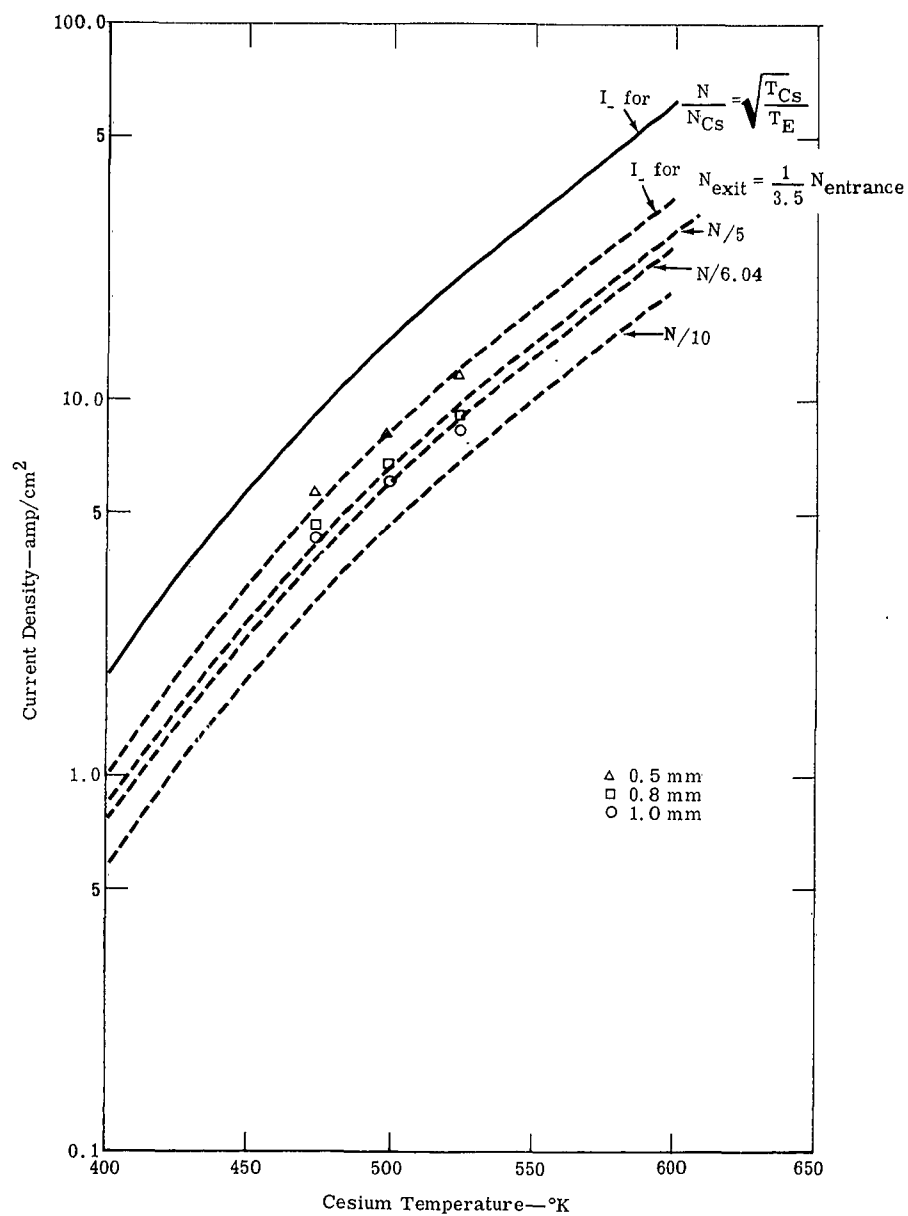
Figure 15. Comparison to Random Current Model at 2100°K

A more detailed analysis was made of some specific I-V curves obtained in the temperature range from 1800 to 2100°K. Figures 16 and 17 show the passive mode curves for d = 0.3 mm and T_{Cs} = 473°K. The curves at close spacing were selected because the pressure drop across the capillaries is a minimum. With this condition the operation approximates a hollow cathode structure. The collector temperature was 673°K for these curves.
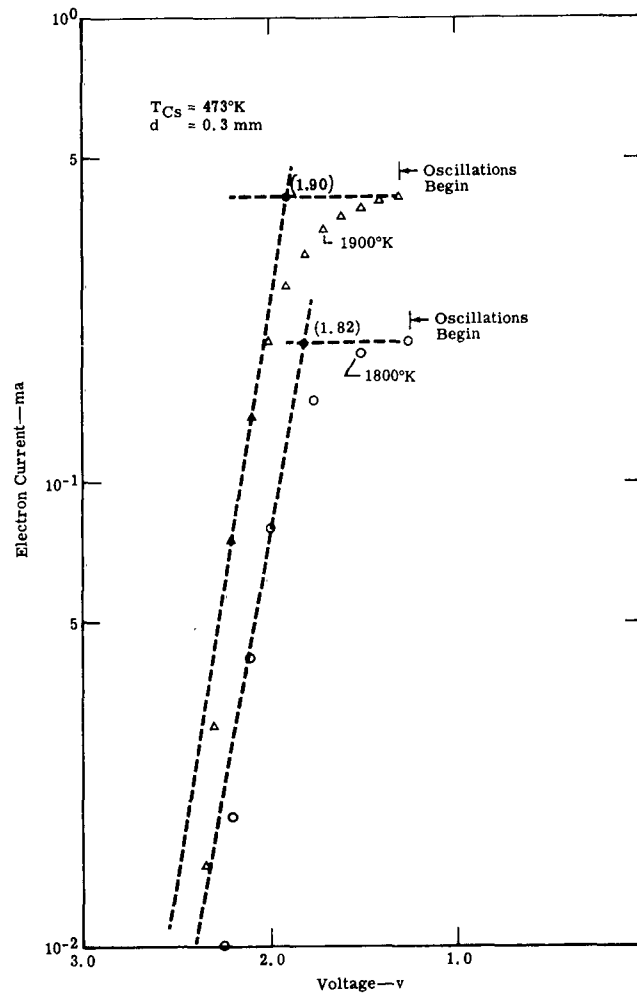
Figure 16. Passive Mode Power at 0.3 mm for 1800 and 1900°K
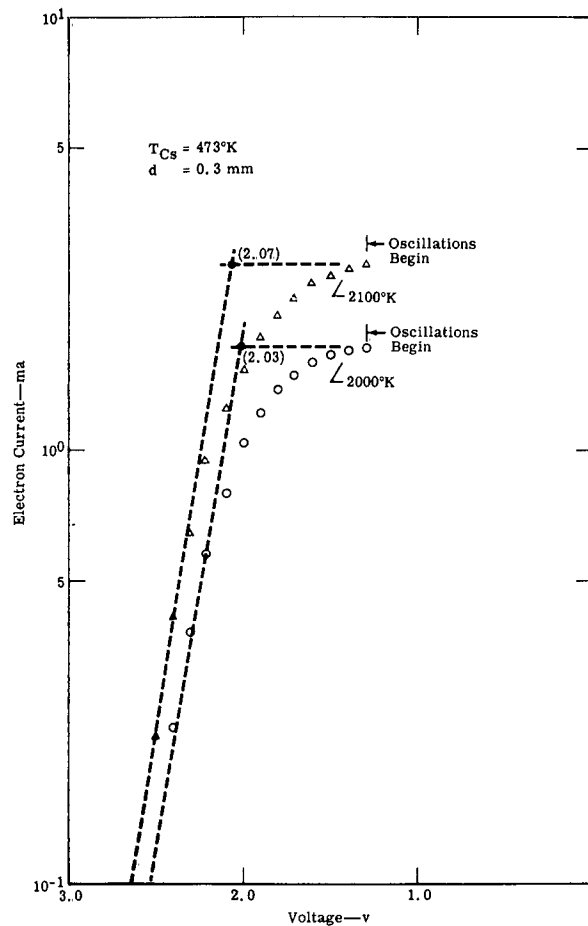
Figure 17. Passive Mode Power at 0. 3 mm for 2000 and 2100°K

In Figures 16 and 17 the contact potential was estimated by the intercept method. Although there is no clear Boltzmann region, a line with a slope approximating the emitter temperature was fit to the points. The following values are noted:

T_E (°K)	Contact Potential (v)
1800	1. 82
1900	1. 90
2000	2. 03
2100	2. 07

23

Two models of the capillary emitter were compared to the observed saturation currents. In the first model the emission current was calculated assuming the total inside wall of the capillary-emitted saturation current. The second model was the random current approach described in EDR 3207. The following calculation procedure was used:

1. Compute the experimental current from one capillary assuming the emitter consists of 320 capillaries.

2. For the given T_E and T_{Cs}, obtain the work function of the capillary wall.

3. Assume that the work function obtained in (2) is present over the total capillary wall. This is tantamount to assuming there is no pressure drop across the capillary. Compute the saturation current from the Richardson equation.

4. Calculate the current that would be emitted by a single capillary if the total inside wall emitted the saturation current computed in (3)---area of capillary wall is 0.1065 cm^2.

5. Determine the plasma potential assuming no pressure drop across the capillary.

6. Calculate the emission current from the capillary with a capillary cross sectional area of 0.91×10^{-3} cm^2.

7. Compare the results of (4) and (6) with (1).

Table III summarizes the results.

A study of Table III reveals the following points:

1. The experimental currents agree better with the random current.

2. Since the random current cannot be higher than the wall current, there is some type of discrepancy in the 2000 and 2100°K data.

3. If a collector work function of 1.9 volts is assumed, then the contact potential is in better agreement with experimental values when the wall work function is used rather than the plasma potential.

TABLE III

Comparison of Experiment and Theory

T_E (°K)	T_{Cs} (°K)	d (mm)	Experimental Current (μa)	ϕ_E (v)	Richardson Current (ma/cm^2)	Wall Current (μa)	Plasma Potential (v)	Plasma Current (ma/cm^2)	Random Current (μa)
1800	473	0.3	625	3.7	17	2130	3.02	1500	1360
1900	473	0.3	1310	3.9	19.5	2080	3.09	2300	2090
2000	473	0.3	5470	4.1	21.5	2290	3.15	6000	5460
2100	473	0.3	8450	4.3	24	2550	3.22	10000	9100

In the evaluation of these data there are three possible explanations for the high currents observed. First, the emitter temperature is actually higher than measured. This does not seem to be a reasonable explanation because an extensive temperature study was made on this type of emitter. As reported in EDR 3207 pyrometer readings were calibrated against a thermocouple. A gradient of up to 100°C from center to edge of the emitter was observed, but a given value observed by the pyrometer should be accurate within 20°C. Second, it is possible that emission from the structure surrounding the emitter is contributing to the measured current because there are no guard rings. Figures 18 and 19 show the pertinent areas surrounding the emitter. In Figure 18 a temperature distribution is postulated for 2000°K. The area immediately adjacent to the emitter is assumed to be at 2100°K---the temperature is then reduced in one hundred degree steps following the results reported in Figure 37 of the Second Quarterly Progress Report (EDR 2791). Saturation currents from each of these areas are indicated. Also noted on the figure are the measured saturation currents as a function of d for a cesium temperature of 473°K. As can be seen, the current contributed by the surrounding areas is small compared to the measured values. The cesium temperature is so low that the cesium coverage is zero for all of the support structure surfaces. Another fact which makes side emission an unlikely possibility is the large change in current which occurs for a small change in spacing. Such behavior cannot readily be explained as being due to extraneous emission surfaces. Finally, a third possibility is that Schottky enhancement of the emission from the capillary wall occurs due to a strong positive sheath. This seems to be the most reasonable explanation at the present time.

In summary, recent data obtained on the multicapillary converter indicates that operation in the temperature range of 2000 to 2100°K yields competitive power density with the added advantages of wider spacing and high voltage. At the present time the formulation of a theory to fully explain the experimental result is not complete. However, it appears that the basic operation of the converter does not depend upon the continuous circulation of cesium through the emitter.

25

At T_{Cs} = 473 K L-T Plot Indicates ϕ_{Ta} = 4.1

Observed Current at T_{Cs} = 473°K

d (mm)	I (ma)
1.4	1350
1.0	1400
0.8	1500
0.5	1780
0.3	2400

45 ma
84 ma
194 ma
2100° K
2200
2100
2000
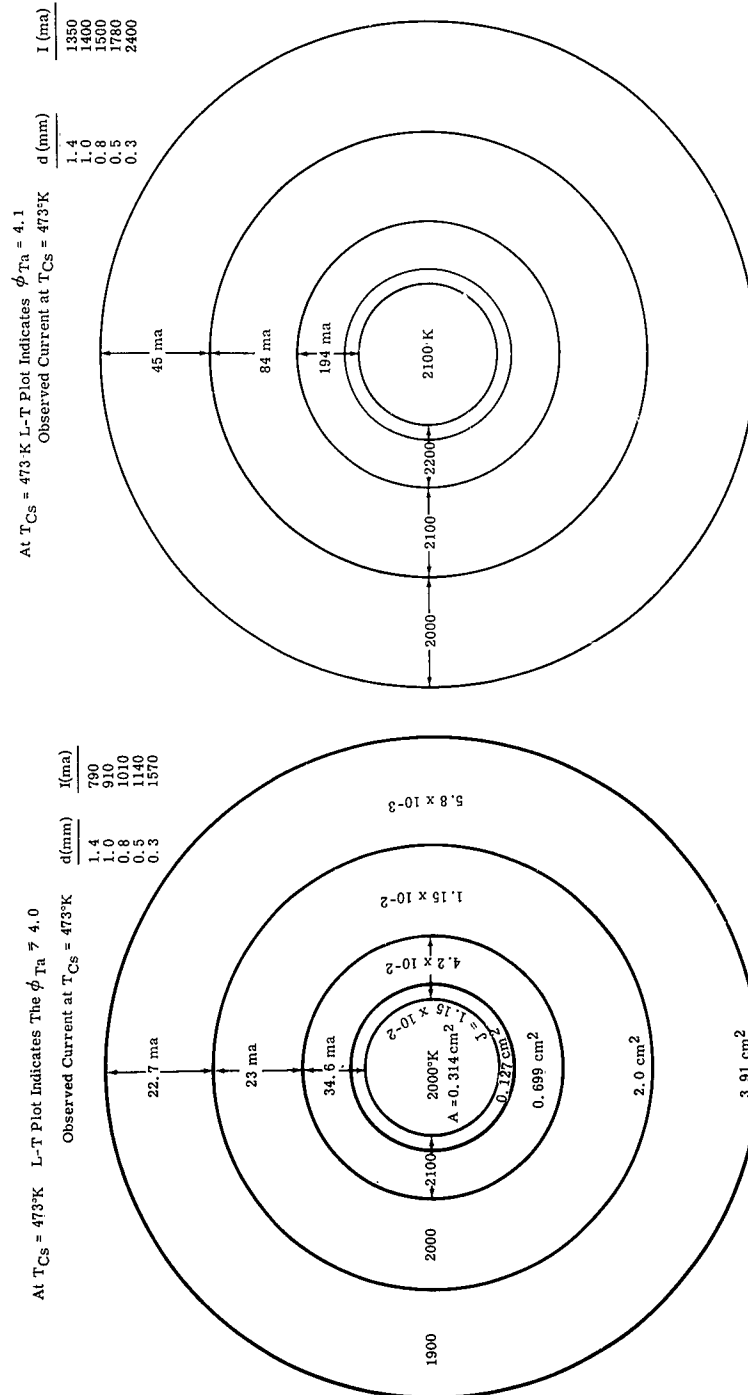
Figure 19. Emitter Temperature Distribution at 2100°K

At T_{Cs} = 473°K L-T Plot Indicates The ϕ_{Ta} ≈ 4.0

Observed Current at T_{Cs} = 473°K

d(mm)	I(ma)
1.4	790
1.0	910
0.8	1010
0.5	1140
0.3	1570

5.8×10^{-3}
1.15×10^{-2}
4.2×10^{-2}
1.15×10^{-2}
$J = 1.15 \times 10^{-2}$

22.7 ma
23 ma
34.6 ma
2000°K
$A = 0.314 \, cm^2$
$0.127 \, cm^2$
$0.699 \, cm^2$
$2.0 \, cm^2$
$3.91 \, cm^2$
2100
2000
1900

Figure 18. Emitter Temperature Distribution at 2000°K

26

ION CURRENT

In EDR 3207 experimental results were reported concerning the effect of collector temperature on the I-V characteristic. It was shown that, as the collector temperature was reduced, the following changes occurred:

1. Ion current decreased rapidly and then leveled off at about 373°K

2. Interelectrode pressure decreased as evidenced by the disappearance of the arc mode in certain cases

3. Open circuit voltage reached a peak value at 473°K

4. Passive mode electron current remained essentially constant

5. At the lowest T_C value, 323 to 373°K, the electron and ion currents were sensitive to spacing

In the analysis of these experimental results it was stated that a complete explanation of the observations had not been formulated. However, as the temperature of the collector was reduced, the evaporation rate of cesium from the collector surface was reduced. This cesium impinging on the hot emitter surface was the main source of ion current, and also contributed to creating a back pressure in the interelectrode space. ·In comparing the measured ion currents to the values predicted by the random current model, it was found that the measured values were higher than predicted by as much as two orders of magnitude.

Ion currents were again measured on Converter G for the T_E values of 1400, 1500, 1600, 1700, and 1800°K; and T_{Cs} values of 473, 523, and 573°K. Figures 20, 21, 22, and 23 demonstrate the typical results. Figure 24 is a summary plot of the measurements. Shown on the summary plot are the ion currents as predicted by the random current model---the theoretical calculation assumes the cesium density at the capillary exit is 1/20 of the entrance density, a result predicted by the Knudsen flow equation. As can be seen from the summary plot, the ion currents measured are again much higher than predicted by the random current model.
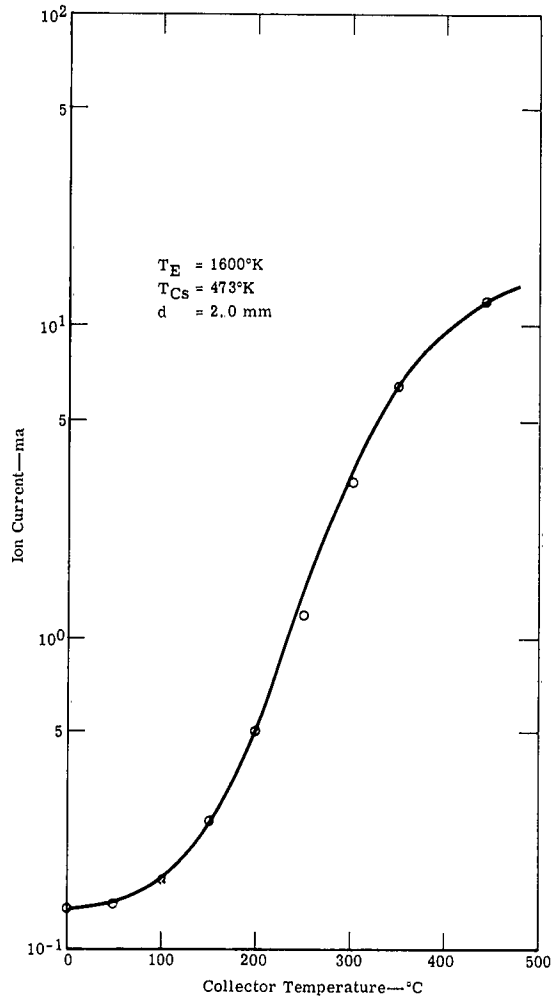
Figure 20. Ion Current as Function of T_C for $T_E = 1600°K$ and $T_{Cs} = 473°K$

$T_E = 1600°K$
$T_{Cs} = 473°K$
$d = 2.0$ mm

Ion Current—ma

Collector Temperature—°C

$T_E = 1800°K$
$T_{Cs} = 473°K$
$d = 2.0$ mm

Ion Current—ma

Figure 21. Ion Current as Function of T_C for $T_E = 1800°K$ and $T_{Cs} = 473°K$

Collector Temperature —°C

28
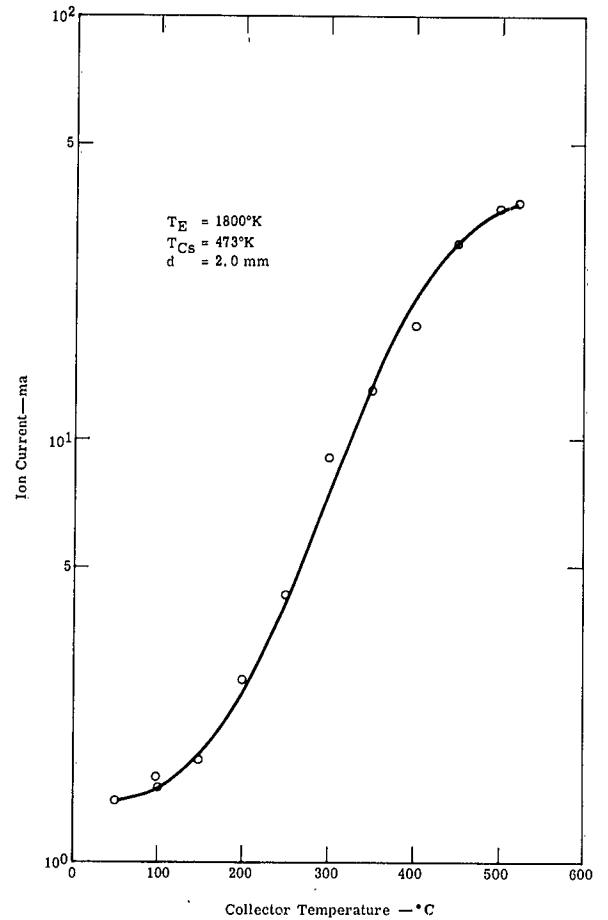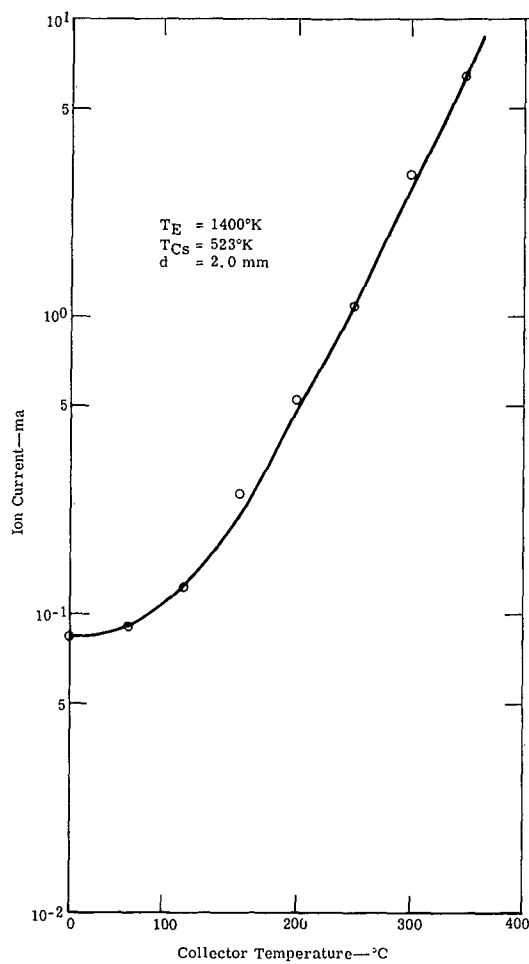
Figure 22. Ion Current as Function of T_C for $T_E = 1400°K$ and $T_{Cs} = 523°K$

$T_E = 1400°K$
$T_{Cs} = 523°K$
$d = 2.0$ mm

Ion Current—ma

Collector Temperature—°C

$T_E = 1800°K$
$T_{Cs} = 573°K$
$d = 0.8$ mm

Ion Current—ma

Figure 23. Ion Current as Function of T_C for $T_E = 1800°K$ and $T_{Cs} = 573°K$

Collector Temperature—°C

29
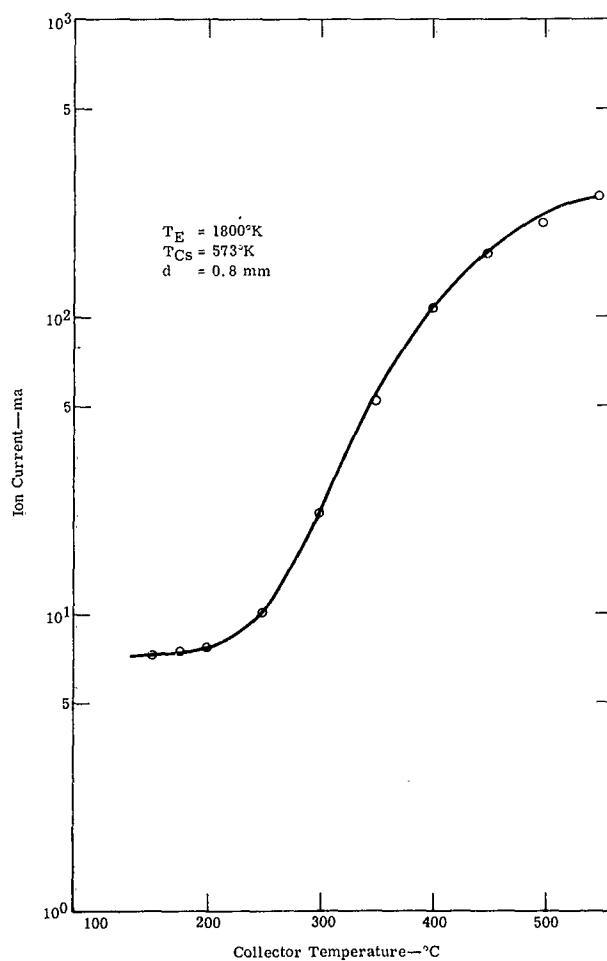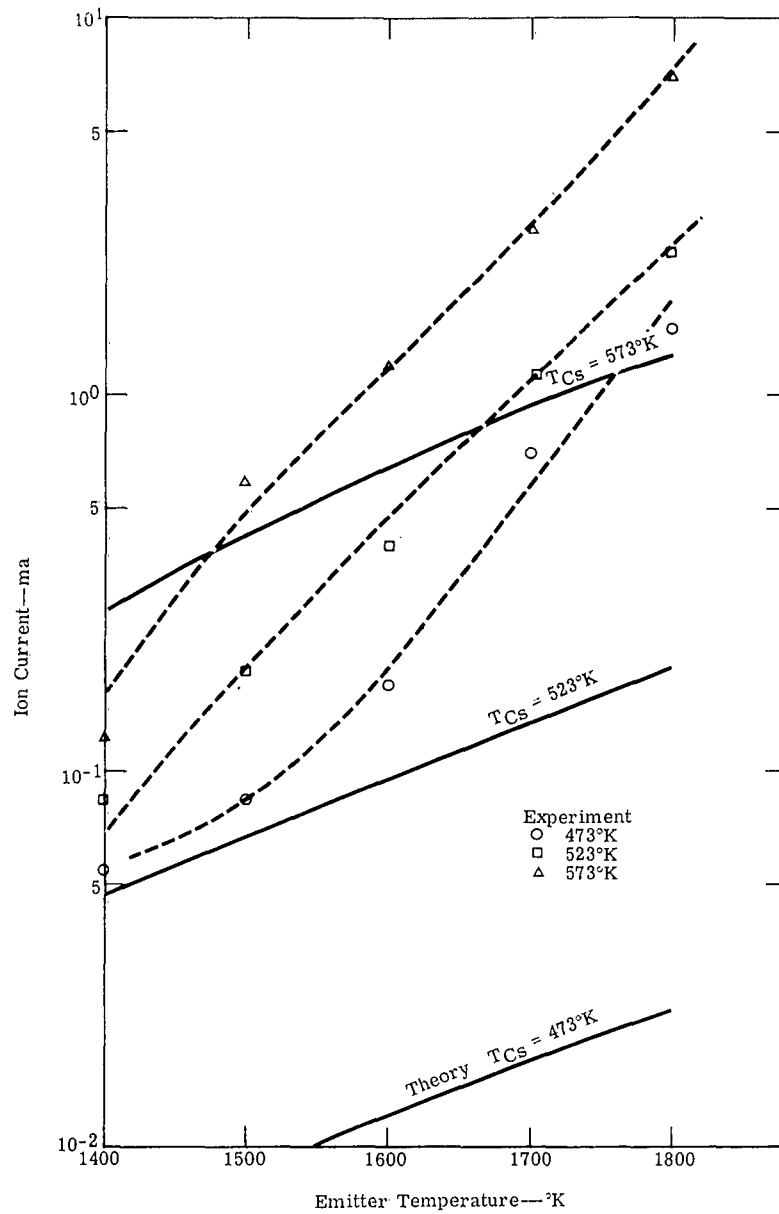
Figure 24.   Ion Current Summary Plot

There appear to be four possible sources for the observed ion current:

1. Thermionic electrons from the collector

2. Photoelectrons from the collector

3. Some type of discharge which creates the ions by volume processes

4. Ions generated at the emitter surface

Considering each of these in more detail, the pertinent surface areas in the collector volume chamber are shown in Figure 25. Current density as a function of work function is given as follows for $T_C = 700°K$:

Work Function	Current Density (ma/cm^2)
1.7	0.027
1.6	0.175
1.5	0.9
1.4	4.8
1.3	25.5

Referring to Figure 20, a typical value of 11 ma was observed at a $T_C = 700°K$. A work function of 1.3 would be required on the collector surface (0.314 cm^2 area) to explain the observed current (see Figure 25). If all of the collector area including the trapazoidal section were emitting, then a work function of slightly less than 1.5 volts would be necessary. Other data have been obtained which do not support the premise that the current is electrons from the collector.

Figure 26 shows the reverse current for two T_C values, 603 and 638°K, as a function of T_E for a $T_{Cs} = 473°K$ and d = 2.0 mm. As seen from the graph, the ion current increases rapidly as T_E increases. Since T_C is constant, the reverse current should remain constant if due to electrons from the collector. Finally, no investigator has reported conclusive evidence that a work function as low as even 1.5 volts has been obtained in a cesium thermionic converter.

Photoelectric currents from cesium covered surfaces are difficult to predict since the yield factor is not well known. Dr. L. R. Kollar of National Research Corporation has made an estimate of the photoelectric current from a Cs-O-W surface. The details are given in Appendix A. He concludes that the photoelectric current for 1800°K tungsten radiation would be 0.16 ma/cm^2, a value negligible in comparison to the reverse currents measured.
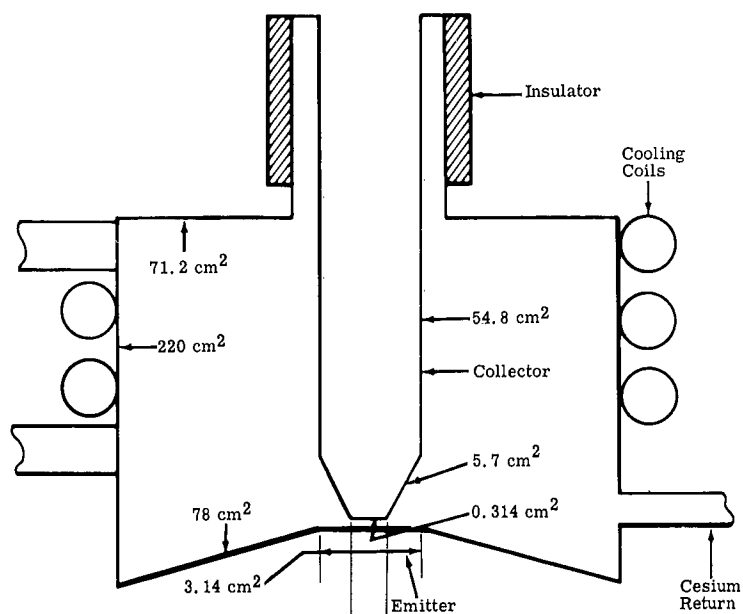
Figure 25. Pertinent Surface Areas in the Collector Volume

It is difficult to understand what type of discharge could be producing ions by volume processes. All discharges or arc phenomena observed on the multicapillary converter, and reported by other workers, are characterized by a sharp rise in current as the voltage is increased, or a discontinuity in the I-V curve. Reverse current was measured to 15 volts negative without a sharp rise on discontinuity in the ion current curve. (See Figure B-22 in Appendix B.)

Finally, the ion current could be due to ions generated on the emitter surface. Two additional experiments were performed to illustrate the nature of reverse current. In Figure 27 the current variation is shown as a function of spacing. In one run the collector temperature was maintained constant---the current increased from 9 ma at 2.0 mm to 23 ma at 0.3 mm. This could be interpreted as due to an increase in the interelectrode pressure. In a second run the collector was permitted to seek an equilibrium temperature---as the spacing was decreased the T_C increased. In this case, at 2.0 mm the current was 8 ma, while at 0.3 mm the current was 42 ma. This could be interpreted to be the cumulative effect of pressure and temperature. In Figure 28 the emitter was raised to 1900°K so that the collector equilibrium temperature was 953°. Upon reducing T_C the ion current actually increased, reached a broad peak around 773°K, and finally decreased as in Figures 20, 21, 22, and 23. This data appears not to support the theory that the ions are due to atom evaporation from the collector to the emitter---if the current
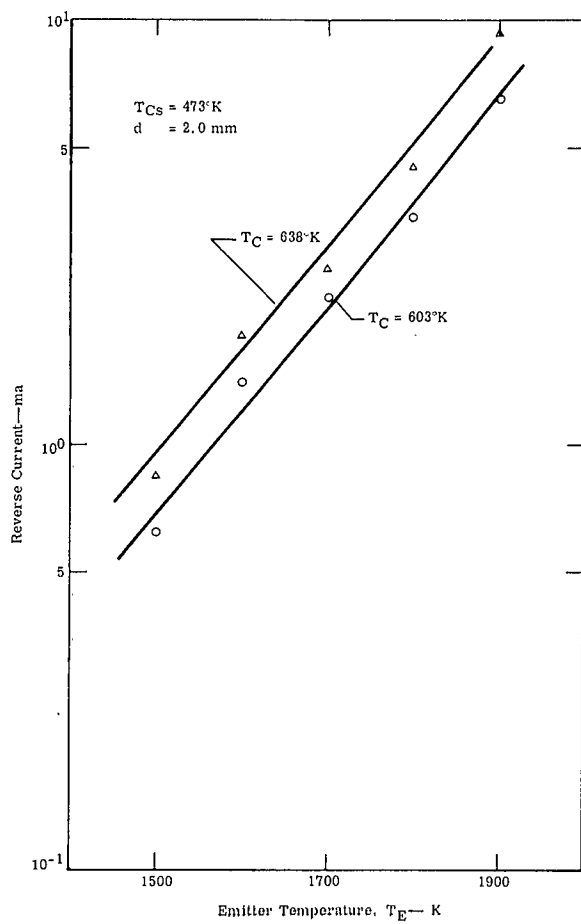
Figure 26. Reverse Current as Function of T_E

Figure 27. Variation in Ion Current with Spacing for Constant T_C and Equilibrium T_C.

33
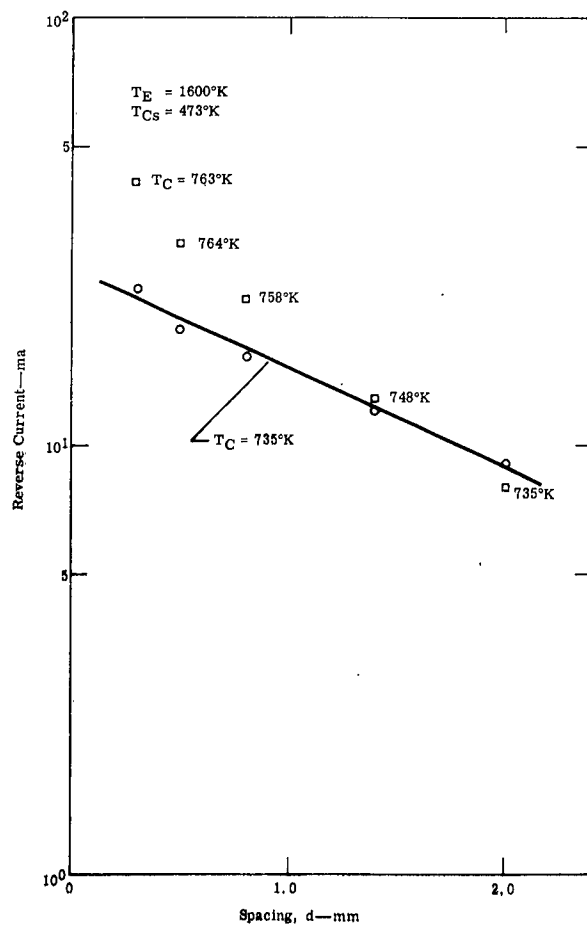
were due to atom impingement on the emitter, the current should saturate at some T_C value, and then remain constant for values above this saturation point.

If the reverse current data are plotted logarithm current as a function of reciprocal temperature, the slope of the line should give the heat of evaporation of cesium, if the current is due to atom evaporation from a collector coated with several layers of cesium (0.79 electron volts/gm atom). The data shown in Figures 20, 21, 22, and 23 are plotted in this form in Figures 29, 30, 31, and 32. In no case is a value of 0.79 obtained—the values vary from 0.28 to 0.55.

If atoms from the collector are being ionized at ·the emitter, it has been pointed out that the emitter surface would have to be electron rich in order to observe currents of the magnitude measured. The presence of ignited mode and high frequency oscillations tend to support this view since Brietwieser, in the previous reference, reports these characteristics are predominant in the electron rather than the ion rich condition.

In summary, the source of the ions has not been identified conclusively. However, evidence still supports the theory that the reverse current is due to atoms evaporating from the collector and being ionized on the emitter surface.
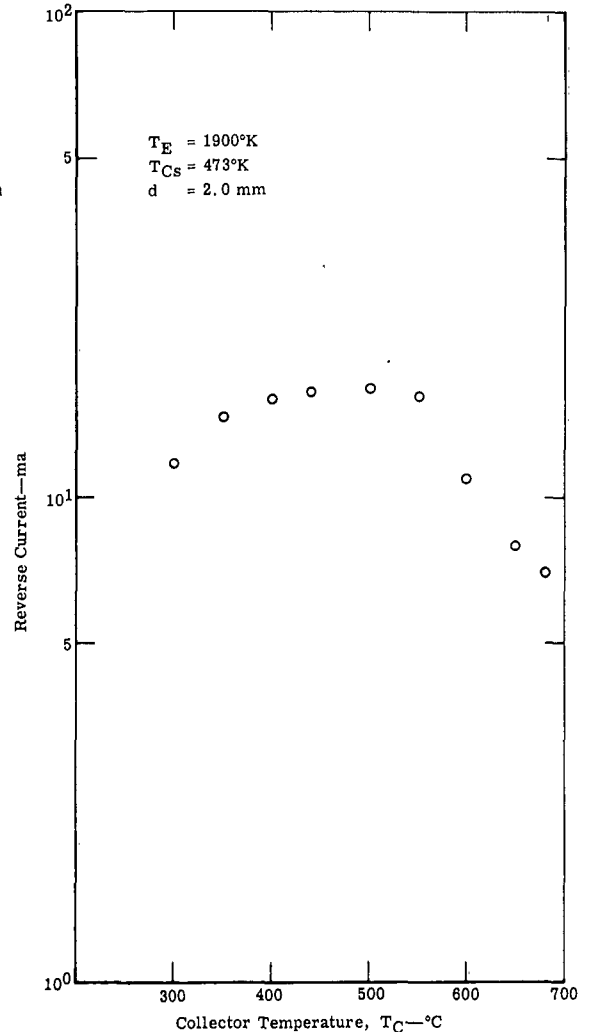
Figure 28. Ion Current at 1900°K
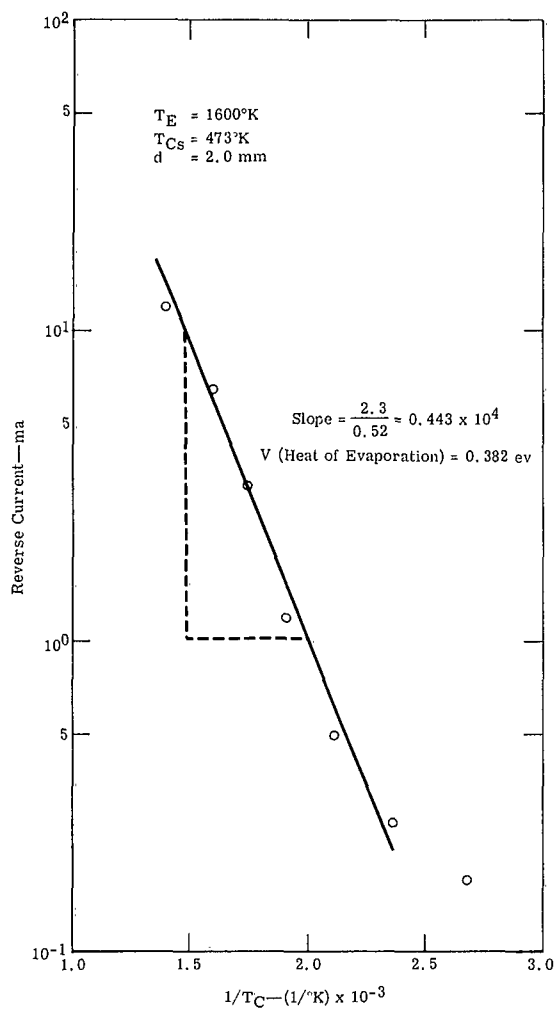
Figure 29. Ion Current as Fun ction of $\dfrac{1}{T_C}$, for $T_E = 1600°K$ and $T_{Cs} = 473°K$

$T_E = 1600°K$
$T_{Cs} = 473°K$
$d = 2.0$ mm

Slope $= \dfrac{2.3}{0.52} = 0.443 \times 10^4$

V (Heat of Evaporation) = 0.382 ev

Reverse Current—ma

$1/T_C$—(1/°K) x 10^{-3}
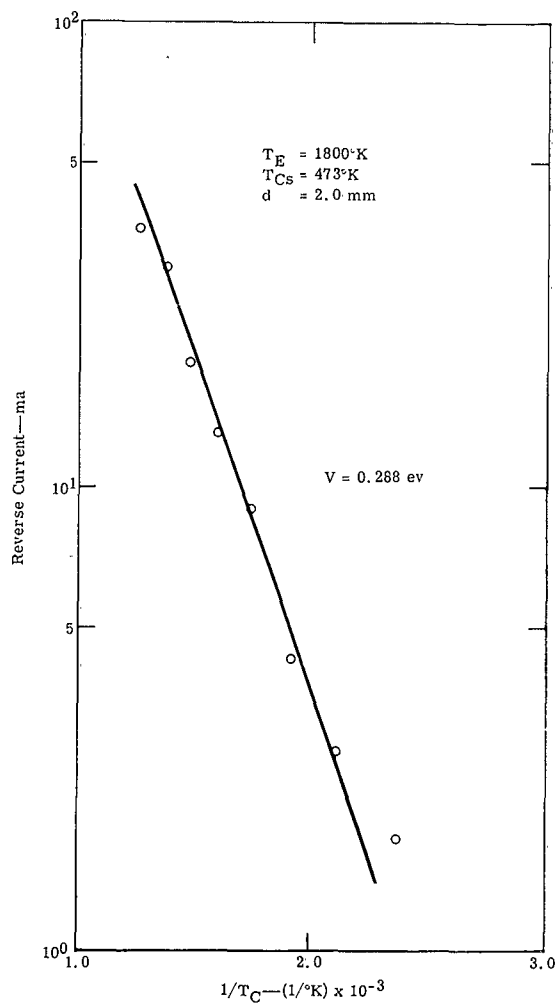
Figure 30. Ion Current as Function of $\dfrac{1}{T_C}$ for $T_E = 1800°K$ and $T_{Cs} = 473°K$

$T_E = 1800°K$
$T_{Cs} = 473°K$
$d = 2.0$ mm

V = 0.288 ev

Reverse Current—ma

$1/T_C$—(1/°K) x 10^{-3}

35
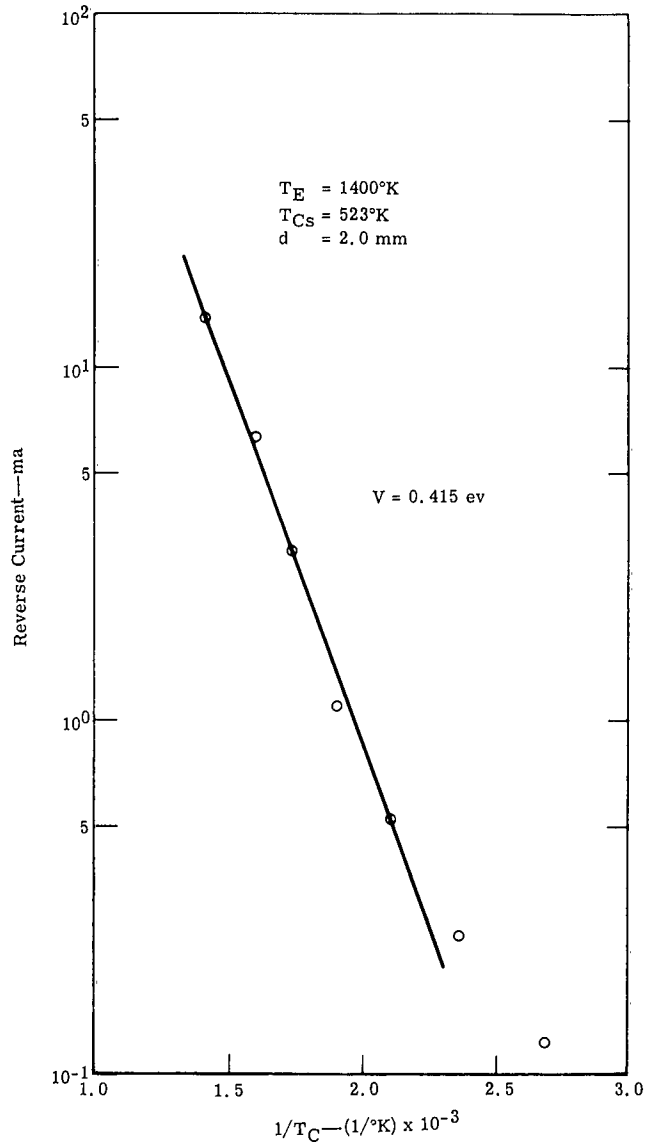
Figure 31. Ion Current as Function of $\frac{1}{T_C}$ for T_E = 1400°F and T_{Cs} = 523°K
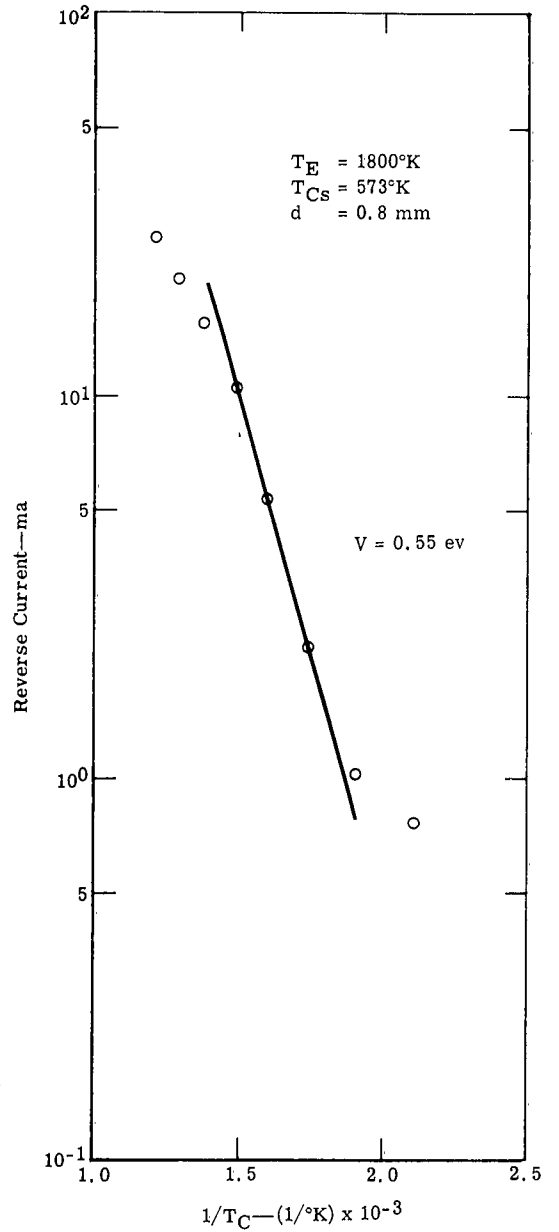
Figure 32. Ion Current as Function of $\frac{1}{T_C}$ for T_E = 1800°K and T_{Cs} = 573°K

36

HIGH FREQUENCY OSCILLATIONS

High frequency oscillations were observed under several conditions. For example, see the data in Figures B-1 to B-21. Considerable difficulty was experienced in recording the oscillations because external circuit inductance produced large inductive pulses when the converter current changed abruptly. From a study of the wave-form, it appeared that the current, under certain conditions, dropped instantaneously towards zero. This was the source of the large inductance pulses.

After considerable investigation, the circuit shown in Figure 33 gave the best results. Two 18-in. lengths of wire twisted together to reduce the inductance gave a short circuit resistance of 0.020 ohms. Figures 34 and 35 show a set of oscillograms taken at T_E = 1800°K and T_{Cs} = 473°K. Note how the inductive pulse increases as the load resistance is reduced towards short circuit.
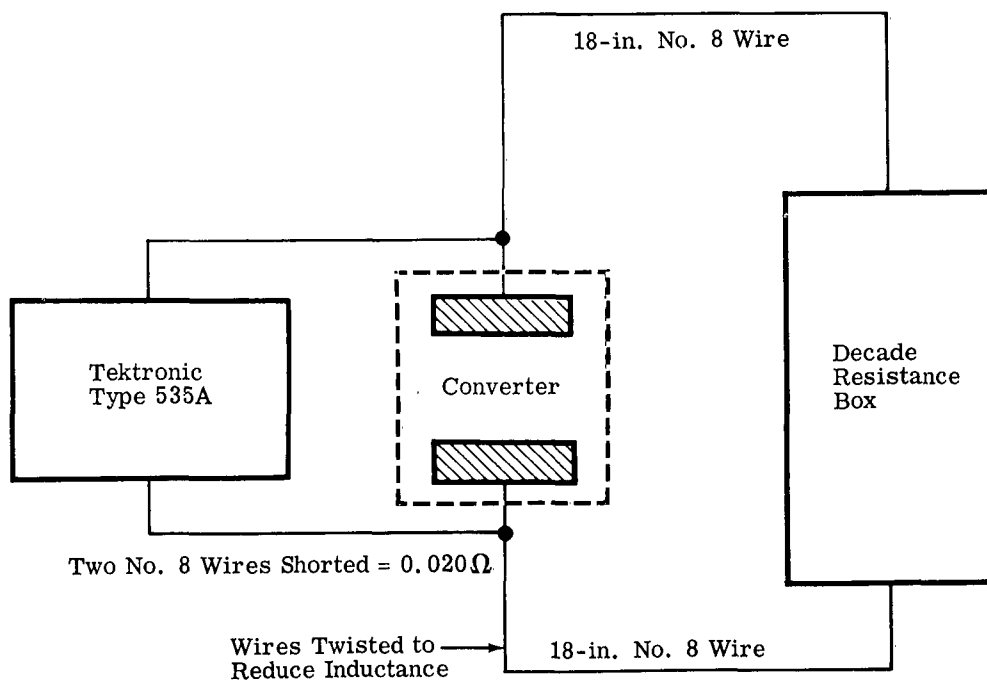
Figure 33. Circuit for Oscillation Study

$T_E = 1800°K$
$T_{Cs} = 473°K$
$d = 1.0$ mm

| R (Ω) | V (v/cm) |

0 — 7 — 0.5

0 — 5 — 0.5

0 — 3 — 0.5

0 — 1 — 0.5

0   2.5   5

μ Sec
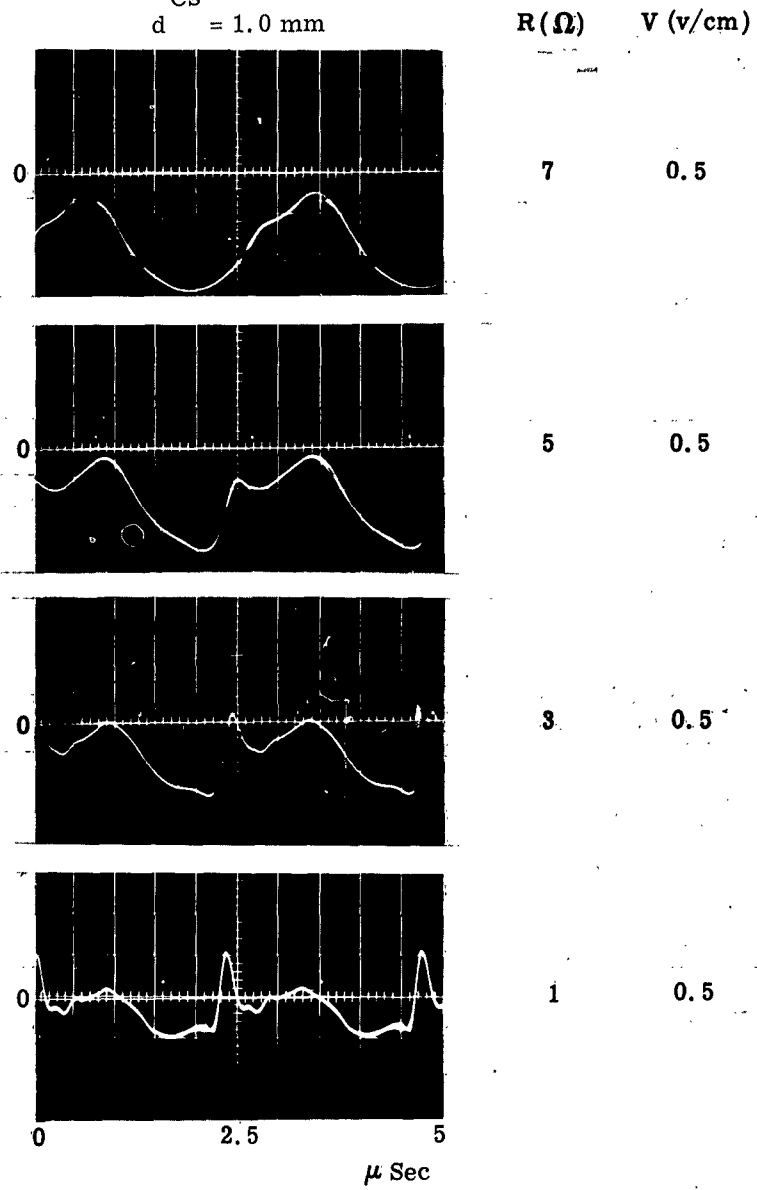
Figure 34.   Oscillation Data for High Resistance Load

38

$T_E = 1800°K$
$T_{Cs} = 473°K$
$d = 1.0$ mm

R (Ω)	V (v/cm)
0.5	0.5
0.02	0.2
0.003	0.2

0   2.5   5.0

μ Sec
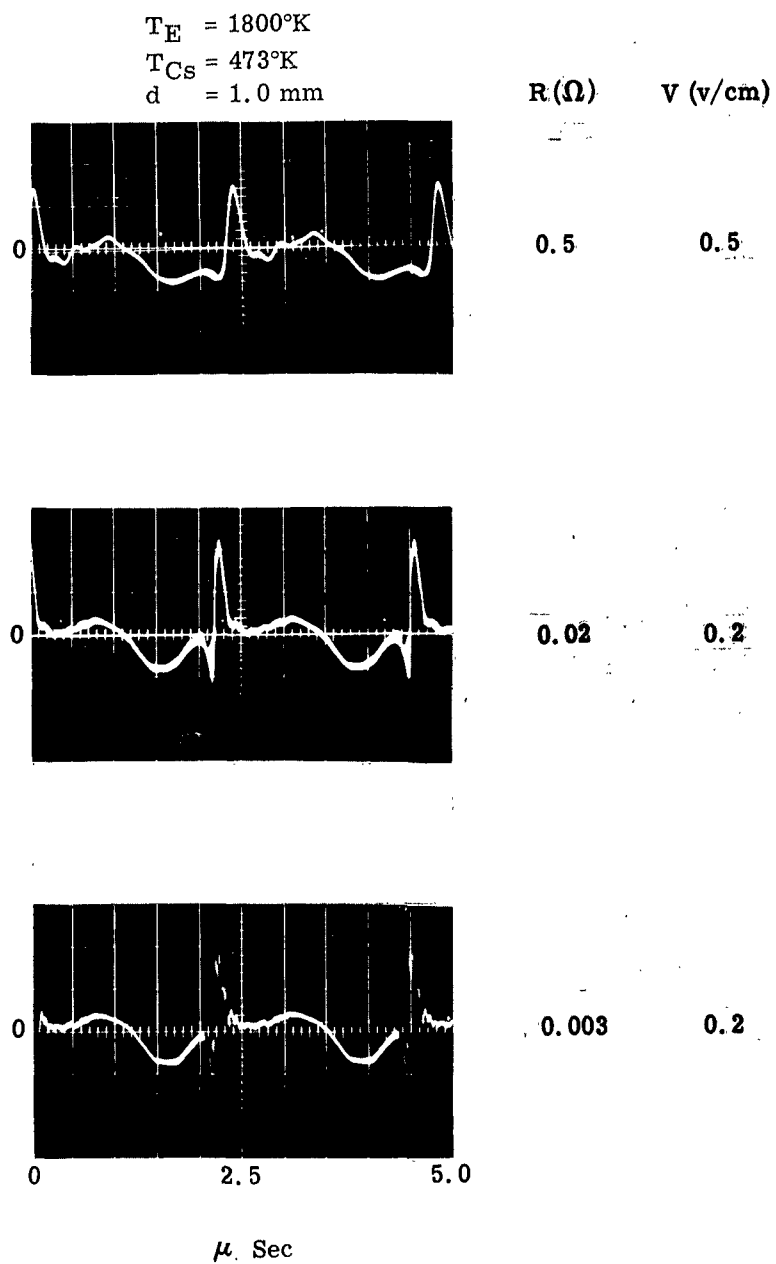
Figure 35. Oscillation Data for Low Resistance Load

39

The peak negative voltage was recorded for a series of load values. The peak current was then computed, and the resultant voltage-current points plotted for comparison with the I-V characteristic recorded on the x-y recorder. The result is shown in Figure B-23. It appears that the converter operates periodically in the arc mode.

Further detailed study of the oscillations as a function of T_E, T_{Cs}, T_C, and d were planned, but failure of the converter prevented this from being accomplished. It may be stated that oscillations were observed over a range of emitter temperatures from 1400 to 2100°K, and up to 573°K cesium temperature at 1500°K emitter temperature. Generally, the higher the emitter temperature, the lower was the cesium temperature at which the oscillations disappeared.

V. SPECTROGRAPHIC STUDY

The object of this investigation was to determine if it is possible to obtain useful information using spectroscopy on a cesium converter operating in the power generating region. The two major points for concern were: (1) if the line intensity would be sufficient to evaluate the spectrum, and (2) if the system were in such a state of nonequilibrium that the spectrum could not be interpreted with existing theory.

EXPERIMENTAL TEST SETUP

The multicapillary diode has a sapphire window located on one side through which the inter-electrode spacing can be observed.

A Hilger Two-Prism Spectrograph (Figure 36) is used to obtain the spectrographic data. The spectrograph is located so that the image of the plasma in the interelectrode space is focused on the entrance slit of the spectrograph. The spectrograph is aligned so that only the radiation from the plasma in the interelectrode space passes through the entrance slit of the spectrograph. The image is magnified by a factor of three by the focusing lens. The entrance slit width is fixed at 10 microns. Thus, the width of the plasma observed is approximately three microns (Figure 37).

EXPERIMENTAL DATA

Spectrographic data were obtained for various emitter temperatures and cesium reservoir temperatures. All data were taken at a constant spacing of 2 mm. Data could have been obtained at spacings down to 1 mm; however, at spacings below 1 mm, background radiation from the emitter makes it difficult to distinguish the weak lines.

Photographs of the plasma line spectra were obtained for a range of operating conditions as follows:

- T_E—1600 to 1900°K
- T_{Cs}—523 to 573°K
- d—2.0 mm

For each photograph taken with the spectrograph, the corresponding position on the current-voltage characteristic curves was recorded.

41

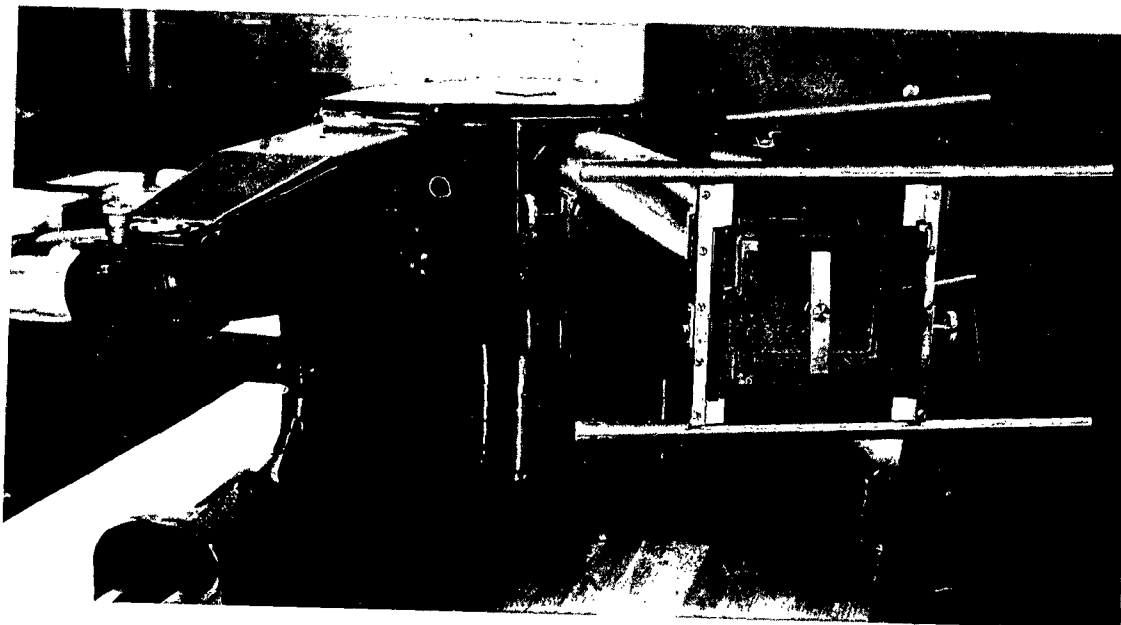Figure 36. Hilger Two-Prism Spectograph

$$\frac{\text{Size Image}}{\text{Size Object}} = \frac{3}{1}$$

Collector

Aperture

Focusing Lens

Sapphire Window

Capillary Emitter

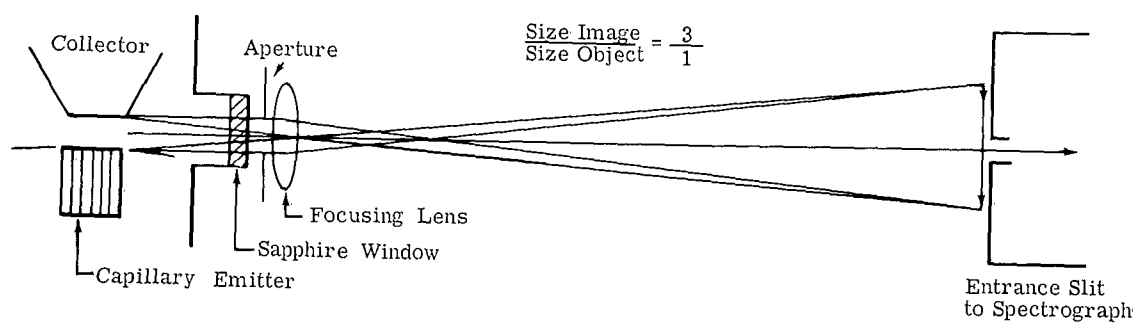Entrance Slit
to Spectrograph

Figure 37. Spectrographic Arrangement

In the range of the converter operating conditions studied, various modes of operation were observed. The different operating modes are described as the passive mode, ignited mode, and arc mode, plus an oscillating region. The different modes of operation are best defined by referring to the current-voltage characteristic curves (Figure B-17). Starting at open circuit voltage, as the output voltage is reduced, the current increases to an apparent saturation value—this is the passive mode of operation. A region of oscillation appears and then the current jumps to some new saturation value where it again levels off—this is the ignited mode. At close spacing (0.3 mm) the current jumps to what appears to be the ignited mode, but the current continues to increase as the voltage is decreased—arc mode operation.

The current-voltage characteristic curves shown in Figures B-24 to B-32 have the points marked where the corresponding spectrographic pictures were taken.

At an emitter temperature of 1600°K and a cesium reservoir temperature of 523°K the passive mode and an oscillating region are observed (Figures B-24 to B-26). Spectroscopic pictures were taken at the points shown. Of particular interest are the data at points before and after the transition into the oscillating region, as will be discussed later.

For the emitter temperature at 1600°K and the cesium reservoir temperature raised to 573°K, the characteristic curves are shown in Figures B-27 and B-28. The converter goes from the passive mode of operation into the arc mode (Figure B-27). Just prior to the transition, plasma oscillations were observed.

Figures B-28 through B-30 are for an emitter temperature of 1800°K and a cesium reservoir temperature of 573 and 523°K. At the cesium reservoir temperature of 523°K the current drops to a negative value in going from the passive to the arc mode (Figure B-30). At the higher cesium temperature of 573°K the converter appears to be in the arc mode at all times (Figure B-29). Figure B-24 also shows the characteristic curve with the emitter at 1900°K with a cesium reservoir temperature of 523°K. Again the converter appears to be in the arc mode only.

One interesting observation—in the transition from the passive mode to the ignited or arc mode, a region of oscillation was always observed. In the arc mode no oscillations were observed with the scope.

The effect of cooling the collector and thus reducing the ion current observed in the capillary was studied. The collector temperature was reduced from 758°K to 373°K and the plasma line spectrum was observed at two points on the I-V curve—(1) open circuit, and (2) short circuit (Figures B-31 and B-32).

Additional spectrographic studies were planned; however, the capillary converter failed after three months of operation, terminating the experimental work.

SPECTROGRAPHIC DATA ANALYSIS

The objectives of the spectrographic study were: (1) to observe the plasma line spectrum for the various modes of operation, (2) to determine the types of impurities which might be observed in the plasma, (3) to determine the energy distribution of ions and electrons in the plasma, and the temperature corresponding to this energy distribution, and (4) the number density of ions and electrons in the plasma.

LINE SPECTRUM FOR DIFFERENT MODES OF OPERATION

In the passive mode of operation only the cesium resonance lines are observed with long exposure times. Cesium lines corresponding to higher excited states cannot be detected. This result is to be expected if the electrons have a Maxwellian distribution corresponding to the emitter temperature. The relative number of electrons having energy equal to or higher than the energy corresponding to the first excited state of the cesium atoms is quite small (tail of the Maxwell-Boltzman distribution).

As an example, the relative number of electrons with energy greater than the first excited state of cesium for a temperature of 1800°K is:

$$\frac{N_c}{N} = 4.4 \times 10^{-4}$$

where N_c is the number having an energy greater than 1.39 ev and N is the total number of electrons.

44

Figure 38 shows the different excited states of a cesium atom and the corresponding energy and wavelength for each excited state. To excite a cesium atom to the first excited state requires energies of 1.39 and 1.45 ev. Energy will be radiated at wavelengths of 8943 and 8521 angstroms in going from the first excited state to the ground state. A dimensionless plot (Figure 39) gives the relative number of electrons having an energy greater than a selected relative energy expressed as (C/Co), where C is the speed of the electron corresponding to some energy (E), and Co is the most probable speed.

For a temperature of 1800°K the square of the most probable speed for electrons is (Figure 40):

$$Co^2 = 5.461 \times 10^{14} \text{ cm}^2/\text{sec}^2$$

For an energy of 1.39 ev the corresponding speed squared of an electron is (Figure 41):

$$C^2 = 4.89 \times 10^{15} \text{ cm}^2/\text{sec}^2$$

The ratio of $(C/Co)^2$ is:

$$(C/Co)^2 = 9.06$$

Using Figure 39, the relative number of electrons having an energy greater than 1.39 ev is:

$$\frac{N_c}{N} = 4.4 \times 10^{-4}$$

Another consideration of importance is the ratio of the λ/d, where λ is the mean free path of the electrons and d is the spacing. In a conventional converter the mean free path in a cesium vapor may be evaluated by using the equation developed by Nottingham.[*] This equation is based on collision probability data reported by Brode.[**] However, in the capillary converter the number density is reduced by approximately one order of magnitude at the exit. This would increase the mean free path by approximately one order of magnitude. For example, at an emitter temperature of 1800°K, a cesium reservoir temperature of 473°K, and a gas temperature of 1800°K, the mean free path for a conventional device would be approximately 0.25 mm.

---

[*] W. B. Nottingham, General Theory of Plasma Diode Converter. Thermo Electron Engrg. Corp., Tech. Rept. No. TEE-7002-5.

[**] R. B. Brode, "Quantitative Study of the Collisions of Electrons with Atoms." Rev. Mod. Phys., Vol. 5, Oct. 1933.
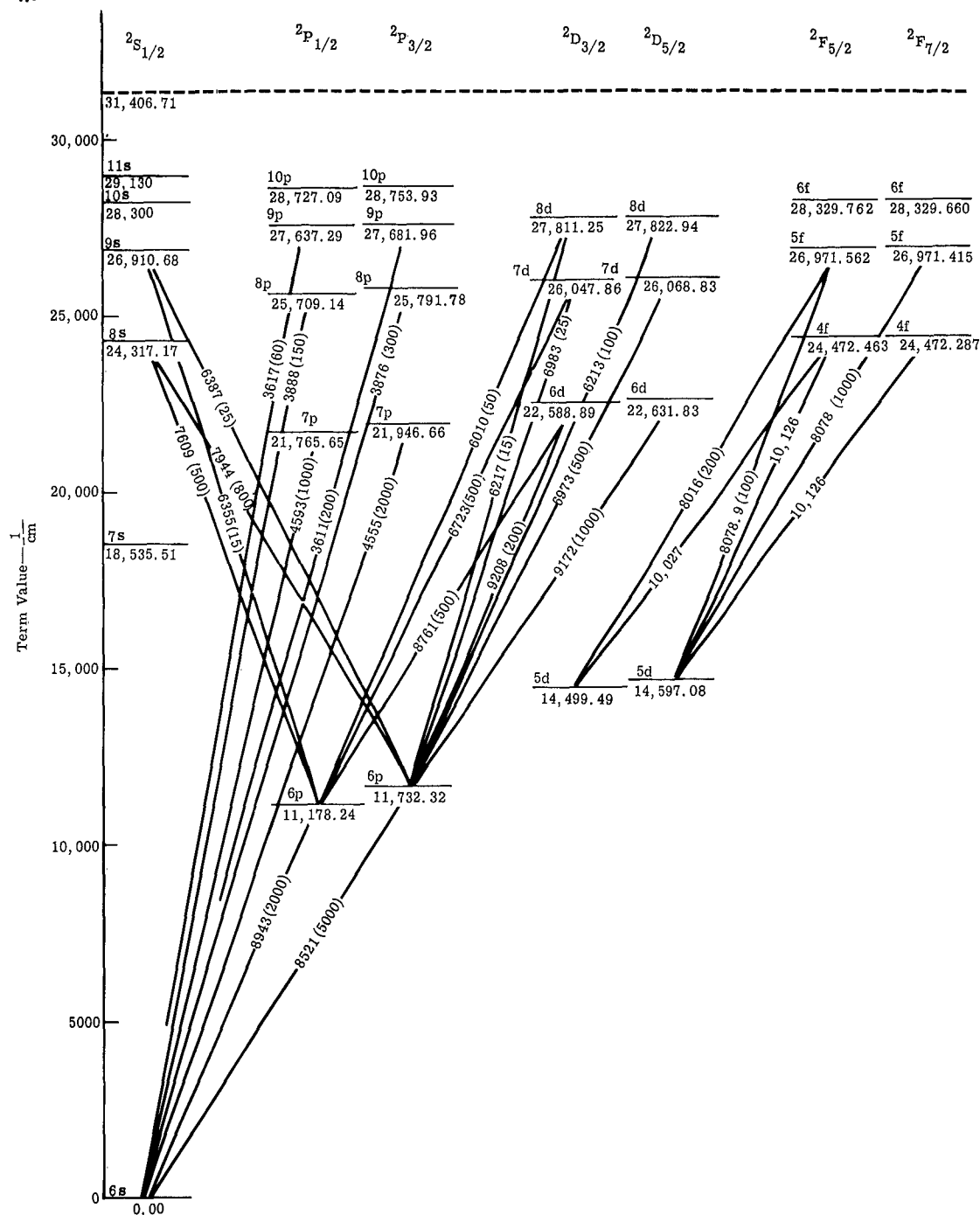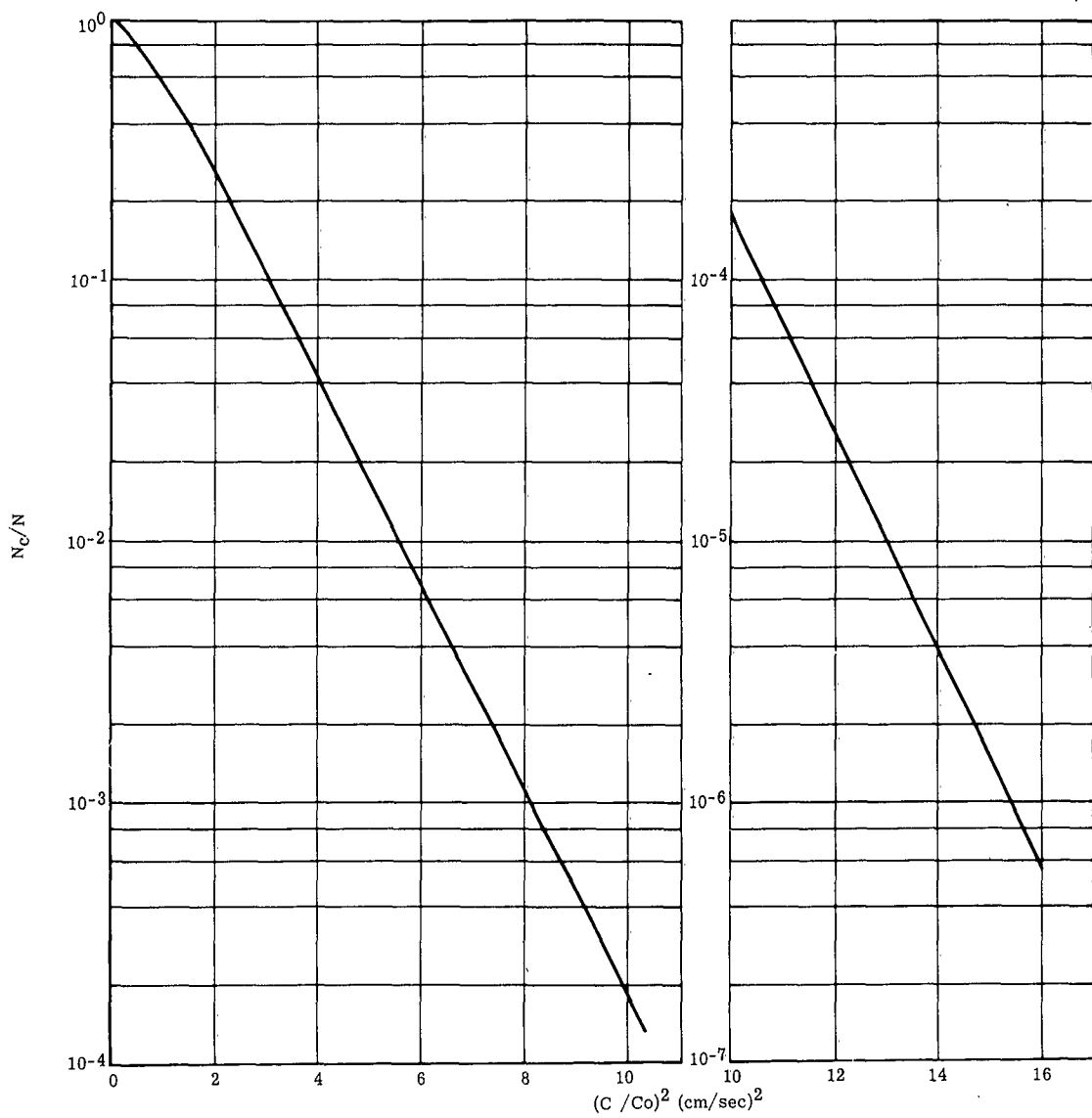
Figure 38. Energy Level Diagram for Cesium Atom

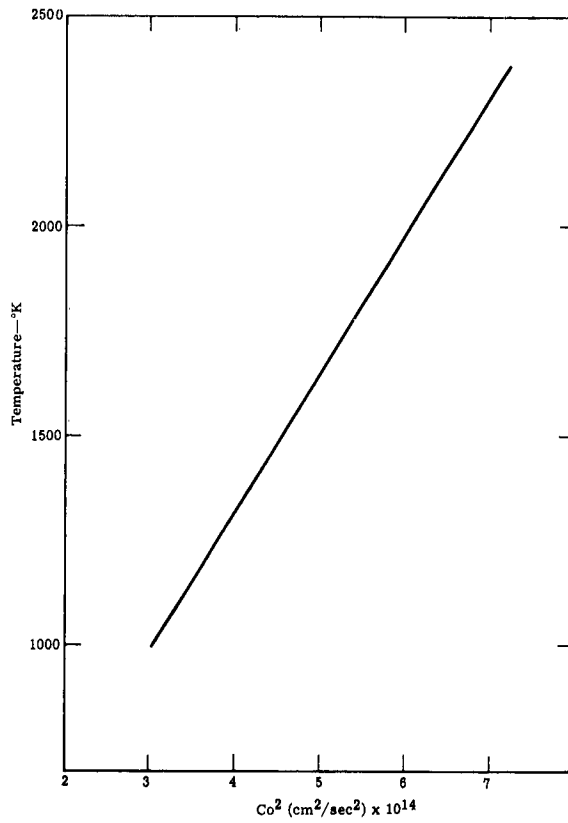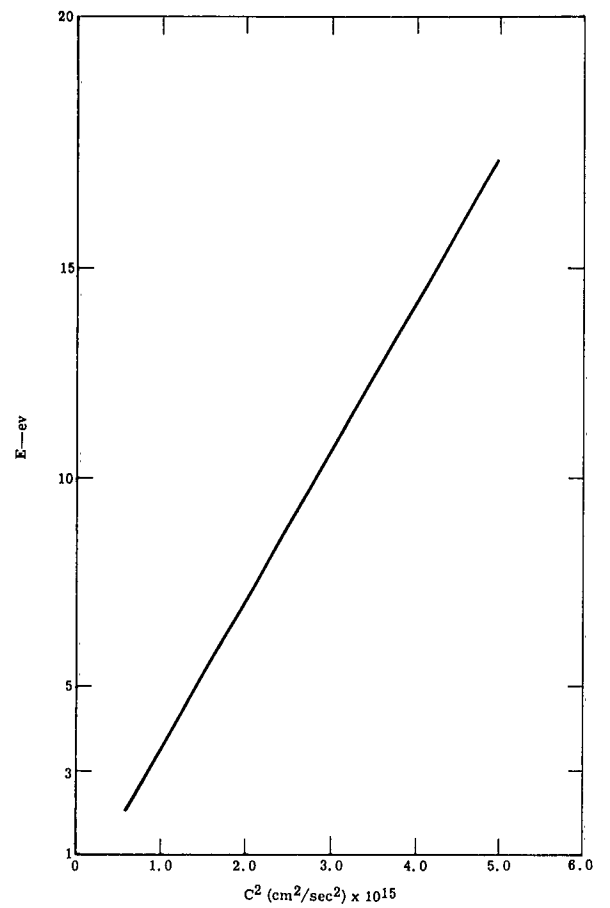Figure 39. Fraction of Electrons Above a Given Energy in a Maxwellian Distribution

47

Figure 40. Temperature vs Co^2

Figure 41. Kinetic Energy vs C^2

48

However, for the capillary converter at the same operating conditions, the mean free path would be 2.5 mm. Over the range of operating conditions studied, λ/d varies from 0.1 to 0.475.

In summation, for the passive mode of operation, the number of electrons having energy equal to or greater than the energy required for excitation of the cesium atoms is small. The mean free path for electrons in the cesium gas is of the same order of magnitude as the spacing, thus the number of collisions is small. The combination of relatively few collisions plus relatively few high energy electrons explains the absence of the cesium line spectrum for the passive mode.

EFFECT OF PLASMA OSCILLATIONS

Plasma oscillations have a very definite effect on the intensity of the cesium lines. In the passive mode the cesium lines were not observed, even with long exposure times. However, as soon as the plasma oscillations start, cesium lines for the higher energy states are observed. As the output voltage is reduced, the intensity of the cesium lines increases. A reduction in output voltage also increases the amplitude of the plasma oscillations. Figures B-24 and B-25 show the points on the characteristic curve at which the spectrographic data were taken going from the passive mode into the plasma oscillating region. The corresponding photographs of the line spectra are shown in Figure 42. The increase in cesium line intensities with a reduction in the output voltage can be observed.

A qualitative explanation of the effect of plasma oscillations would be that the oscillations increase the number of collisions occurring in the plasma. The plasma oscillations are normally considered to be due to ions sweeping back and forth between the electrodes. At the same time the electrons must be oscillating but probably at a higher frequency. The effect of the oscillations is to increase the distance traveled by the electrons in passing from the emitter to the collector. If the electron path is increased, then the number of collisions should increase by the same proportion.

A second effect may be to increase the energy of the electrons. Assuming that the electrons oscillate as a result of accelerating fields being established by the ions, then the electrons may gain kinetic energy during these oscillations. The net effect would be to increase the number of electrons with sufficient energy to excite cesium atoms.

However, for the capillary converter at the same operating conditions, the mean free path would be 2.5 mm. Over the range of operating conditions studied, λ/d varies from 0.1 to 0.475.

In summation, for the passive mode of operation, the number of electrons having energy equal to or greater than the energy required for excitation of the cesium atoms is small. The mean free path for electrons in the cesium gas is of the same order of magnitude as the spacing, thus the number of collisions is small. The combination of relatively few collisions plus relatively few high energy electrons explains the absence of the cesium line spectrum for the passive mode.

EFFECT OF PLASMA OSCILLATIONS

Plasma oscillations have a very definite effect on the intensity of the cesium lines. In the passive mode the cesium lines were not observed, even with long exposure times. However, as soon as the plasma oscillations start, cesium lines for the higher energy states are observed. As the output voltage is reduced, the intensity of the cesium lines increases. A reduction in output voltage also increases the amplitude of the plasma oscillations. Figures B-24 and B-25 show the points on the characteristic curve at which the spectrographic data were taken going from the passive mode into the plasma oscillating region. The corresponding photographs of the line spectra are shown in Figure 42. The increase in cesium line intensities with a reduction in the output voltage can be observed.

A qualitative explanation of the effect of plasma oscillations would be that the oscillations increase the number of collisions occurring in the plasma. The plasma oscillations are normally considered to be due to ions sweeping back and forth between the electrodes. At the same time the electrons must be oscillating but probably at a higher frequency. The effect of the oscillations is to increase the distance traveled by the electrons in passing from the emitter to the collector. If the electron path is increased, then the number of collisions should increase by the same proportion.

A second effect may be to increase the energy of the electrons. Assuming that the electrons oscillate as a result of accelerating fields being established by the ions, then the electrons may gain kinetic energy during these oscillations. The net effect would be to increase the number of electrons with sufficient energy to excite cesium atoms.
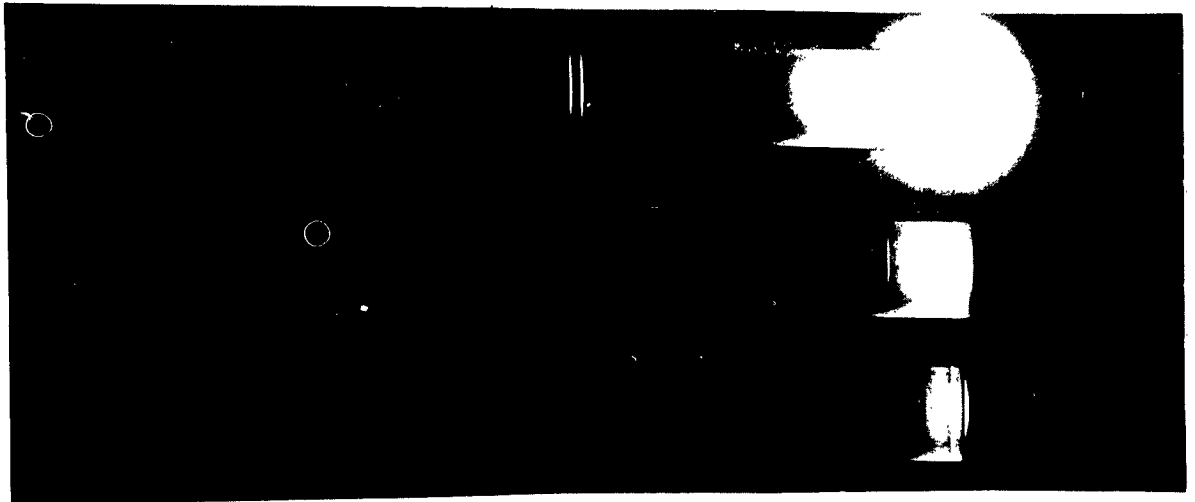
P-20
Exposure Time—5 sec, 15 sec, and 5 min

Passive Mode

P-23
Exposure Time—5 min, 15 sec, and 5 sec

Oscillating Region

Figure 42. Line Spectra of Passive Mode and Oscillation Region

TRANSITION FROM THE PASSIVE MODE TO THE IGNITED OR ARC MODE

The transition from the passive mode to the arc mode is shown by the characteristic I-V curve (Figure B-27).

The transition from the passive to arc mode of operation is explained as the result of volume ionization creating a large positive sheath at the emitter. Electrons are accelerated through this positive sheath into the plasma. The kinetic energy of the electrons leaving the emitter is increased by the amount of the sheath potential. Therefore, a large fraction of the electrons entering the plasma may have sufficient energy to excite the cesium atoms.

In going from the oscillating region into the arc mode an increase in the cesium line intensity is observed. The spectrographic data (shown in Figure 43) corresponds to the I-V characteristic curve (Figure B-27) in line intensity.

IMPURITIES IN THE PLASMA

Impurity lines were observed in the plasma—the impurities were identified as potassium and rubidium. The existence of potassium and rubidium can only be explained by assuming that these impurities were present in the cesium used in the reservoir. Two potassium lines at wavelengths of 7698 and 7665 angstroms and one rubidium line at a wavelength of 7800 angstroms were observed. These lines are the resonance lines of the respective elements. The manufacturer stated that the cesium was 99.9% pure. Thus, all the impurities constitute only 0.1% by weight of the cesium.

The appearance of the potassium and rubidium lines depended on the mode of operation and the emitter temperature. In the oscillating region the potassium and rubidium lines were weak as compared to the adjacent cesium lines for an emitter temperature of 1600 to 1800°K. However, in the arc mode at an emitter temperature of 1800°K and a cesium temperature of 573°K the potassium lines were very strong. The potassium lines were stronger than the adjacent cesium lines (Figure 44). At an emitter temperature of 1600°K and a cesium temperature of 573°K weak potassium lines are observed in the arc mode. A comparison of the line spectrum for an emitter temperature of 1600 and 1800°K operating in the arc mode at a cesium temperature of 573°K is shown in Figure 45.

P-40
Exposure Time 1 sec, 5 sec, and 2 min
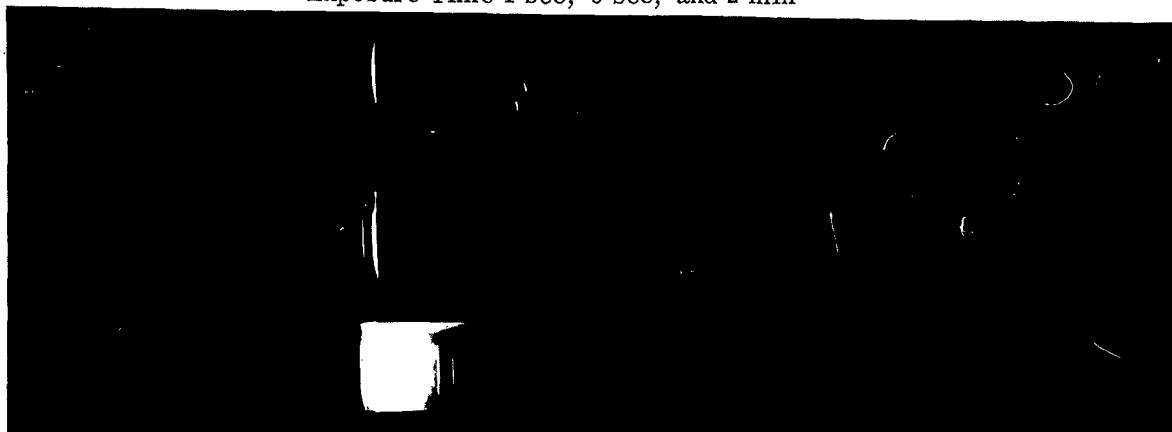
Oscillation Region

P-41
Exposure Time—2 min, 5 sec, and 1 sec
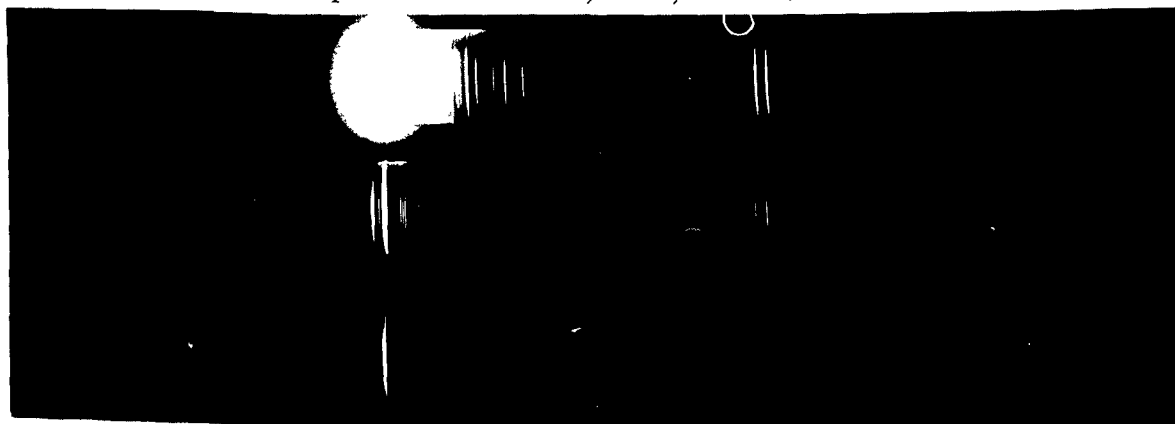
Ignited Mode

Figure 43. Line Spectra of Oscillation Region and Arc Mode

Exposure Times 5 Sec, 30 Sec, 2 Min

Cs 7609
K {7698
  {7665
Rb 7800

Figure 44.   Line Spectra in Arc Mode at 1800°K

Cs   7609
K   {7698
    {7665
Rb   7800

$T_E = 1600°K$ $T_E = 1800°K$

P-41   P-61

Figure 45.   Impurity Lines at 1600 and 1800°K

ELECTRON TEMPERATURE

In the arc mode the electron temperature was measured using the line ratio method. The radiation power in ergs/sec/cm^3 as a function of electron temperature is shown for different cesium lines in Figure 46. This curve was obtained for cesium lines with known transition probabilities. Using Figure 46 the intensity ratio between two cesium lines at a given temperature can be determined. Figure 47 shows the densitometer traces for P-34 (Figure B-27) and P-51 (Figure 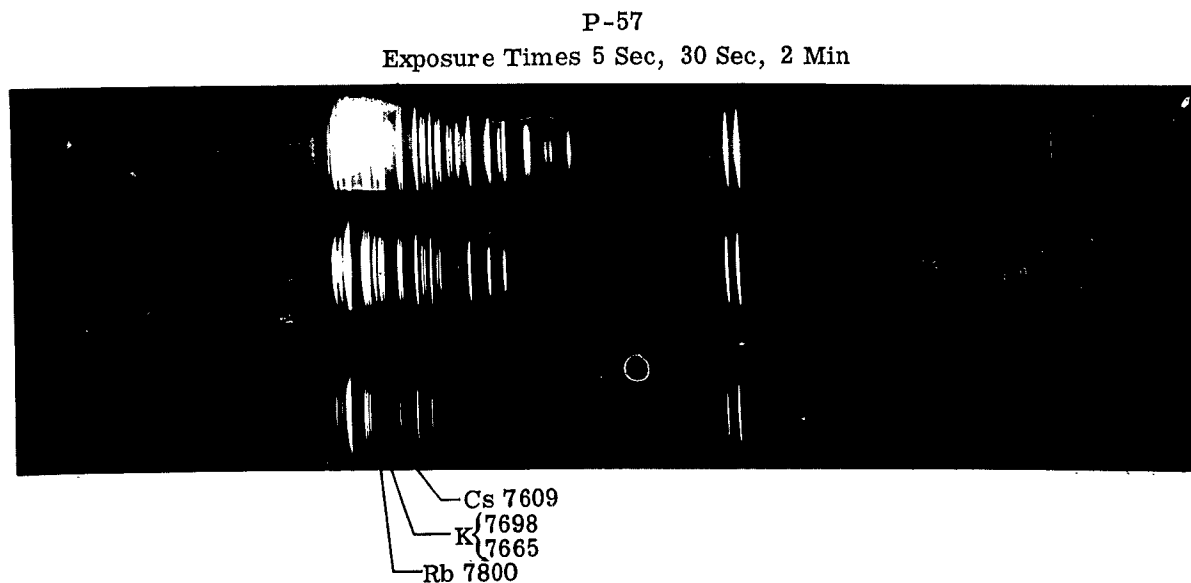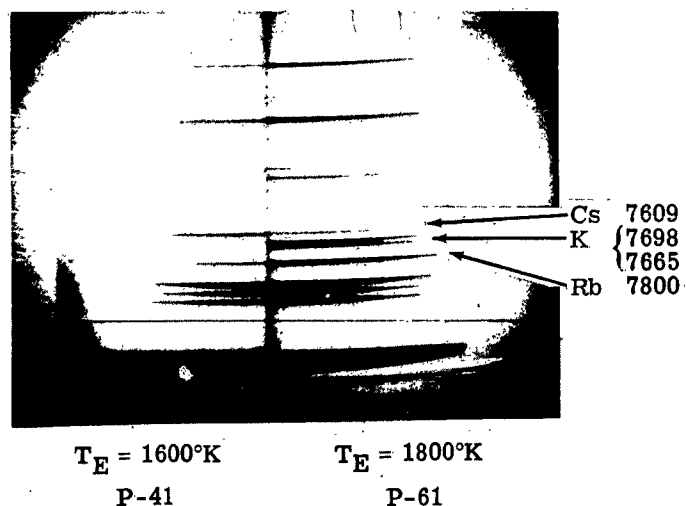B-29). P-34 is for an emitter temperature of 1600°K and P-51 is for an emitter temperature of 1800°K. This example shows an inversion of the intensity ratio of the line pairs 7609/8016, which can be explained as a temperature effect together with the change of sensitivity of the photographic emulsion at different wavelengths. The result indicates that the electron temperature was slightly below 4000°K at 1600°K and slightly above 4000°K at 1800°K.

Extensive measurements were made of intensity ratios of lines originating from higher energy levels. The line ratios used with the corresponding temperature (for P-51) are:

Line Ratio		Measured Temperature
$\dfrac{7608}{6010}$	=	3600°K
$\dfrac{8761}{6010}$	=	4000°K
$\dfrac{6010}{4555}$	=	4290°K
$\dfrac{7609}{6212}$	=	4000°K

The measured electron temperature for these line ratios in arc mode operation is thus 4000°K ± 20% from the spectroscopic study.

Additional work is being done to better establish the electron temperature. However, the important result is that the electron temperature is higher than the emitter temperature in the arc mode. This is to be expected since a positive sheath must exist at the emitter which accelerates electrons into the plasma.
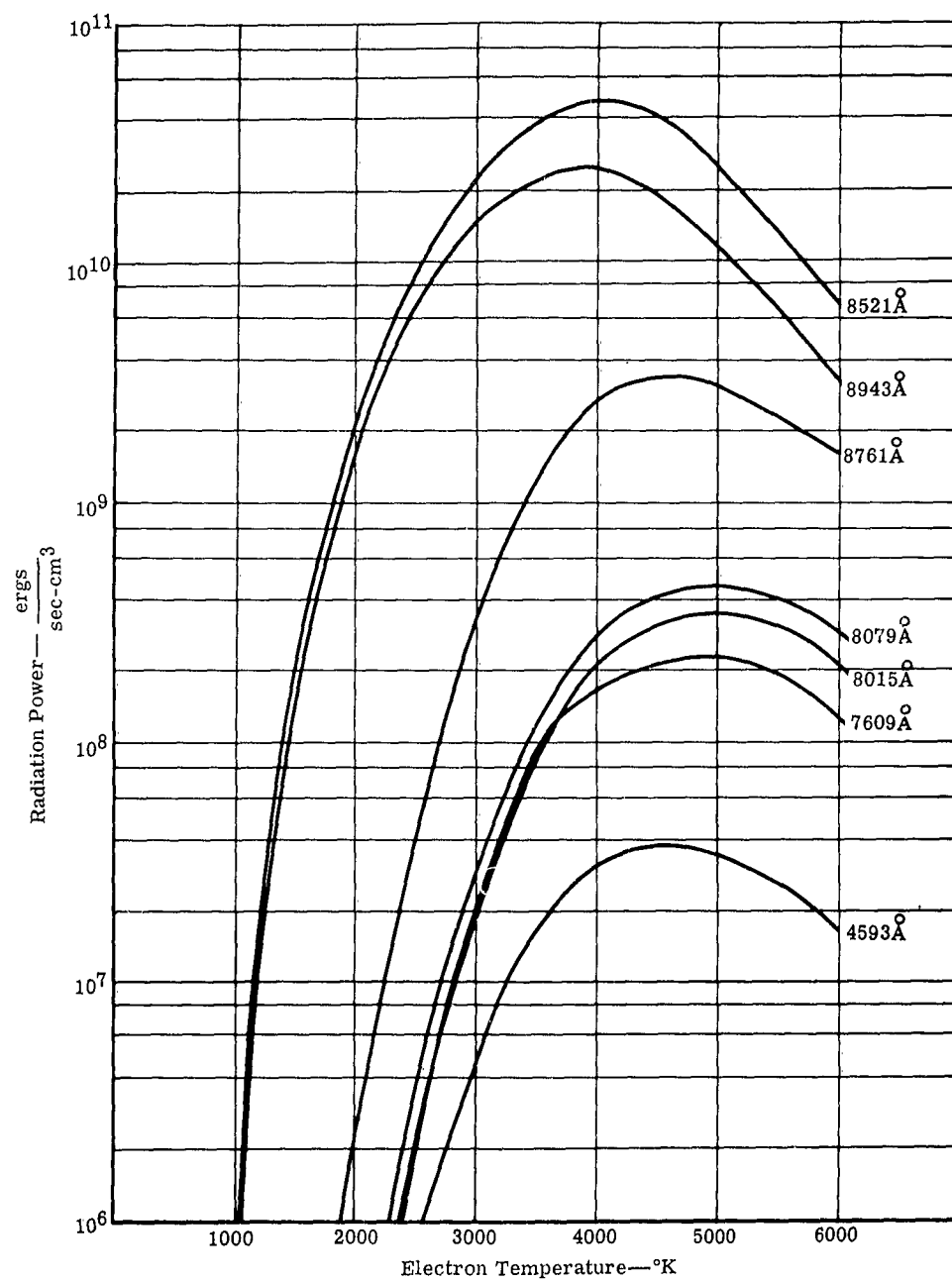
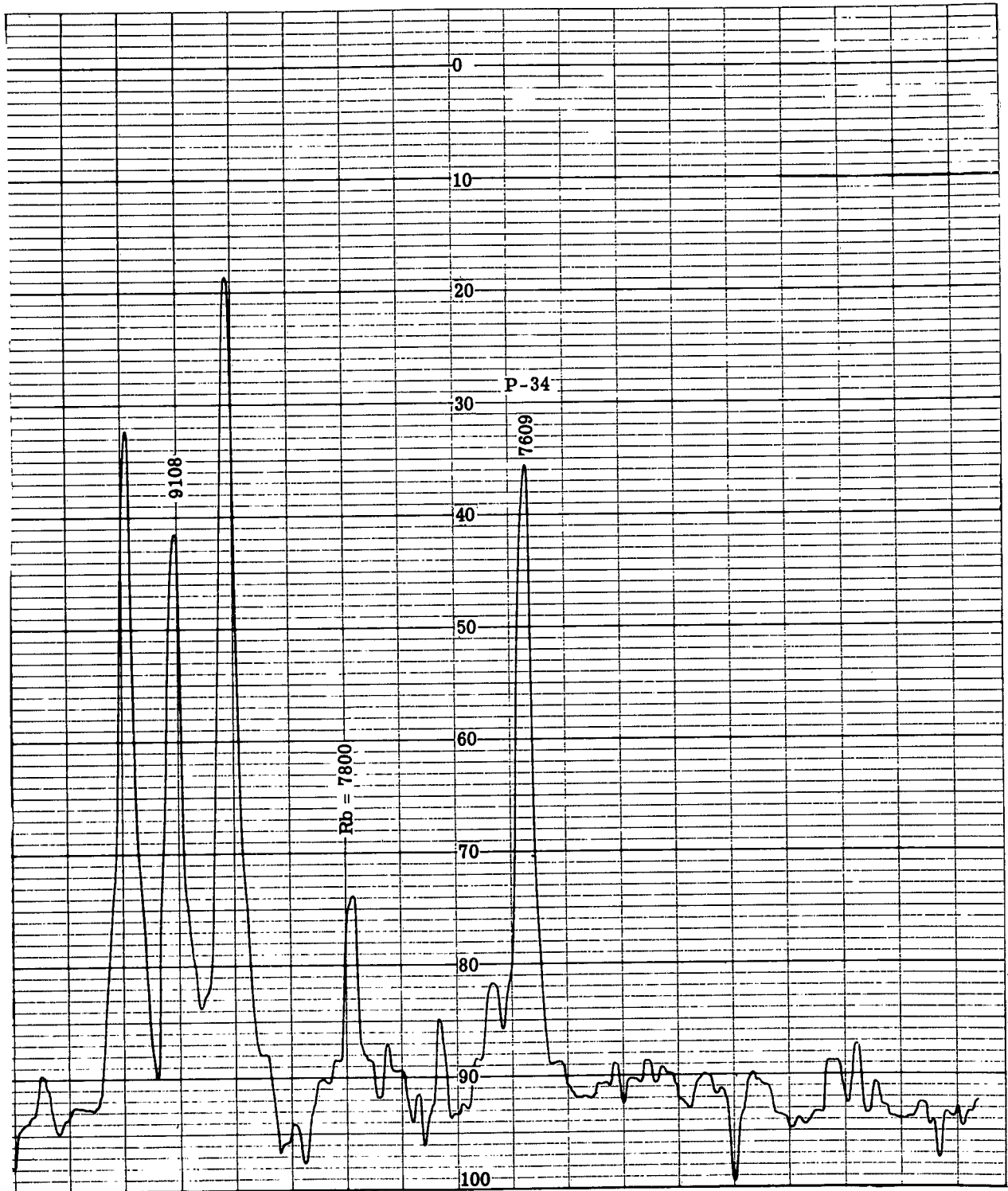Figure 46. Radiation Power as Function of Electron Temperature

NUMBER DENSITY OF IONS AND ELECTRONS

Using the cesium lines 6288, 6250, 6472 and 6432 the electron density was estimated by line broadening measurements. The value obtained was $2 \times 10^{14}/cm^3$ in the arc mode for an emitter temperature of 1800°K and cesium temperature of 573°K. The theoretical values for the line broadening used to make this estimate were taken from H. Griem, a consultant for General Motors Research. His work will be published in 1964---"Plasma Spectroscopy," by H. Griem, McGraw Hill (1964).

The ion density, determined by the random current model, for an emitter temperature of 1800°K and a cesium temperature of 573°K is estimated to be 5.15×10^{13} ions/cm^3. The total number density at the exit of the capillary is estimated to be 1.7×10^{15} atoms/cm^3. The results from the spectroscopic study indicate an ion density somewhat higher than predicted by the random current model. This result would agree with a positive sheath formed at the emitter in the arc mode resulting in a higher electron temperature, which in turn would increase the volume ionization rate, sustaining the discharge.

EFFECT OF COOLING THE COLLECTOR

The effect of cooling the collector to reduce the ion current did not seem to change appreciably the intensity of the line spectrum for the diode operating in the oscillating region. With the collector at 373°K the line intensity was slightly less than with the collector at 673°K.
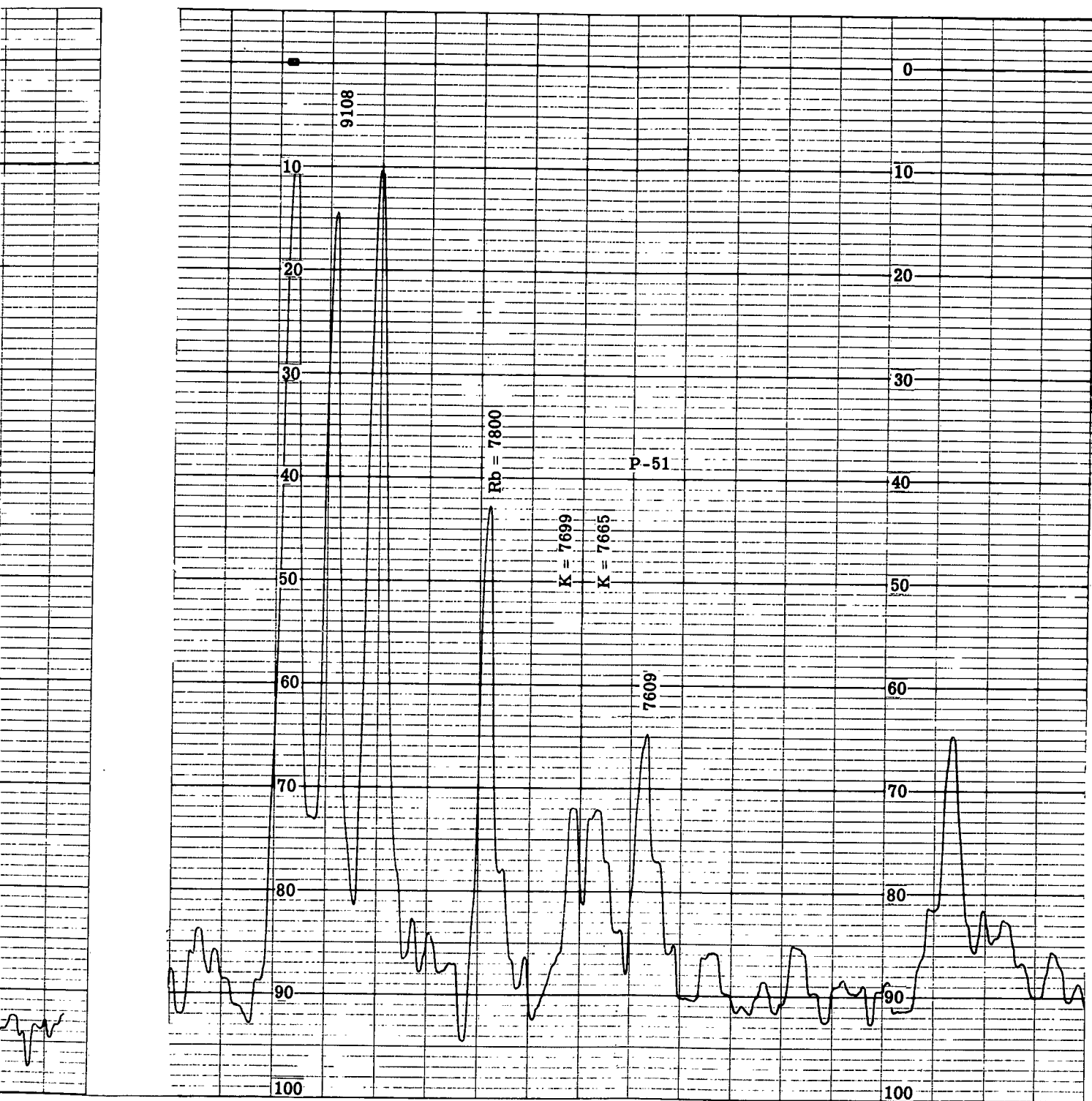
Chart showing spectral peaks labeled 9108, Rb = 7800, 7609, and P-34, with a vertical scale from 0 to 100. Marked "1".

Figure 47. Densitometer Traces

57

APPENDIX A

Photoelectric Emission in Cesium Converters

APPENDIX A

PHOTOELECTRIC EMISSION IN CESIUM CONVERTERS
by Dr. L. R. Kollar
National Research Corporation

The magnitude of the photoelectric current from the anode of a thermionic converter with tungsten electrodes operating in cesium vapor was calculated. It is probably not more than 0.16 ma/cm^2 for the conditions assumed. These were:

1. The anode operating in Cs vapor at a pressure sufficient to maintain complete coverage

2. The anode receiving all of the radiation from a tungsten electrode at a temperature of 1800°K

The calculation was first made for a Cs-O-Ag surface. This grossly overestimates the photoelectric effect as this surface has the highest known quantum efficiency in the long-wave end of the spectrum where most of the energy from an 1800°K source is radiated. Accordingly the value of 2.0×10^{-3} amp/cm^2 obtained for this case represents the maximum yield to be expected under the most favorable conditions for the best known photoemitter.

The calculation was then made assuming what the writer believes to be an optimistic value for the photoelectric yield of a Cs-O-W surface. This gave the value of 0.16 ma/cm^2.

The data used in these calculations are given in Table A-I. The first column gives the wavelength in μ : the center of the 0.1μ band was used in the computation. The second column gives the energy in watts radiated over a 2π solid angle/cm^2/0.1μ band for a black body at 1800°K. The third column gives the emissivity of tungsten and the fourth column gives the energy radiated by the tungsten source. The fifth column gives the yield for the photoemitter in terms of photoelectric current per watt of energy incident at the various wavelengths and the last column gives the corresponding photoelectric currents. The sum of these values is the total photoelectric current. The top half of Table A-I gives the values for a Cs-O-Ag surface. The lower half gives the values for Cs-O-W. For a Cs on W surface the value might be an order of magnitude smaller.
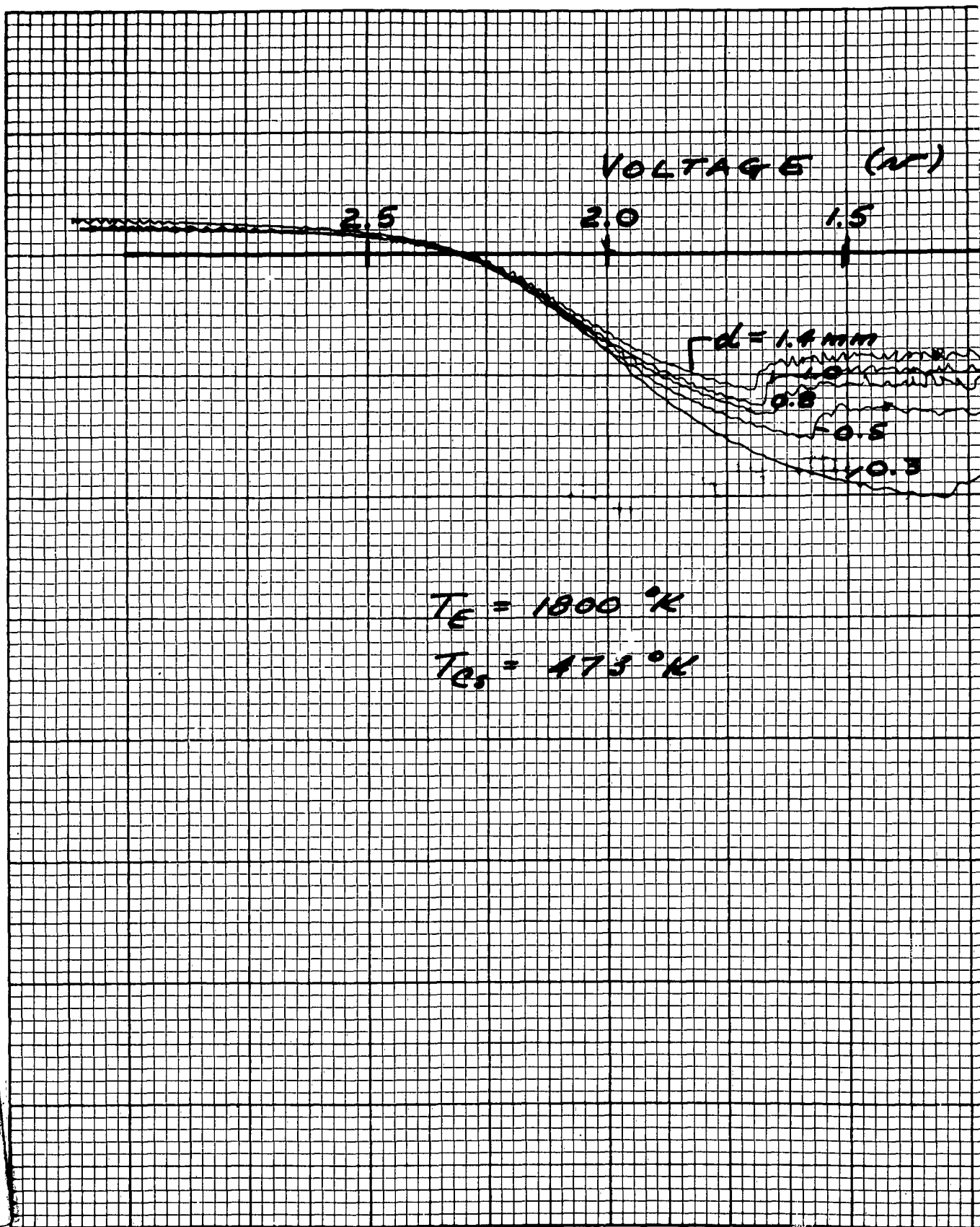
TABLE A-I

Prediction of Photoelectron Yield From Cesium Surface

Wavelength $\lambda(\mu)$	Total Power J_λ (watt)	Emissivity ϵ	Energy Radiated ϵJ_λ(watt)	Photoemitter Yield (amp/watt)*	Photo Currents (amp)
			Cs-O-Ag		
0.1	7.54×10^{-27}				
0.2	5.25×10^{-11}				
0.3	4.19×10^{-6}	0.5	2.1×10^{-6}		
0.4	7.74×10^{-4}	0.48	3.7×10^{-4}	1.5×10^{-3}	5.6×10^{-7}
0.5	1.38×10^{-2}	0.47	6.5×10^{-3}	0.5×10^{-3}	3.3×10^{-6}
0.6	7.94×10^{-2}	0.45	3.6×10^{-2}	1.2×10^{-3}	0.43×10^{-4}
0.7	2.46×10^{-1}	0.43	1.1×10^{-1}	2.0×10^{-3}	2.2×10^{-4}
0.8	5.25×10^{-1}	0.41	2.2×10^{-1}	2.5×10^{-3}	5.5×10^{-4}
0.9	8.85×10^{-1}	0.40	3.5×10^{-1}	1.9×10^{-3}	6.7×10^{-4}
1.0	1.27×10^{0}	0.38	4.8×10^{-1}	0.8×10^{-3}	3.9×10^{-4}
1.1	1.55×10^{0}	0.36	5.6×10^{-1}	0.15×10^{-3}	0.84×10^{-4}
					2.0×10^{-3}
			Cs-O-W		
0.1					
0.2					
0.3			2.1×10^{-6}		
0.4			3.7×10^{-6}	0.5×10^{-3}	1.9×10^{-7}
0.5			6.5×10^{-3}	0.35×10^{-3}	2.3×10^{-6}
0.6			3.6×10^{-2}	0.25×10^{-3}	9.0×10^{-6}
0.7			1.1×10^{-1}	0.2×10^{-3}	2.2×10^{-5}
0.8			2.2×10^{-1}	0.15×10^{-3}	3.3×10^{-5}
0.9			3.5×10^{-1}	0.12×10^{-3}	4.2×10^{-5}
1.0			4.8×10^{-1}	0.1×10^{-3}	4.8×10^{-5}
1.1			5.6×10^{-1}		0.16×10^{-3}

*RCA Review 21, 184, (1960).

APPENDIX B

Typical Multicapillary Data
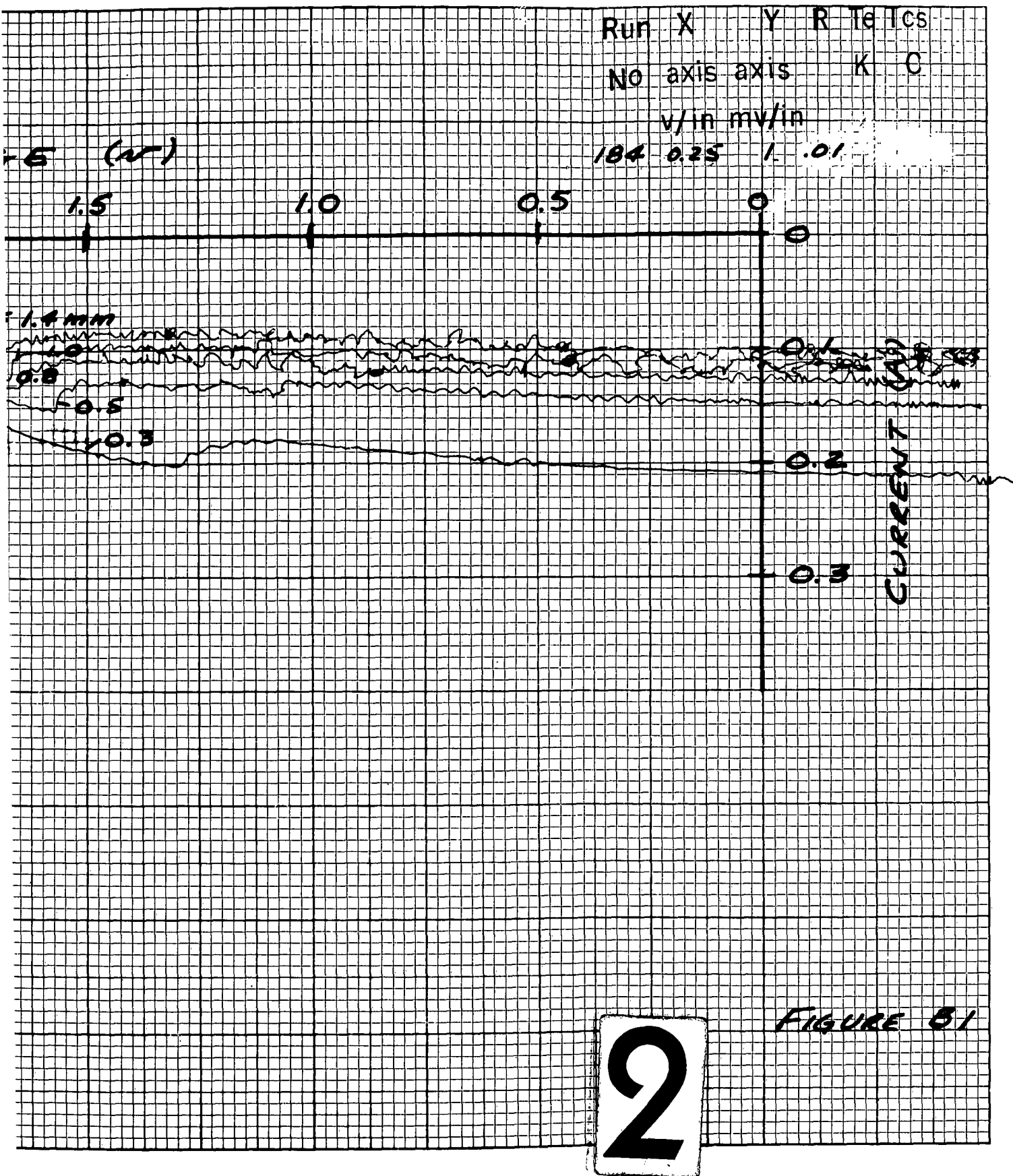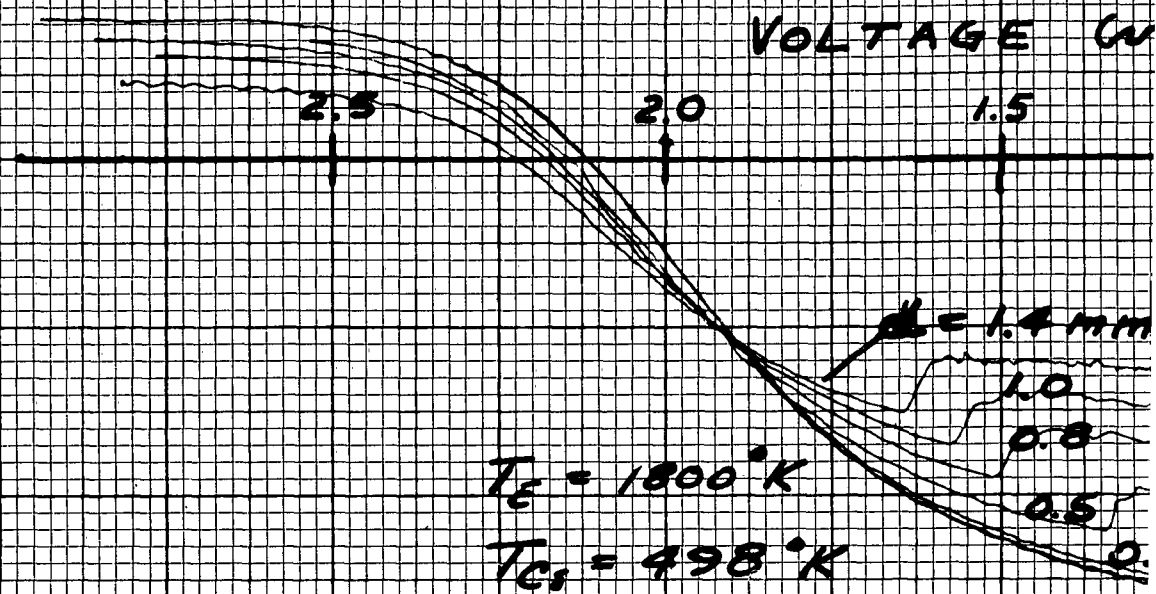
VOLTAGE (v)

2.5   2.0   1.5

d = 1.4 mm
1.0
0.8
0.5
0.3

$T_E = 1800 \,°K$

$T_{Cs} = 475 \,°K$

1

FIGURE 51

VOLTAGE (V)

2.5   2.0   1.5

$d = 1.4\,mm$
1.0
0.8
0.5
0.

$T_E = 1800°K$

$T_{Cs} = 498°K$

Run No	X axis /in	Y axis mv/in	R	Te K	Tcc C
180	0.25	1.0Λ			

1

FIGURE 82

VOLTAGE (V)

2.5   2.0   1.5

α = 1.4

1.0
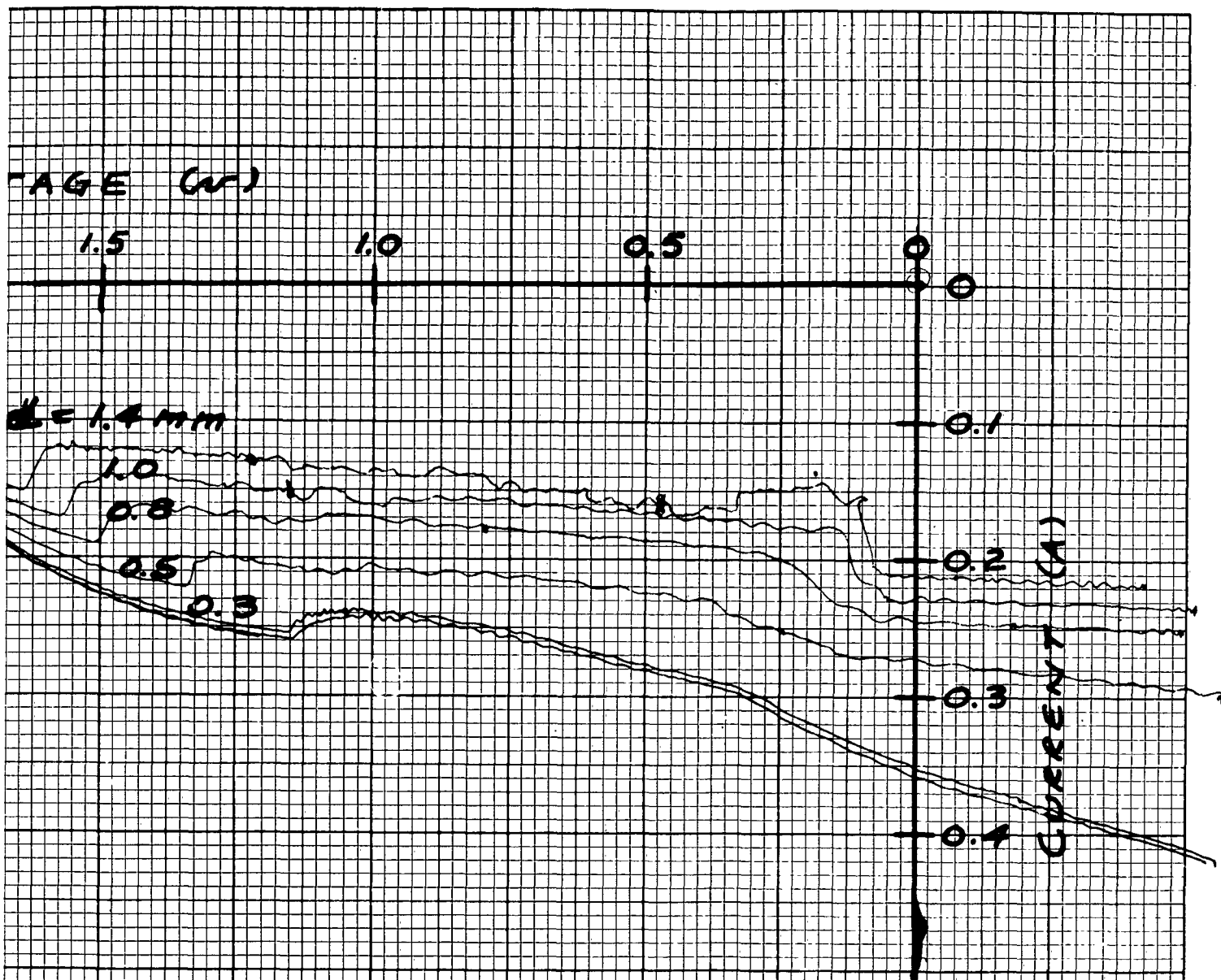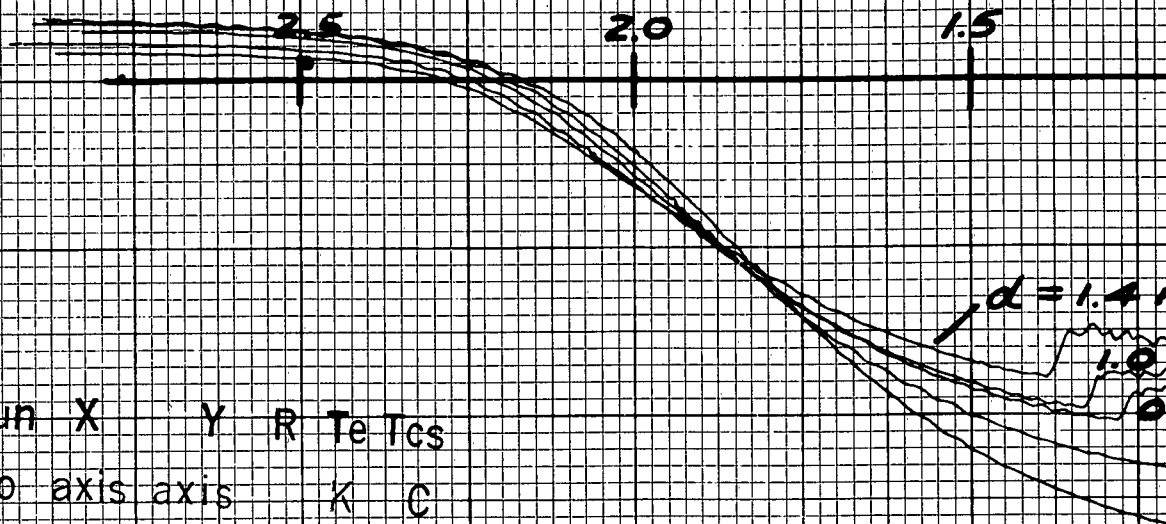
Run   X   Y   R Te Tcs
No   axis   axis   K   C

v/in   mv/in $T_E = 1800\,°K$

176 0.25   1 .01 $T_{CS} = 523\,°K$
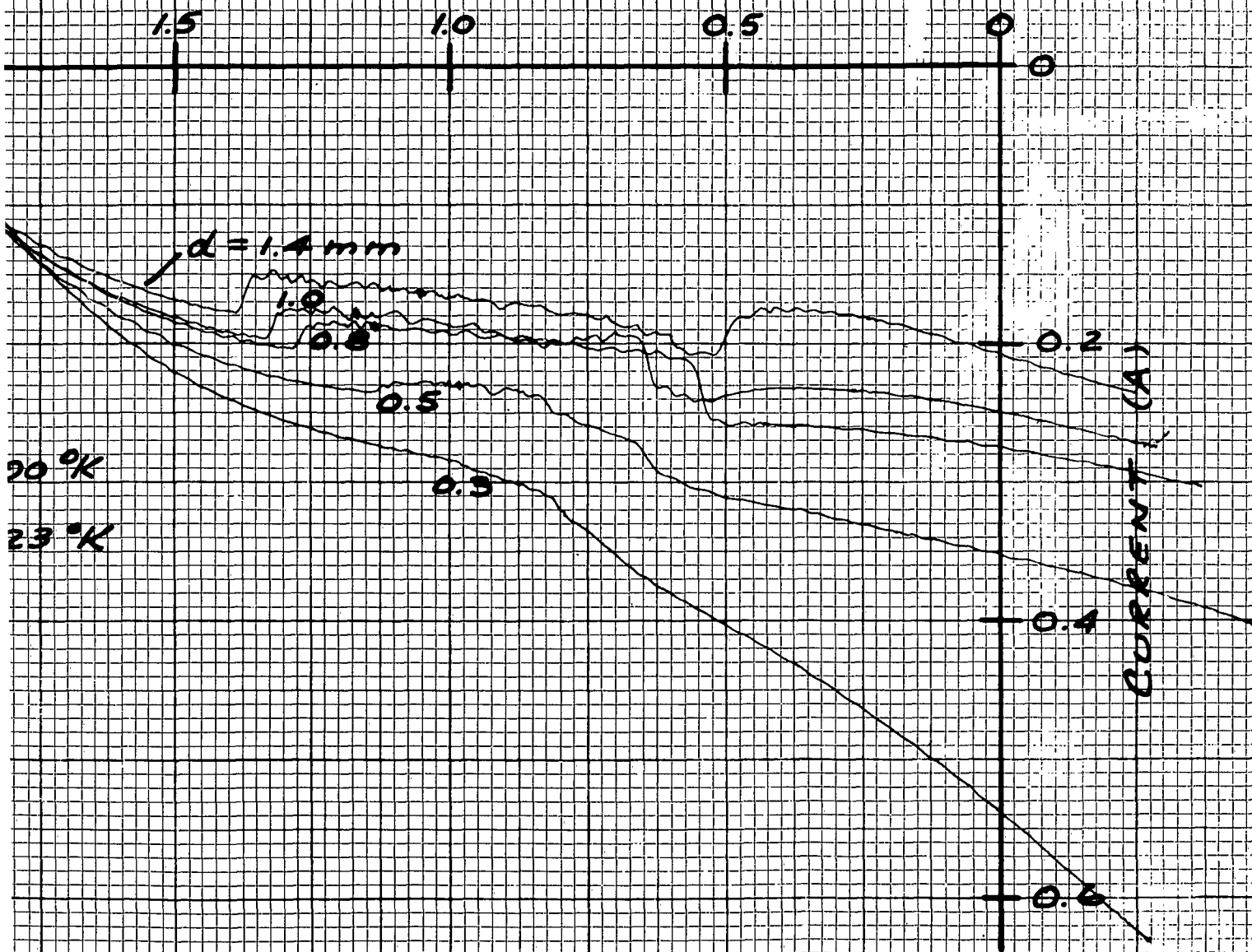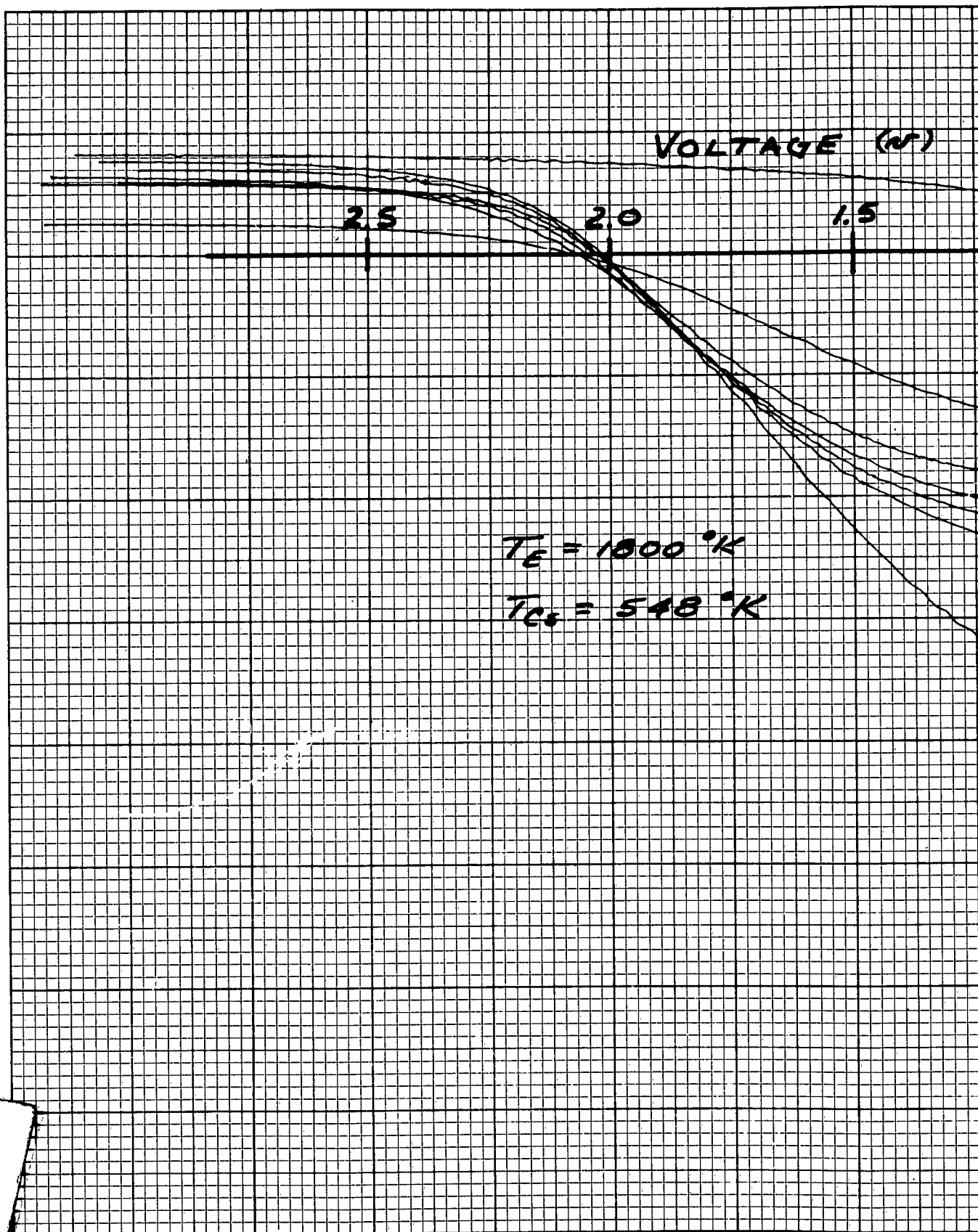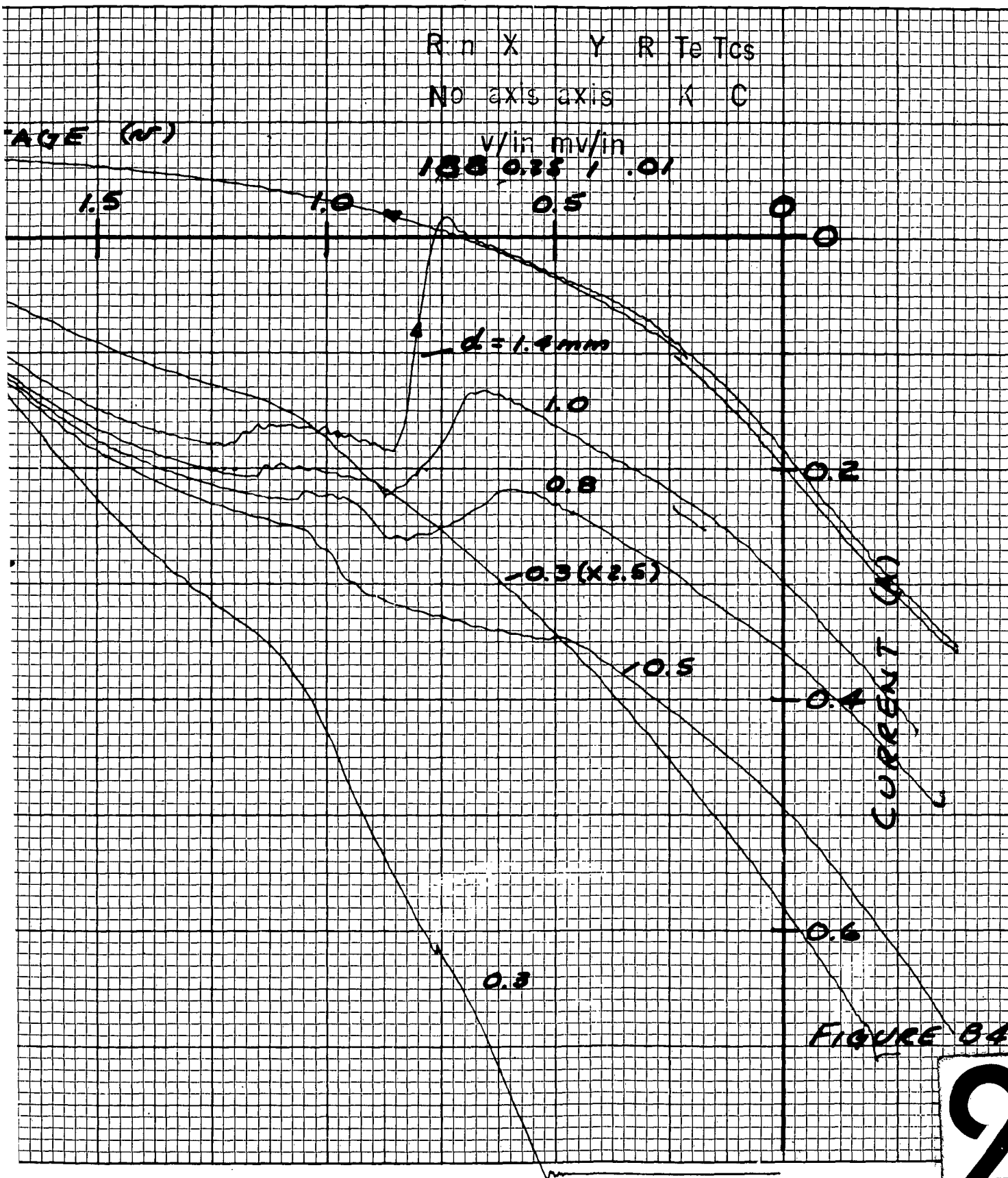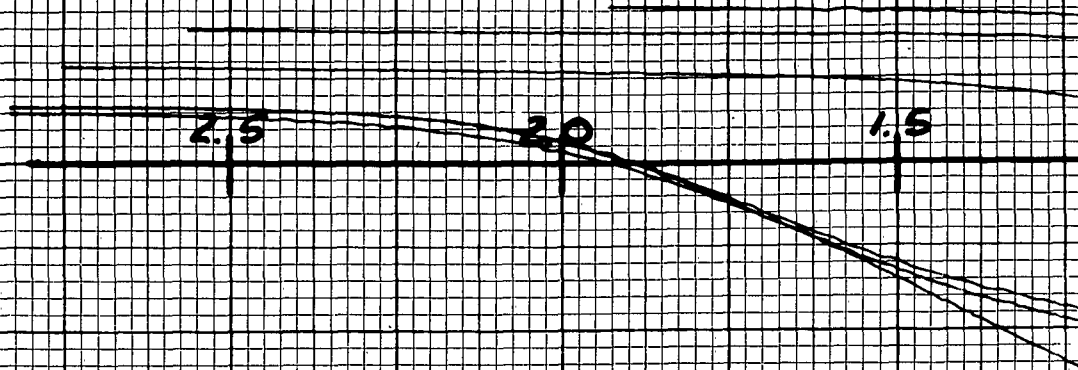
FIGURE 83

VOLTAGE (N)

2.5   2.0   1.5

$T_E = 1800\ °K$

$T_{C_s} = 548\ °K$

1

Figure 84

VOLTAGE (V)

Rin X Y R Te Tcs
No axis axis K C
v/in mv/in
136 0.25 1 .01

1.5   1.0   0.5   0

d = 1.4mm

1.0

0.8

0.3 (x2.5)

0.5

0.4

0.6

0.3

CURRENT (A)

FIGURE 84

2

VOLTAGE (w)

2.5   2.0   1.5

$T_E = 1800\ °K$

$T_{cs} = 573\ °K$

1

FIGURE 85

VOLTAGE (W)

2.5 2.0 1.5

d = 1.4
1.0
0.8
0.5
0.3

$T_E = 1900 \ ^\circ K$

$T_{Cs} = 473 \ ^\circ K$

1
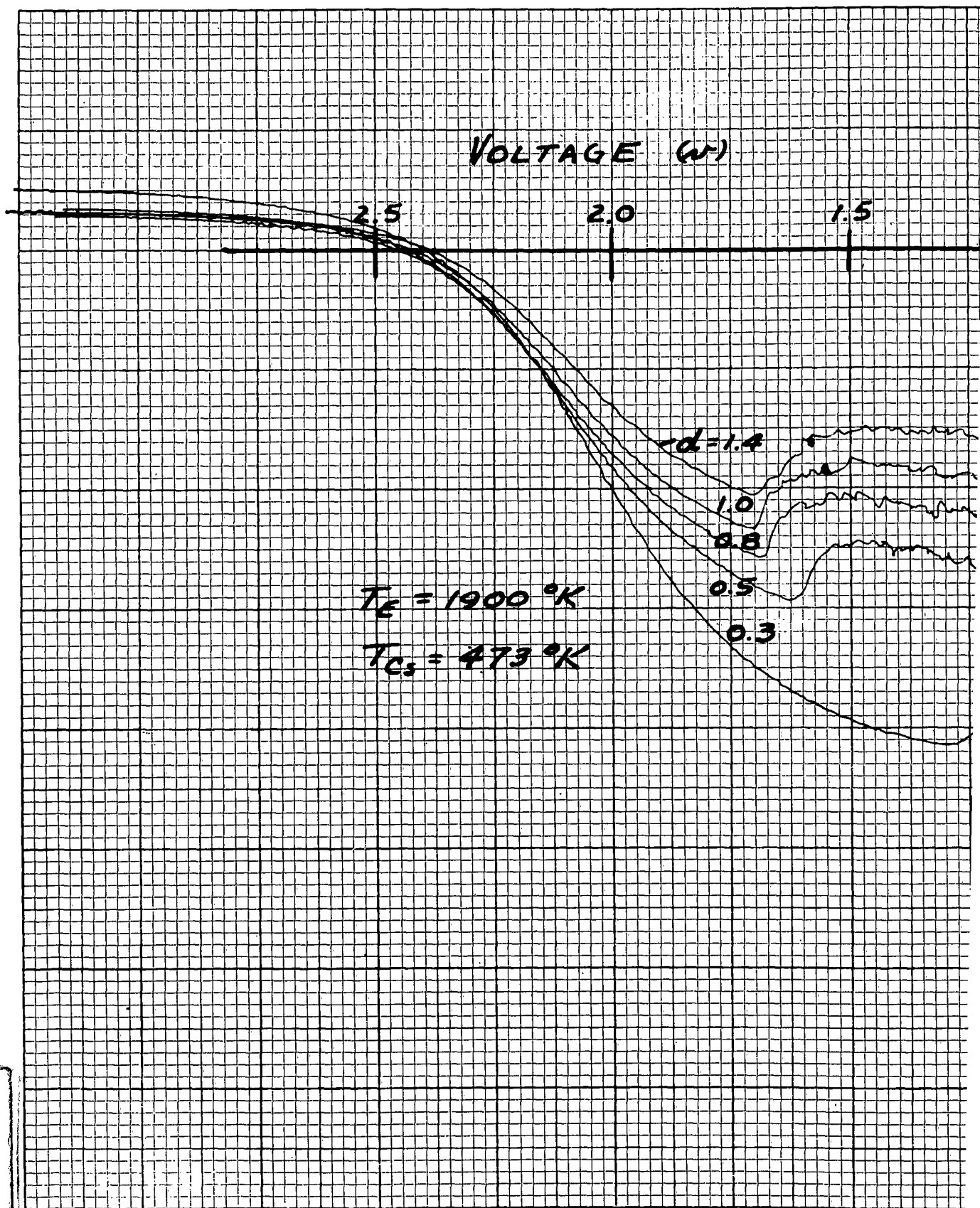
Run X Y R TeTcs
No. axis axis K C
V/in mv/in
1.05 0.25 1 .01

1.5   1.0   0.5   0

.2

.4

.6

CURRENT (A)

FIGURE B6

2

VOLTAGE (W)

2.5   2.0   1.5

$T_E = 1900\,°K$

$T_{cs} = 498\,°K$

d = 1.9mm

1.0

0.8

Run   X   Y   R Te Tcs
No axis axis   K   C
    v/in mv/in

181 0.25   A   91

LTAGE (N)

1.5   1.0   0.5   0

d = 1.4 mm

0.5 (×2.5)

1.0

0.5 (×2.5)

0.8

CURRENT (A)

.2

.4

.6

FIGURE B7

2

VOLTAGE (w)

2.5   2.0   1.5

Run X   Y   R Te Tcs
No   axis axis   K   C
     v/in mv/in
177 0.25 2.5 .01

$T_E = 1900\,°K$

$T_{cs} = 523\,°K$

177

FIGURE 8B

VOLTAGE (w)

2.5   2.0   1.5

$T_E = 1900\,°K$

$T_{Cs} = 548\,°K$

1

Run X Y R Te Tcs
No axis axis K C
v/in mv/in
169 0.25 2.5 .01

1.5   1.0   0.5   0   0

d=1.4mm

1.0

0.8

.5

0.5

1.0

0.3

1.5

FIGURE 89

2

VOLTAGE (N)

2.5   2.0   1.5

$T_E = 1900 °K$

$T_{CS} = 573 °K$

1

FIGURE B10

VOLTAGE (v)

2.5　　　2.0　　　1.5

d = 1.4mm
1.0
0.8
0.5

$T_E = 2000°K$
$T_{CS} = 473°K$

0.3

1

FIGURE B11

VOLTAGE

2.5   2.0   1.5

$T_E = 2000°K$

$T_{Cs} = 498°K$

Run X   Y   R Te Tcs
No   axis axis   K   C
     v/in mv/in
182 0.25   5   .01

1
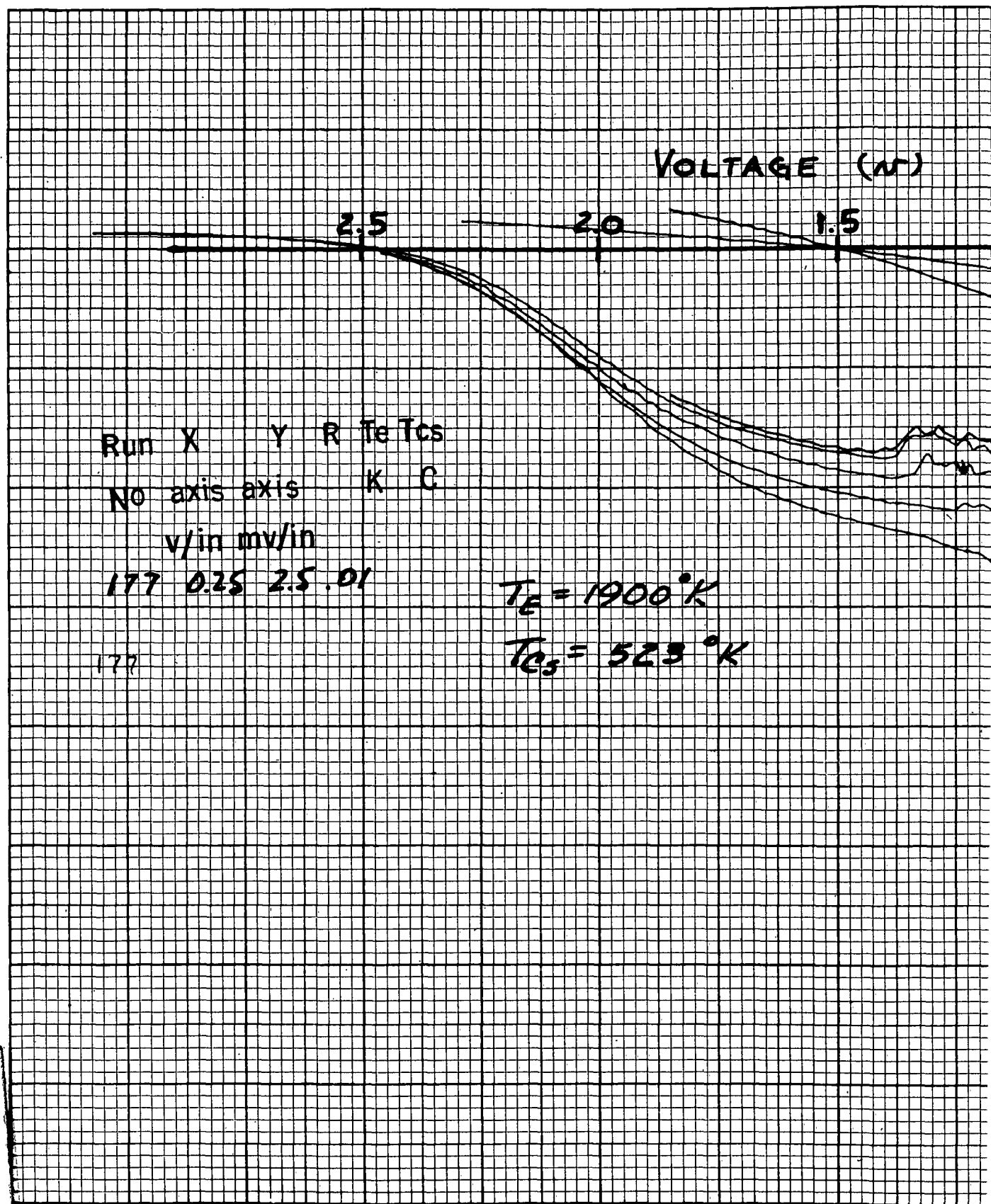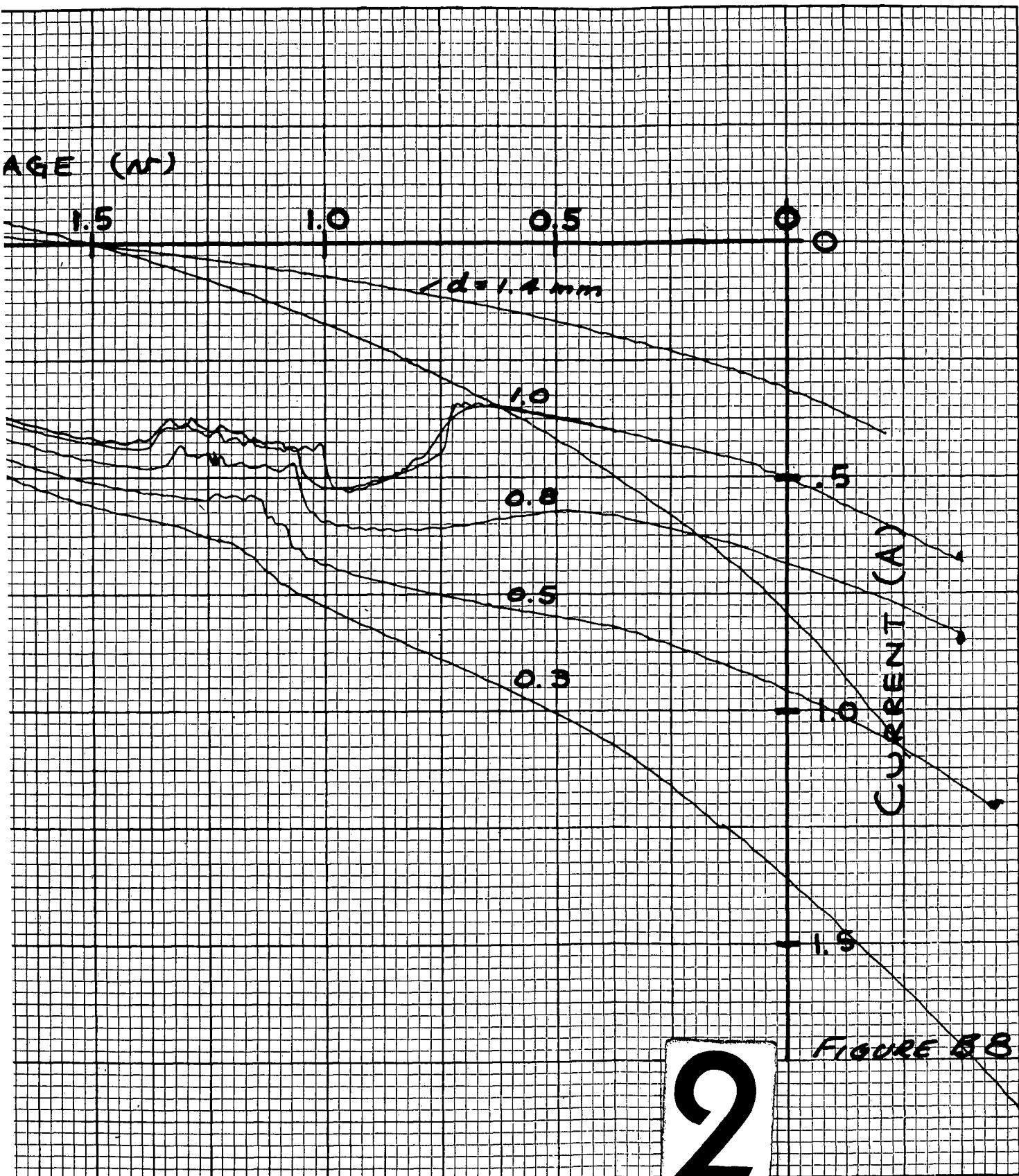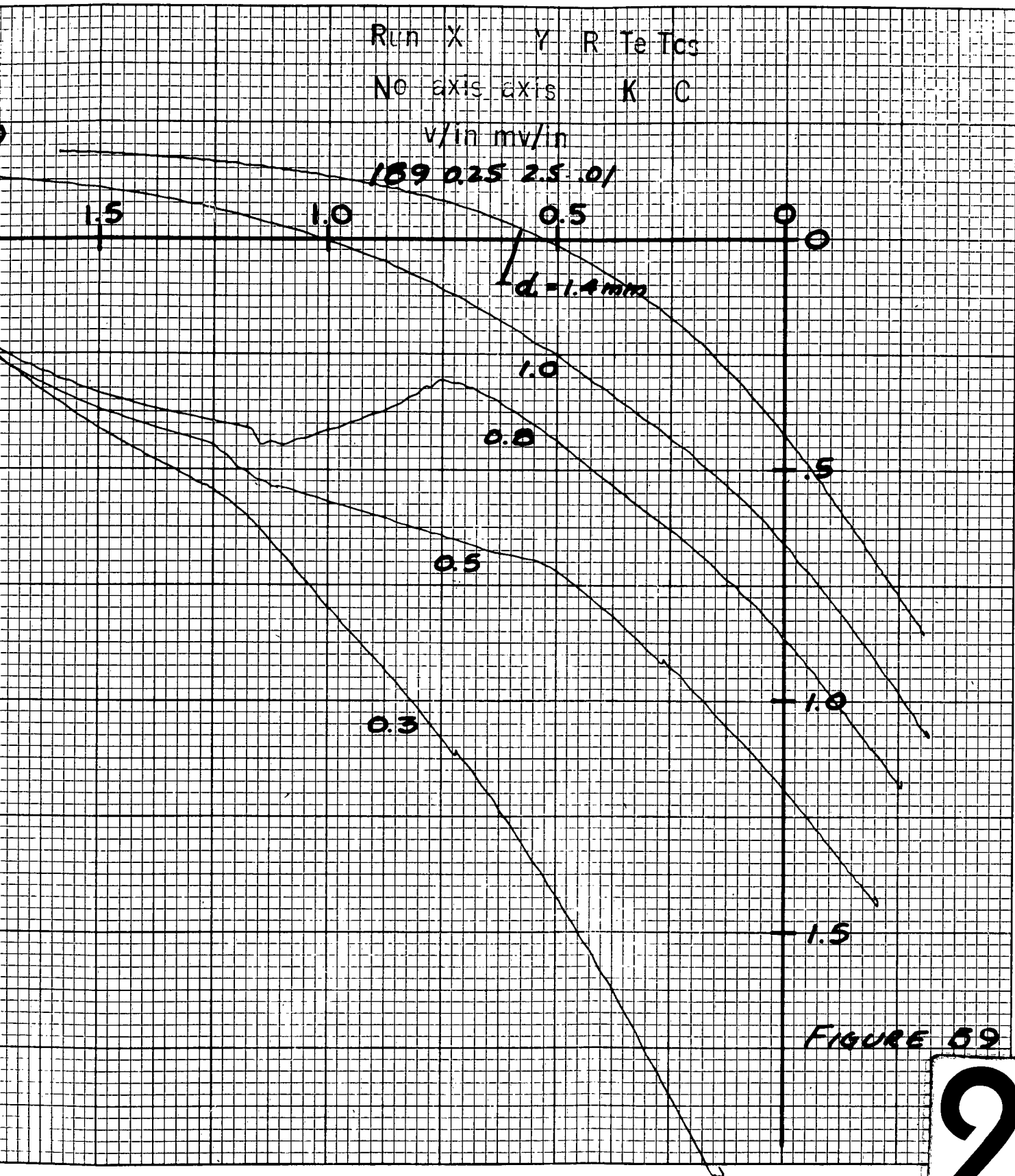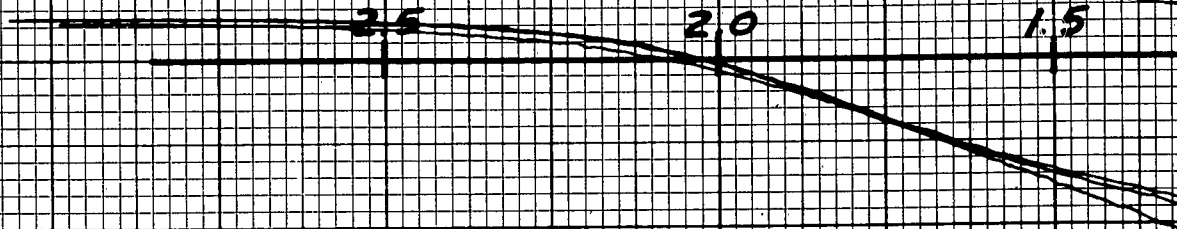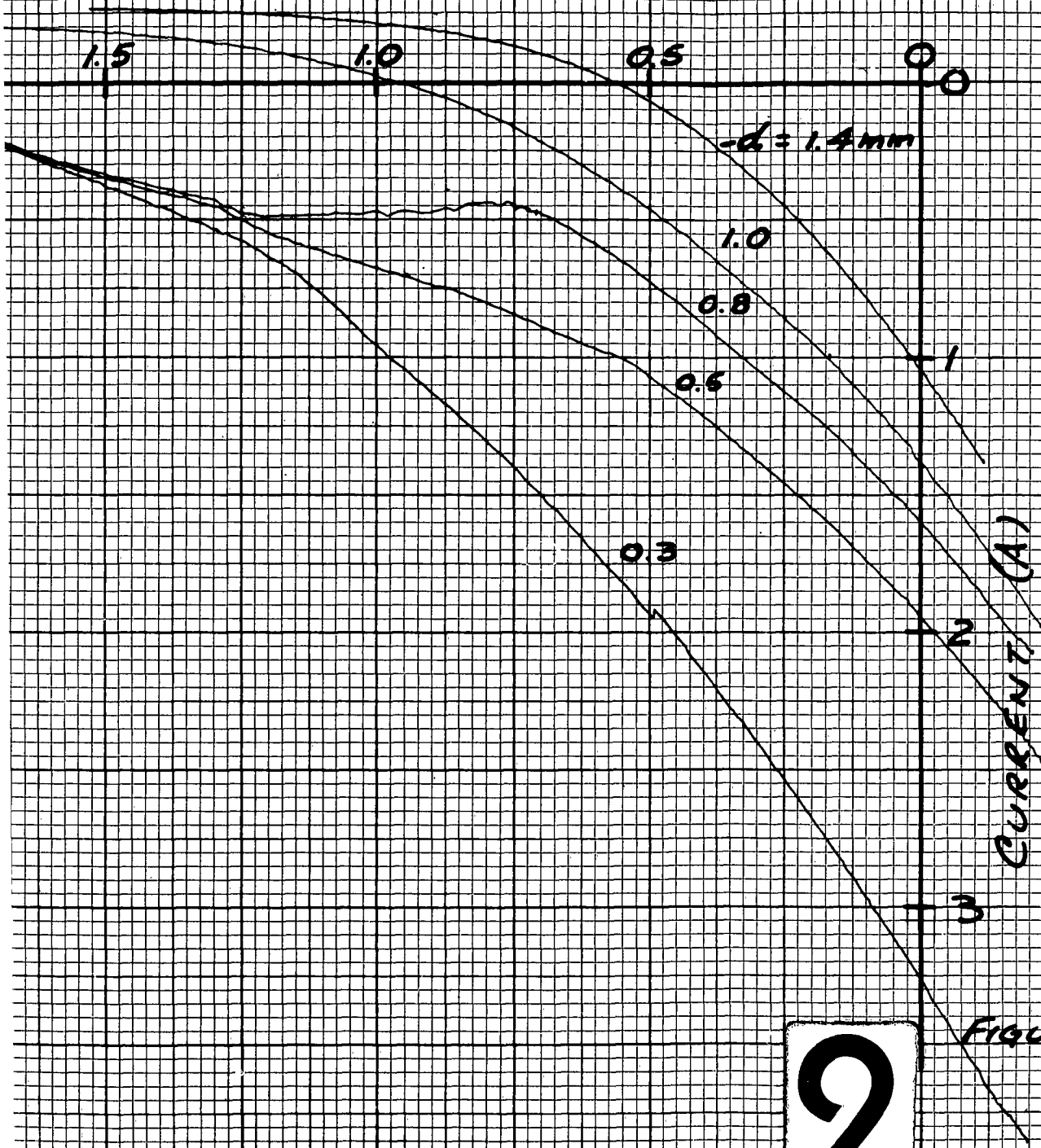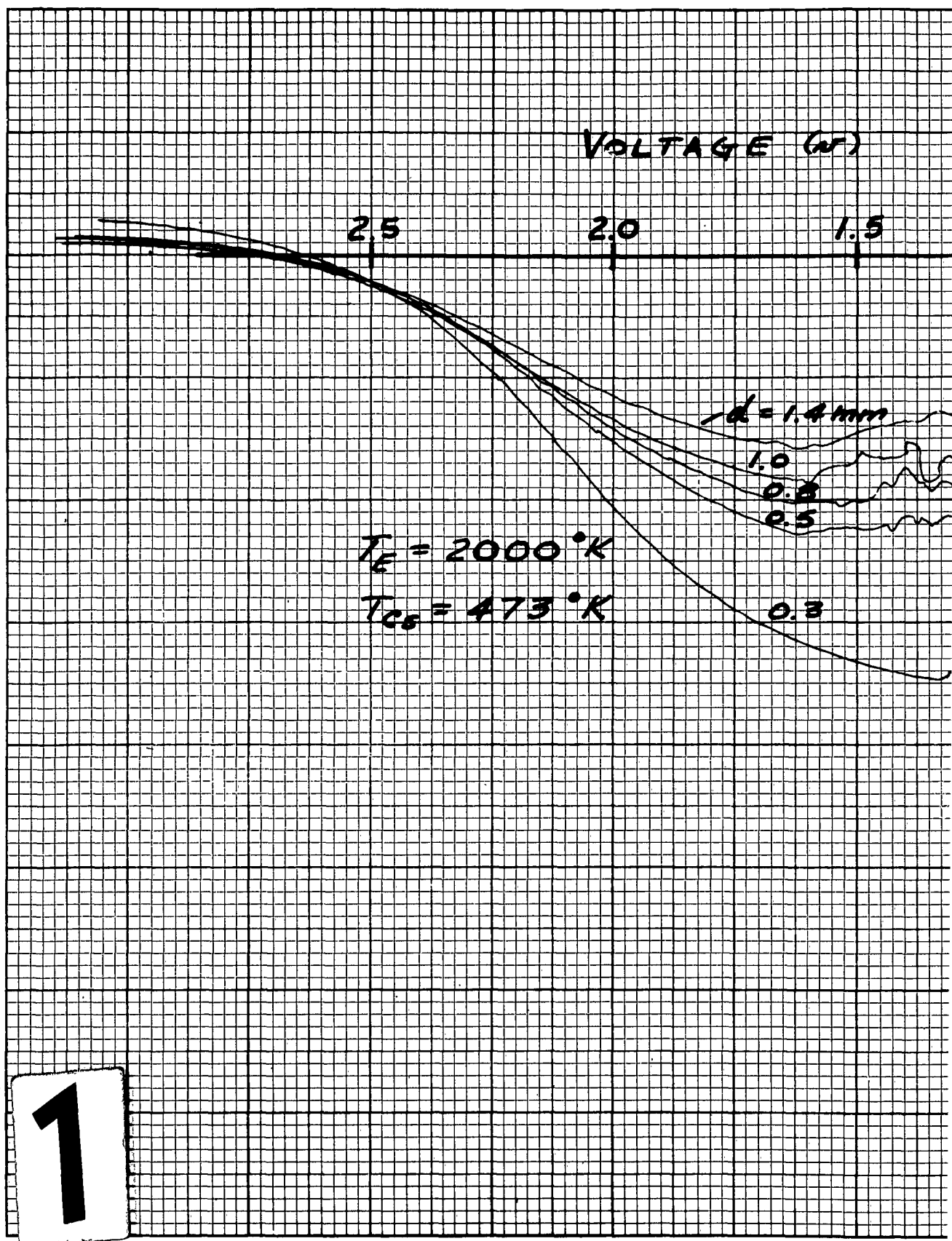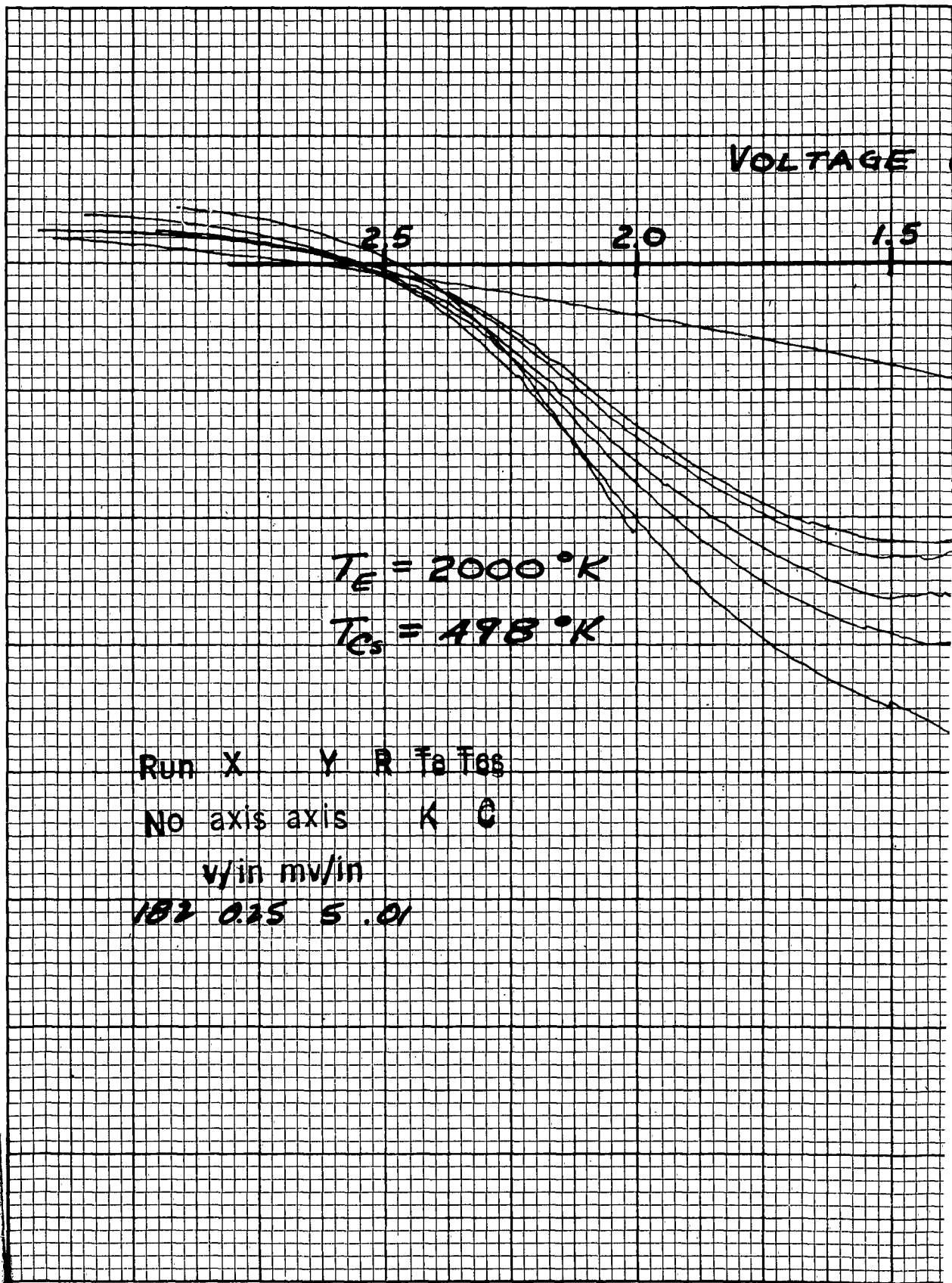
FIGURE B12

VOLTAGE

2.5   2.0   1.5

$T_E = 2000\,°K$

$T_{cs} = 523\,°K$

Run X   Y   R Te Tcs
No axis axis   k   C
    v/in mv/in
178 0.25 10.01

1

VOLTAGE (V)

1.5   1.0   0.5   0

d = 1.4 mm
1.0
0.8
0.5
0.3

CURRENT (A)

2

4

6

2
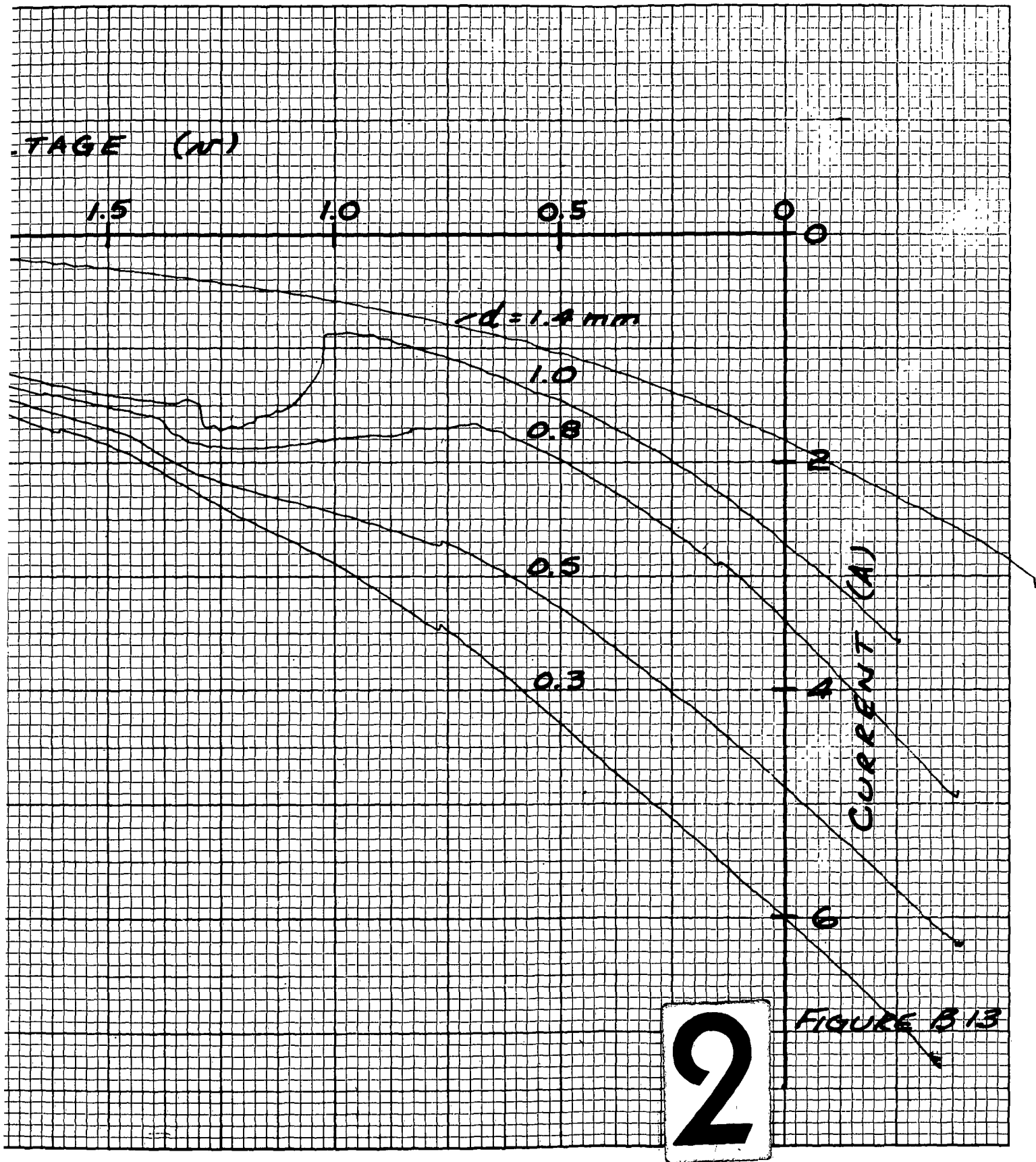
FIGURE B.13

VOLTAGE (V)

2.5 2.0 1.5

$T_E = 2000 \,°K$

$T_{es} = 548 \,°K$

1

Run X Y R Te Tcs
No axis axis K C
v/in mv/in
190 0.25 25.01

1.5   1.0   0.5   0

(w)

d = 1.4 mm
1.0
0.8
0.5
0.3

0
2.5
5.0
7.5

CURRENT (A)

FIGURE B.14

2

VOLTAGE (W)

2.5   2.0   1.5

$T_E = 2000\ °K$

$T_{CS} = 573\ °K$

1
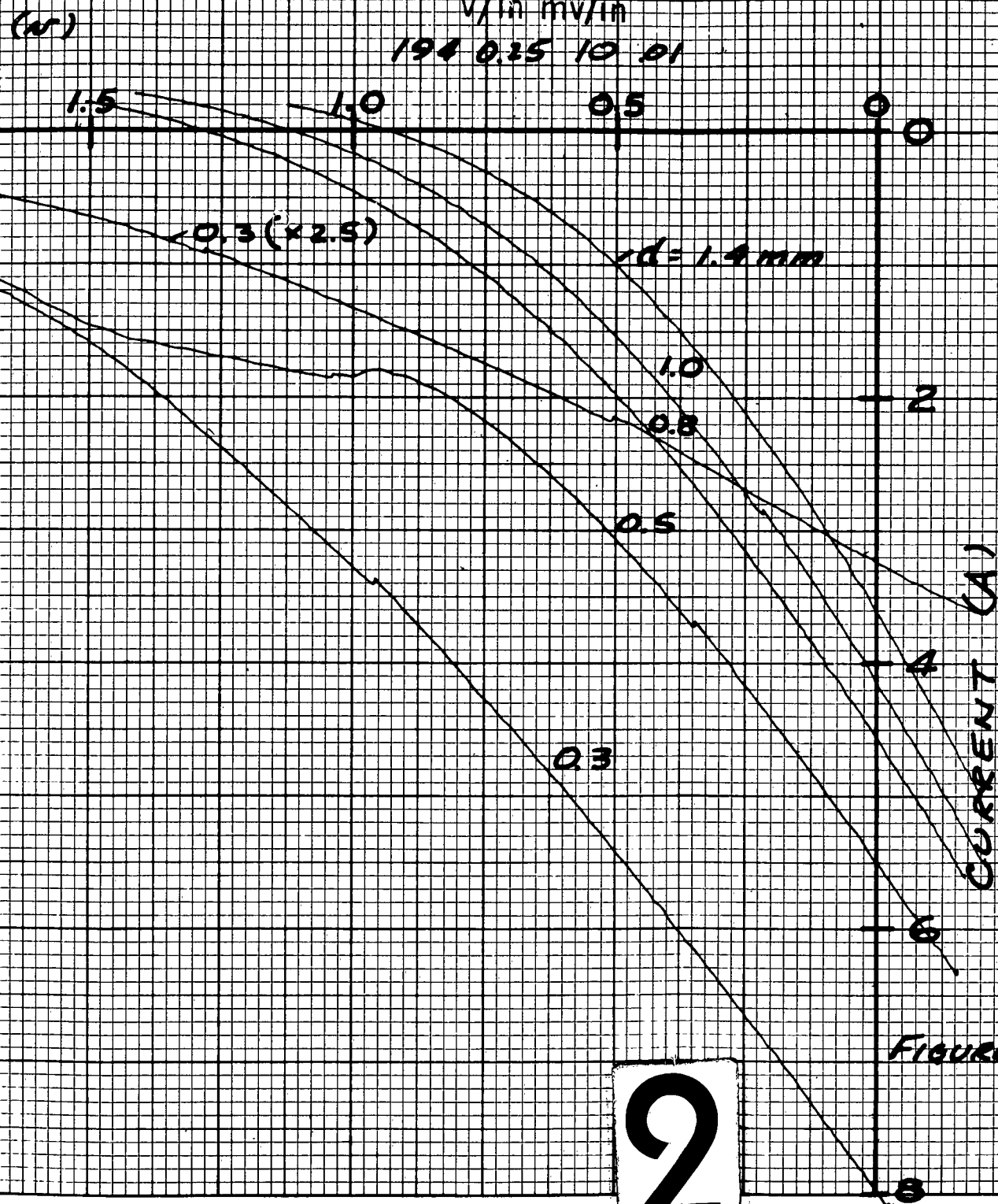
Figure B.15

VOLTAGE

2.5   2.0   1.5

Run X   Y   R Te Tcs
No   axis axis   K   C
     V/in mv/in
P15 025   2.5 .001

$T_E = 2000°K$

$T_{Cs} = 598°K$

1
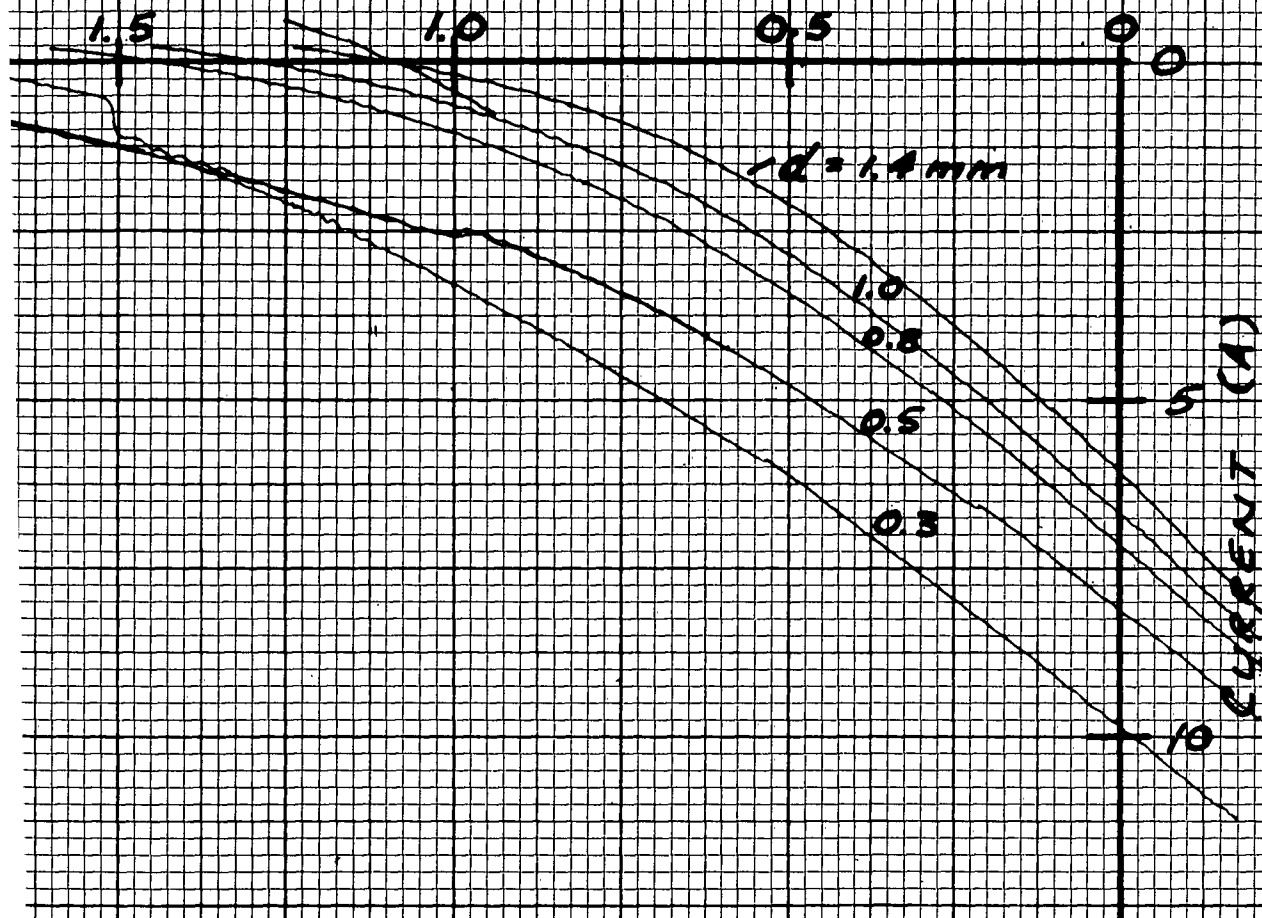
FIGURE B16

VOLTAGE · VOLTS

2.0   2.5   2.0   1.5

(PASSIVE MODE)
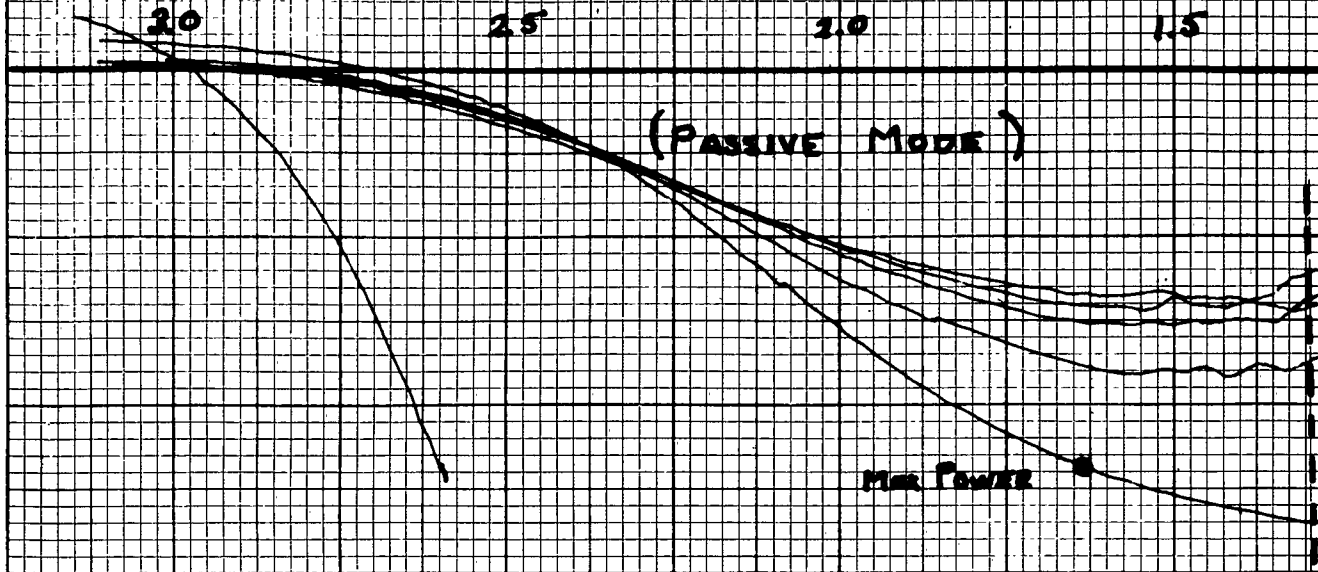
Max Power *

$T_E = 2100 \, °K$

$T_{CS} = 200 °C$

Max Power = 12

1
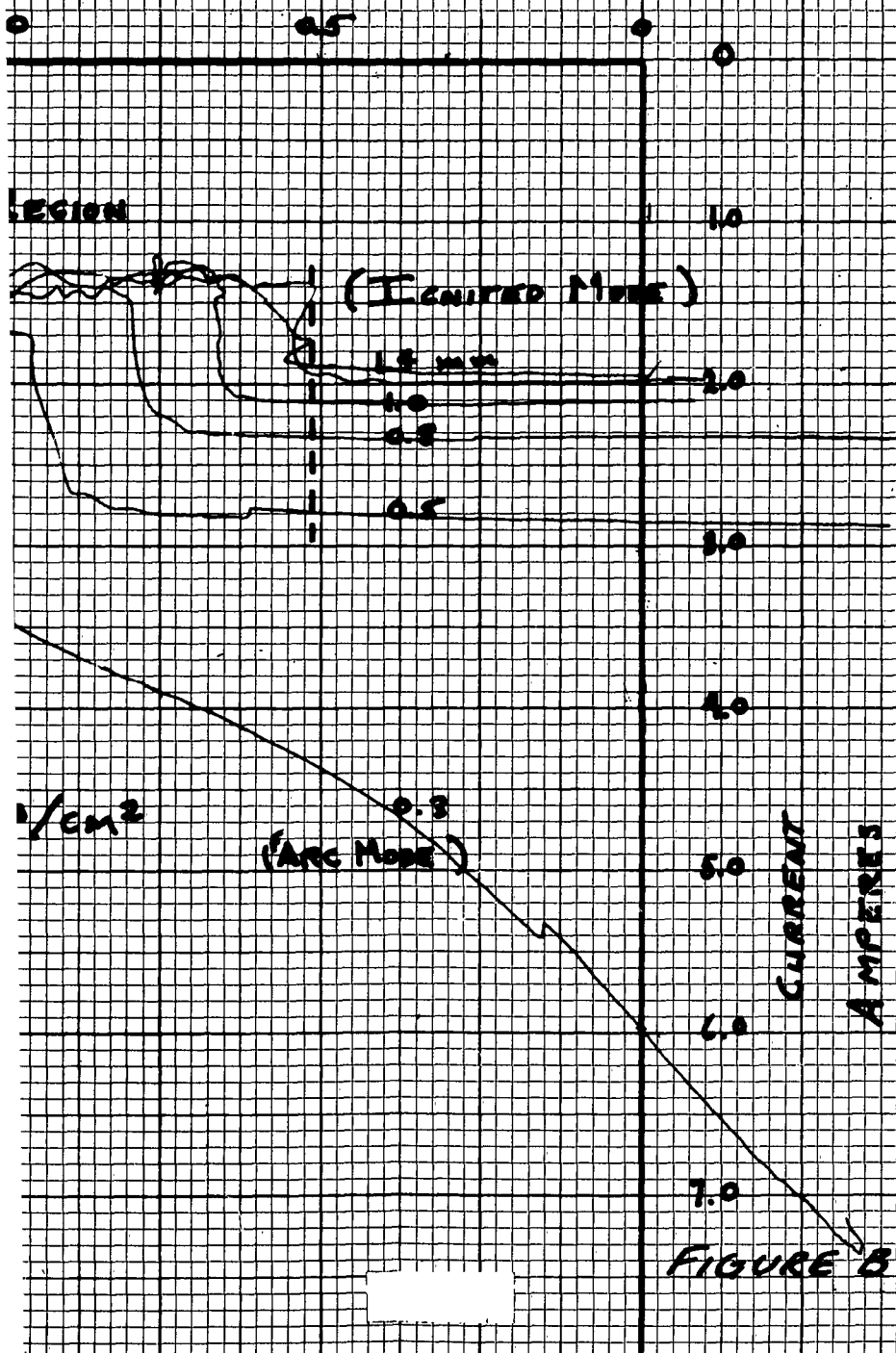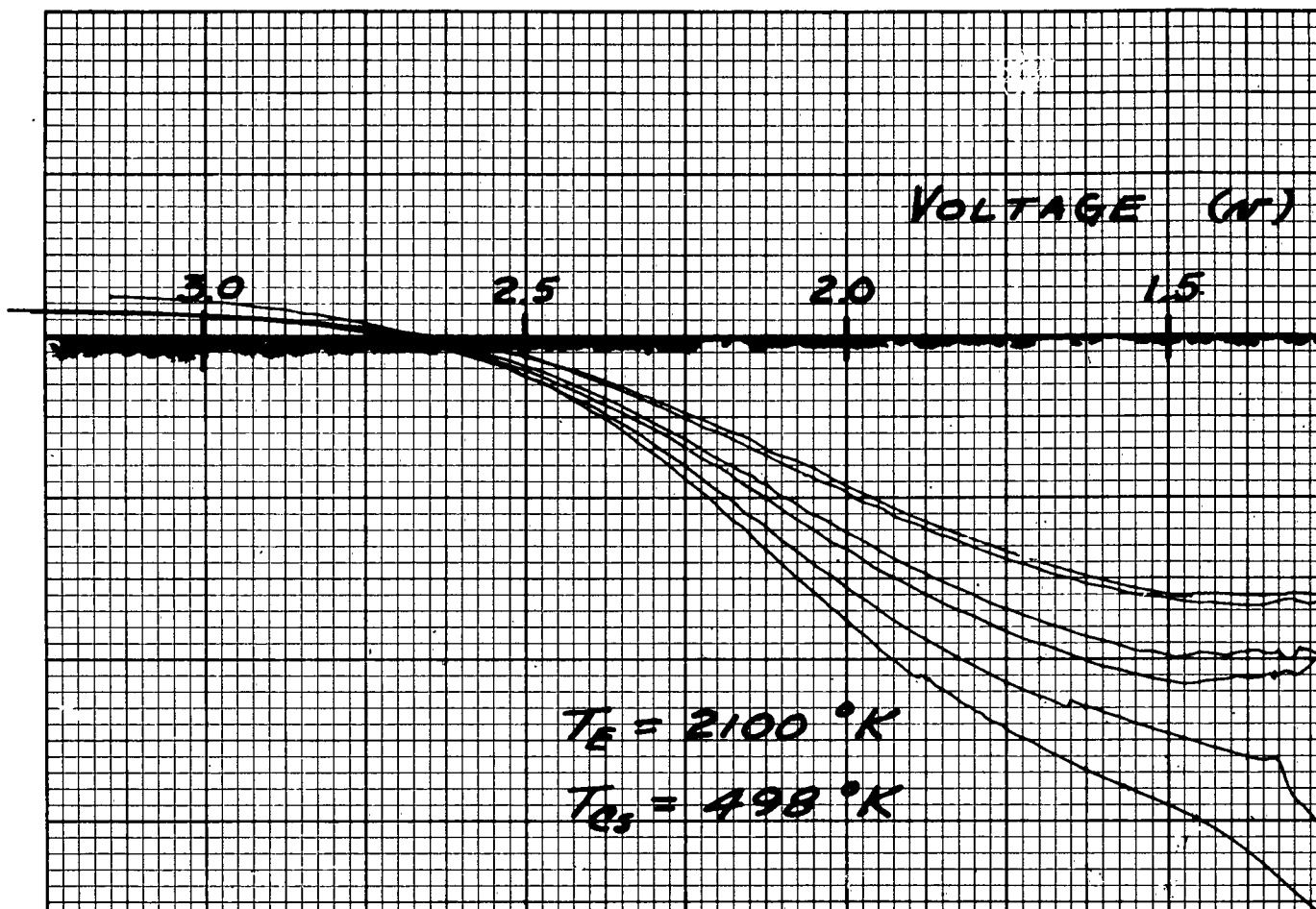
Figure B·17

VOLTAGE (N·)

3.0   2.5   2.0   1.5

$T_E = 2100\ °K$

$T_{cs} = 498\ °K$

Run X   Y   R Te Tcs
No axis axis   C
    v/in mv/in
183 035   10 .01

FIGURE B18

VOLTAGE - VOLTS

2.5   2.0   1.5

Max
Power
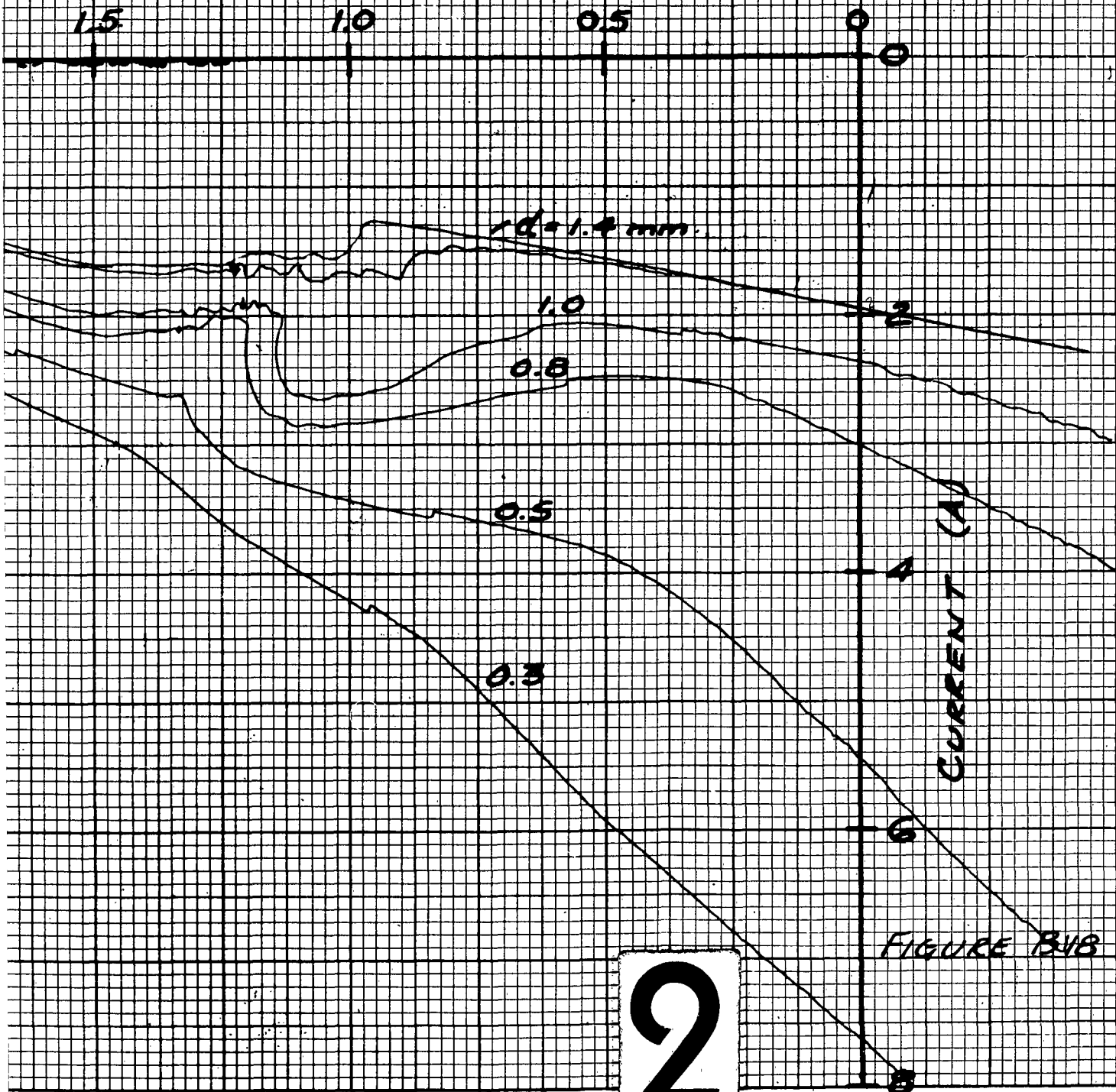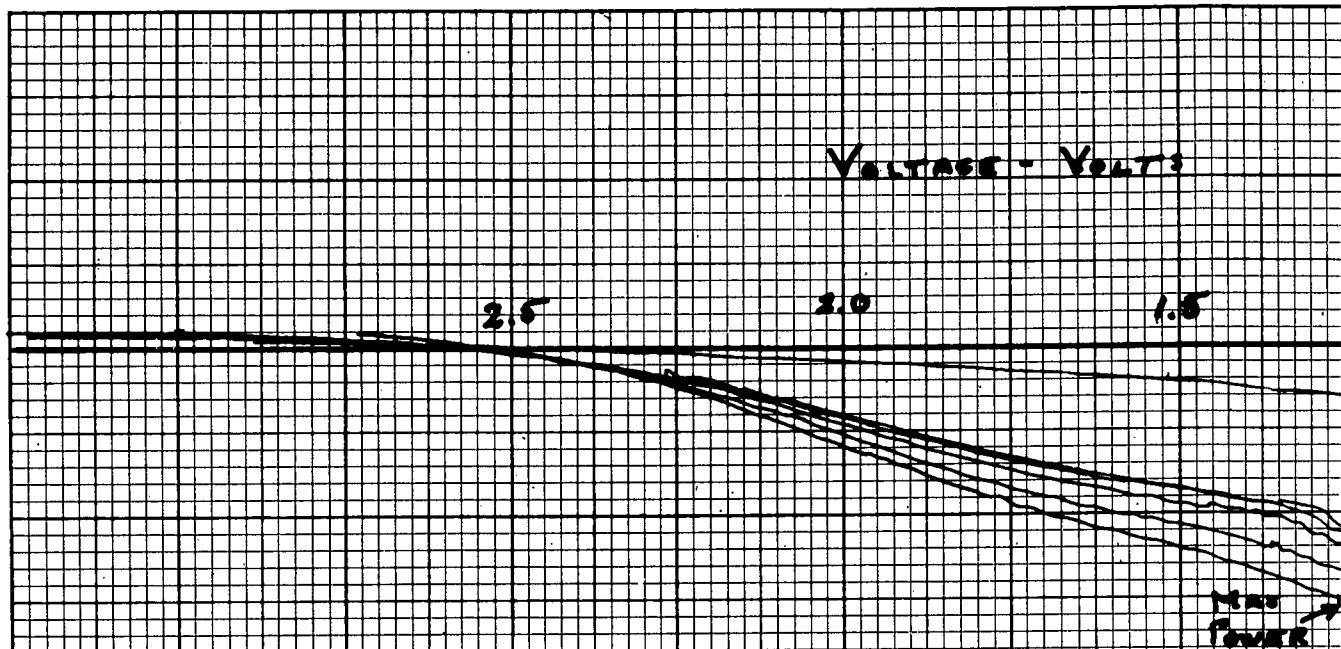
Run	X	Y	R	Te	Tcs		Tz
NO	axis	axis		°K	°C		°C
	V/in	mv/in					
175	0.25	25	0.01	2100	250		250

Te = 2
Tcs =

Max

3/20

1

VOLTS

1.5   1.0   0.5   0

0

1.1 mm

1.0

2.5

0.8

5.0

0.5

0.3

7.5

MAX POWER →

10.0

CURRENT - AMPERES

12.5
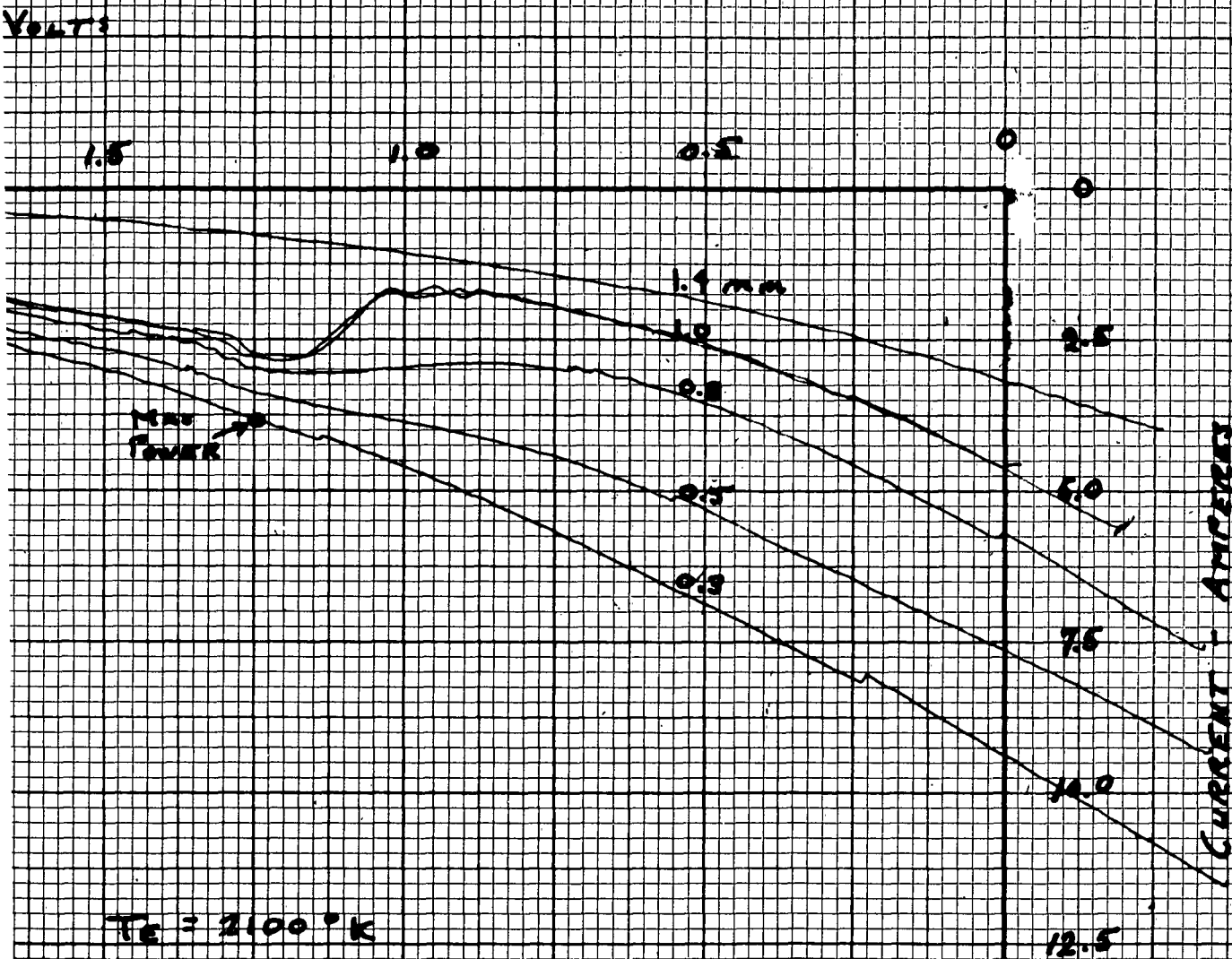
$T_E = 2100°K$

$T_{CS} = 250°C$

MAX POWER   14.8 WATTS/CM^2

3/20/65

FIGURE B19

2

VOLTAGE - VOLTS

2.5   2.0   1.5

Max Pow

Tc =

Tcs =

Max P

3/20

1

Figure B-20: Run No. 191 — X axis 0.25 V/in, Y axis 25.0 mv/in, R 0.01, Te 2100 K, Tcs 275 C

$T_E = 2100\ ^{\circ}K$

$T_{cs} = 275\ ^{\circ}C$

Max Power   14.7 Watts/cm²

3/20/63

FIGURE B-20

VOLTAGE - VOLTS

2.5   3.0   1.5
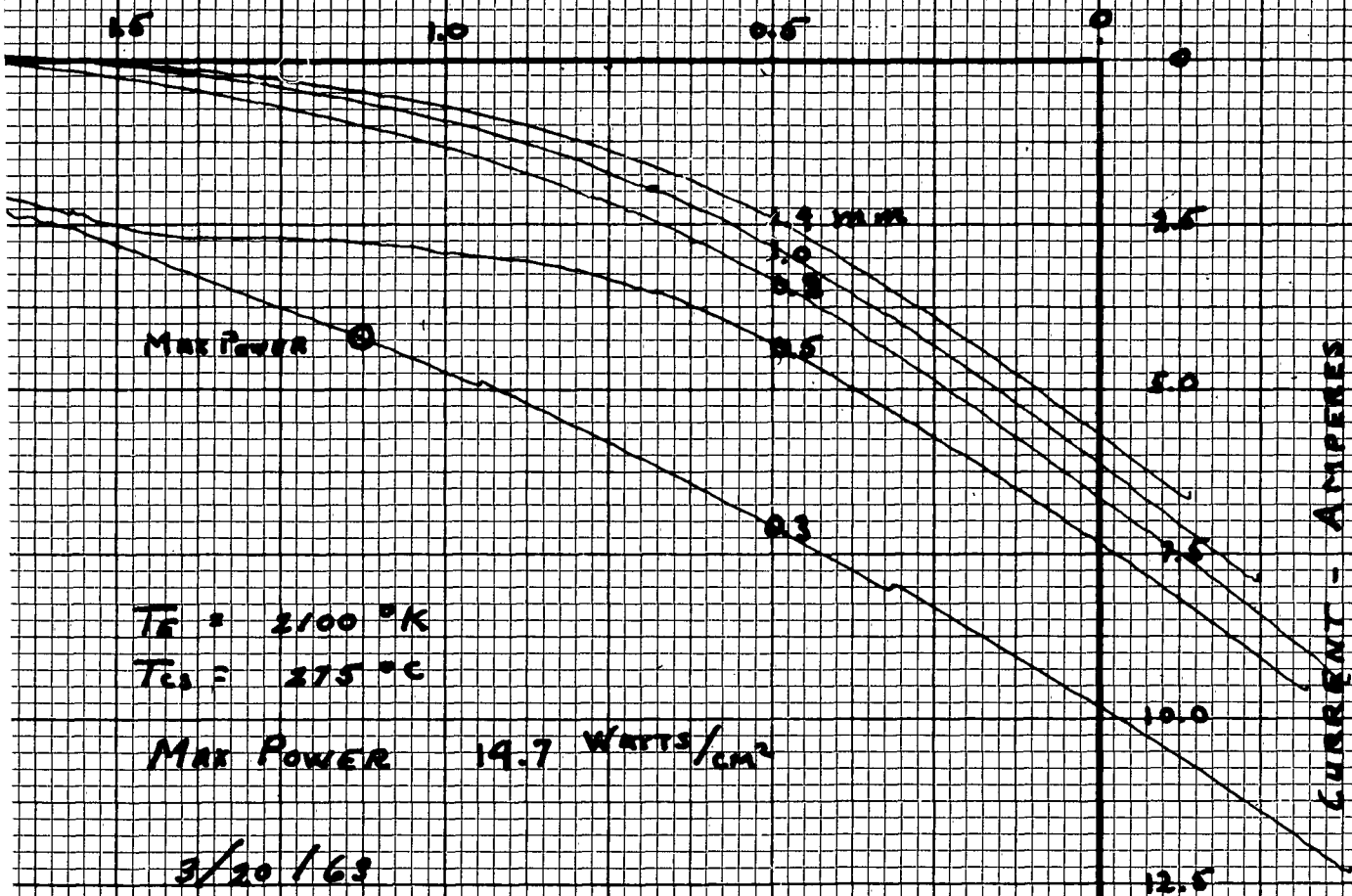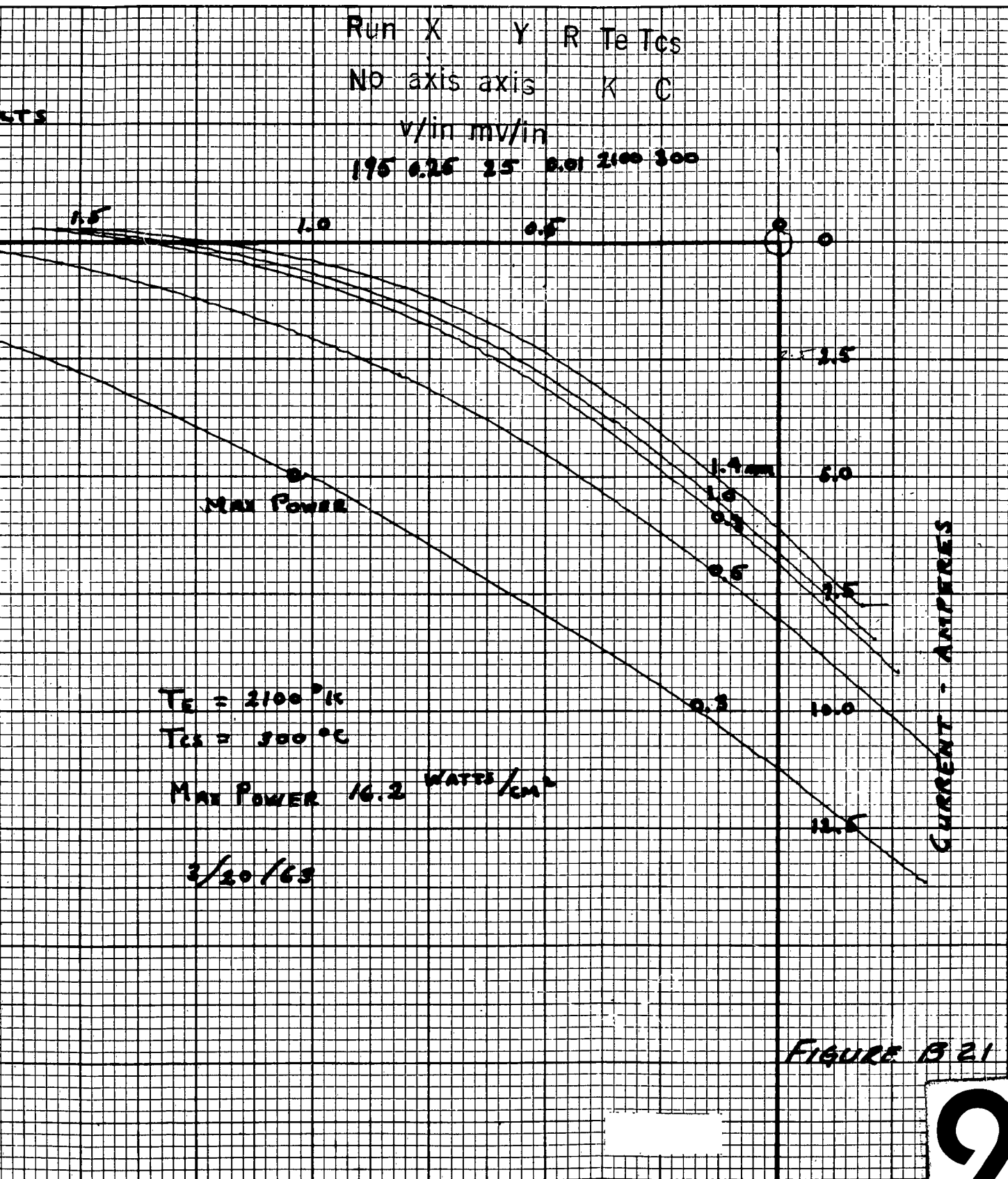
FIGURE B 21

$T_E = 1900 \, °K$

$T_{C_3} = 473 \, °K$

$T_C = 638 \, °K$

$d = 2.0 \, mm$

$1800 \, °K$

$1700 \, °K$

$1600 \, °K$

$1500 \, °K$

14   12   10   8

VOLTAGE   (V)

1

Run X   Y   R Te Tcs
No axis axis   K   C_{10}
        v/in mv/in
        254

7.5

CURRENT (mA)

5

2.5

FIGURE B22

8   6   4   2   0

(W)

2

VOLTAGE ~

2.5　　　　　　2.0　　　　　1.5

DATE　　5/7/63

T_E　　　1800 °K

T_{CS}　　473 °K

d　　　1.0 mm

T_C　　　425 °C

$R(\Omega)$
10.036
9.036
8.036
7.036
6.036
5.036
4.036
3.036
2.036
1.036
0.936
0.836
0.736
0.636
0.536
0.436
0.336
0.236
0.136

1

LTAGE ~ volts

1.5   1.0   0.5   0   0
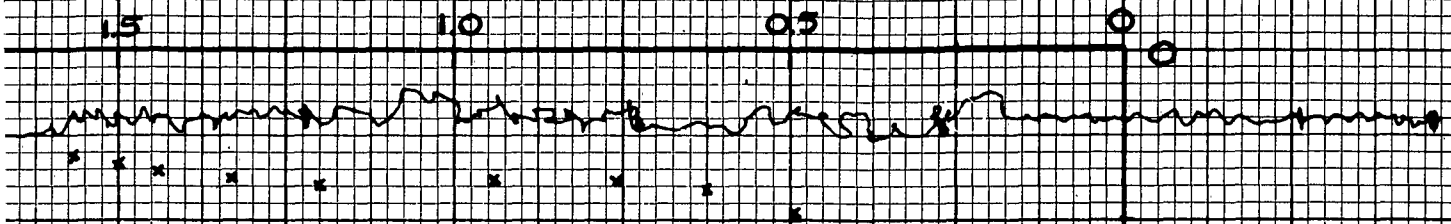
R(Ω)	V(v)	I(ma)
10.036	1.57	156
9.036	1.50	166
8.036	1.44	179
7.036	1.33	189
6.036	1.20	199
5.036	0.94	187
4.036	0.76	189
3.036	0.62	204
2.036	0.49	241
1.036	0.36	348
0.936	0.35	374
0.836	0.34	407
0.736	0.32	434
0.636	0.30	473
0.536	0.29	540
0.436	0.28	640
0.336	0.27	801
0.236	0.26	1100
0.136	0.25	1840

500

CURRENT

(ma)

1000

1500

FIGURE B33
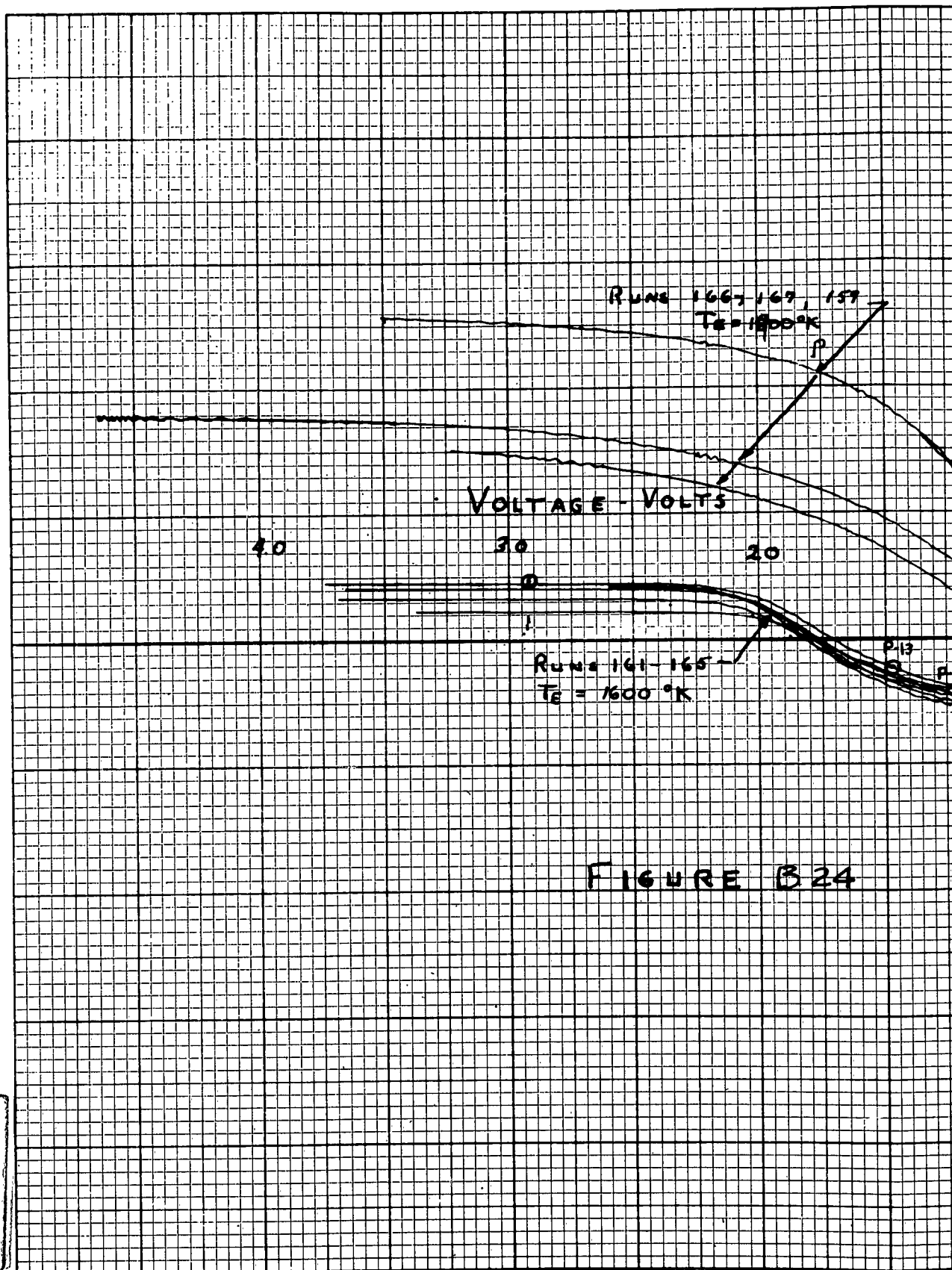
2

FIGURE B 24

Run X Y R Te Tc₃
No axis axis K C
v/in mv/in

Run No	X axis v/in	Y axis mv/in	R	Te K	Tc₃ C	
159, 166, 167	0.5	1.0	0.01	1900	250	2.0
161 – 165	0.5	1.0	0.01	1600	250	2.0

CURRENT - AMPERES

3-3-63

2

VOLTAGE - VOLTS

4.0   3.0   2.0

⊕
P-19

⊕
P-20

FIGURE B25

1
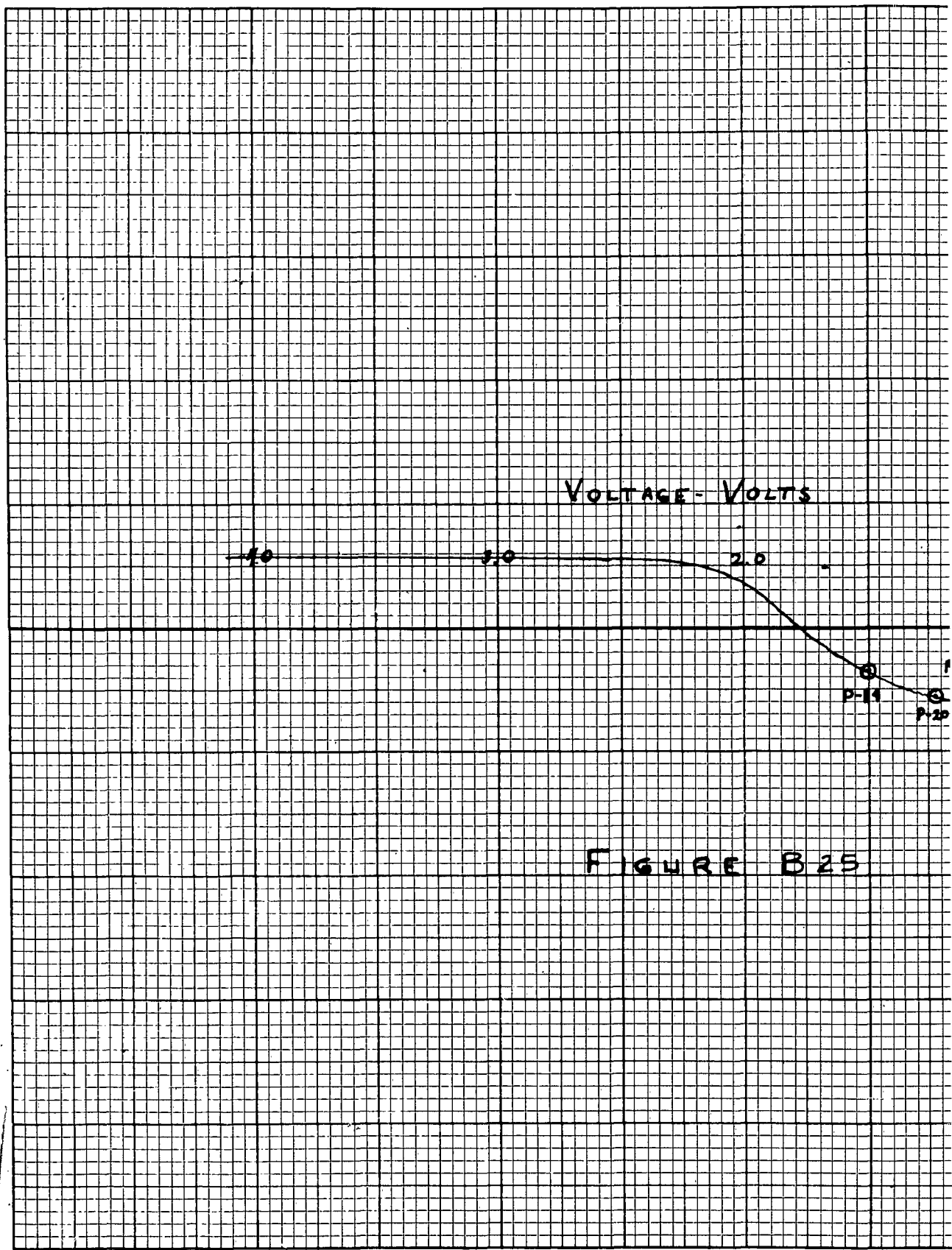
Run   X   Y   R Te Tes
No axis axis   °K °C
v/in mv/in
168 0.5   1.0   0.01 1600 250

VOLTS

0.2

0.1

2.0   1.0   -1.0   -2.0

0   0

P-16 P-21   P-22   P-23   P-12

P-11   P-19

P-20 P-5   P-17

0.1

E   B 25   0.2

CURRENT - AMPERES

3-29-63

2
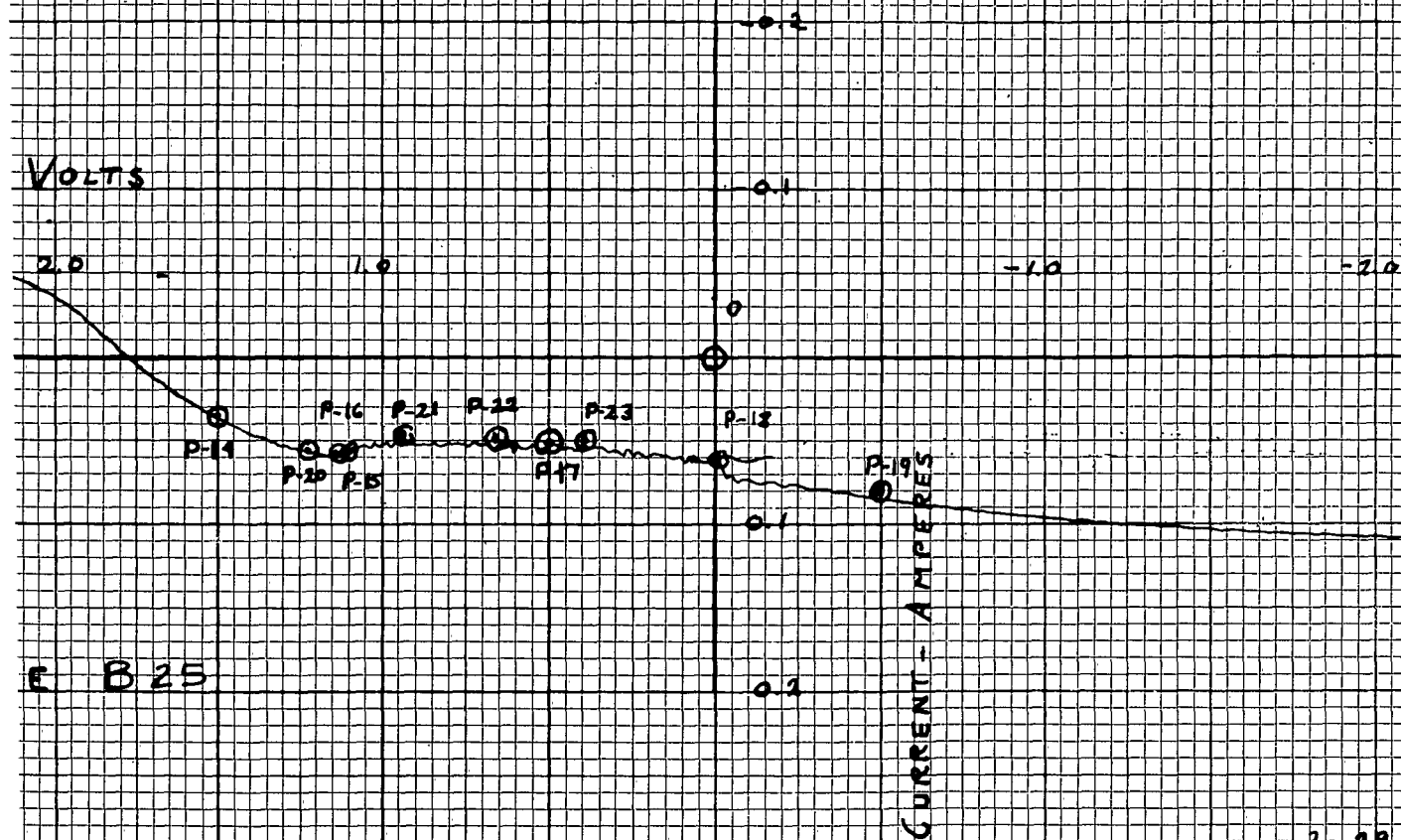
VOLTAGE - VOLTS

4.0   3.0   2.0

FIGURE B-26

1

Run X Y R Te Tcs
No axis axis °K °C
v/in mv/in
178 0.5 1.0 0.01 1600 250
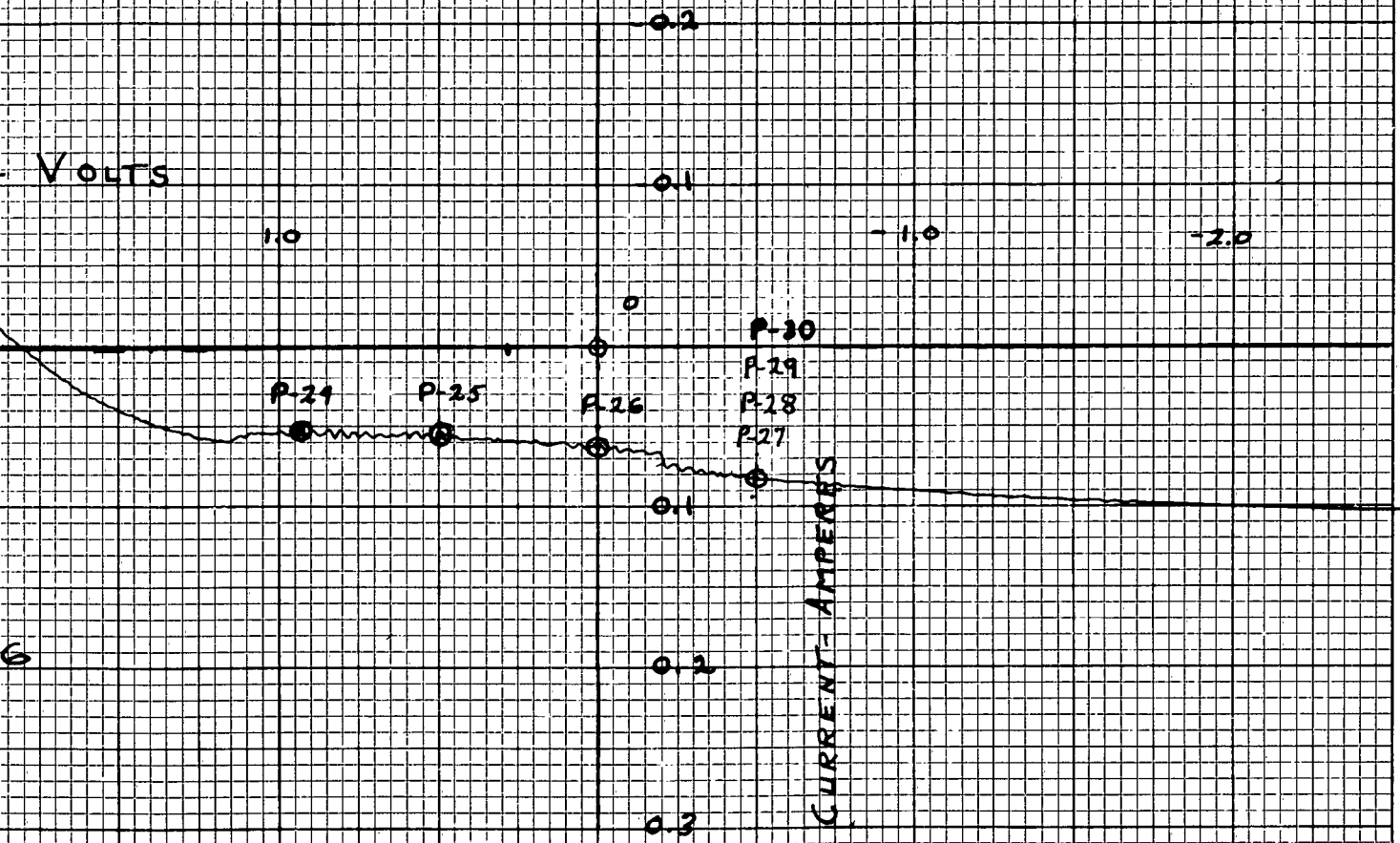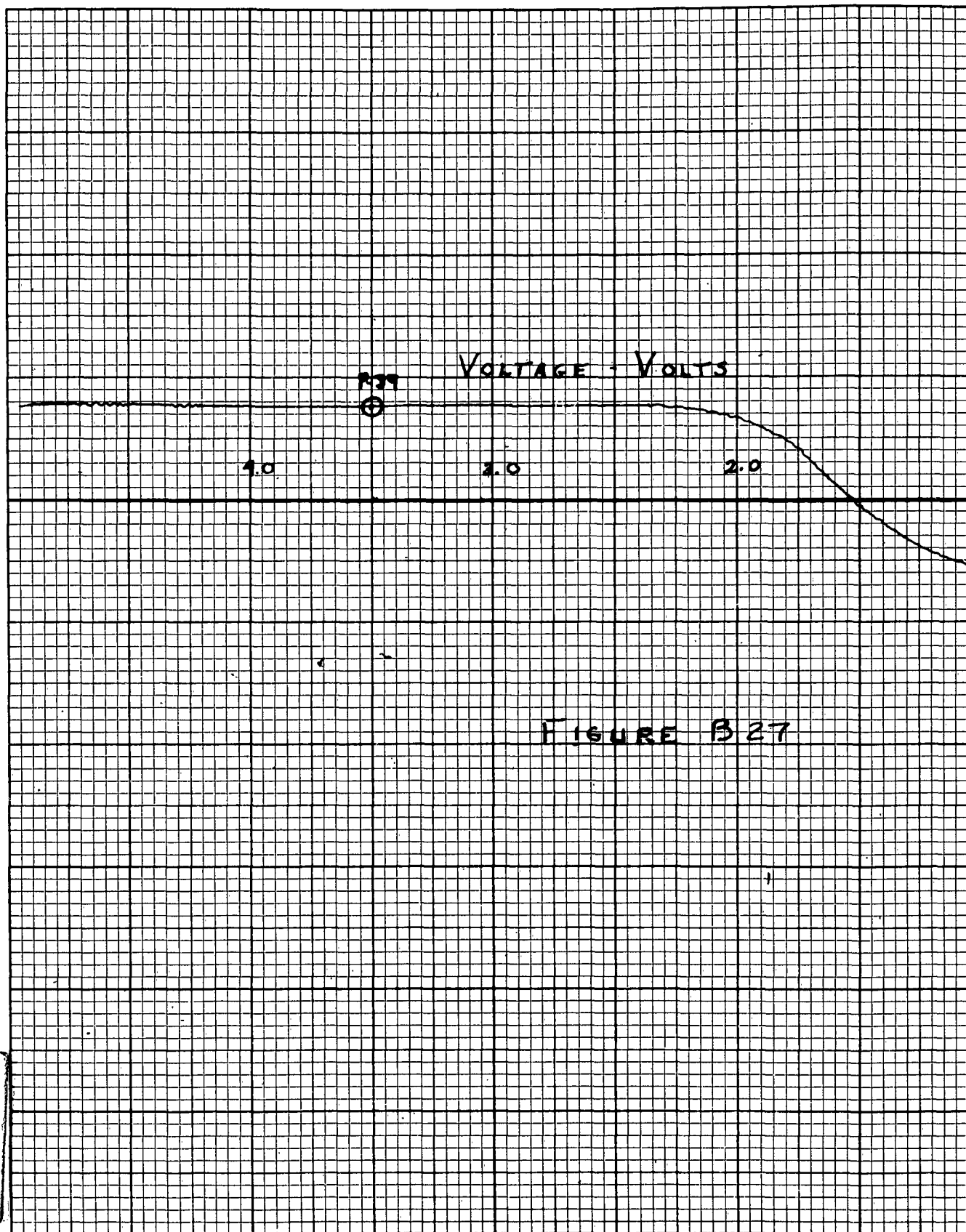
VOLTS

-0.2

-0.1

1.0   -1.0   -2.0

0

P-30
P-29
P-24   P-25   P-26   P-28
P-27

0.1

0.2

0.3

3-9-63

CURRENT-AMPERES

VOLTAGE - VOLTS

4.0   3.0   2.0

FIGURE B 27

Run X Y R Te Tc
No axis axis °K °C
v/in mv/in
193 0.5 1.0 0.01 1600 300

$T_{col} = 475°C$

$T_{col} = 600°C$

CURRENT - AMPERES

4-10-63

P-41
P-40
P-42
P-45
P-43
P-44

2

VOLTAGE - VOLTS

4.0   3.0   2.0

FIGURE B 28

1
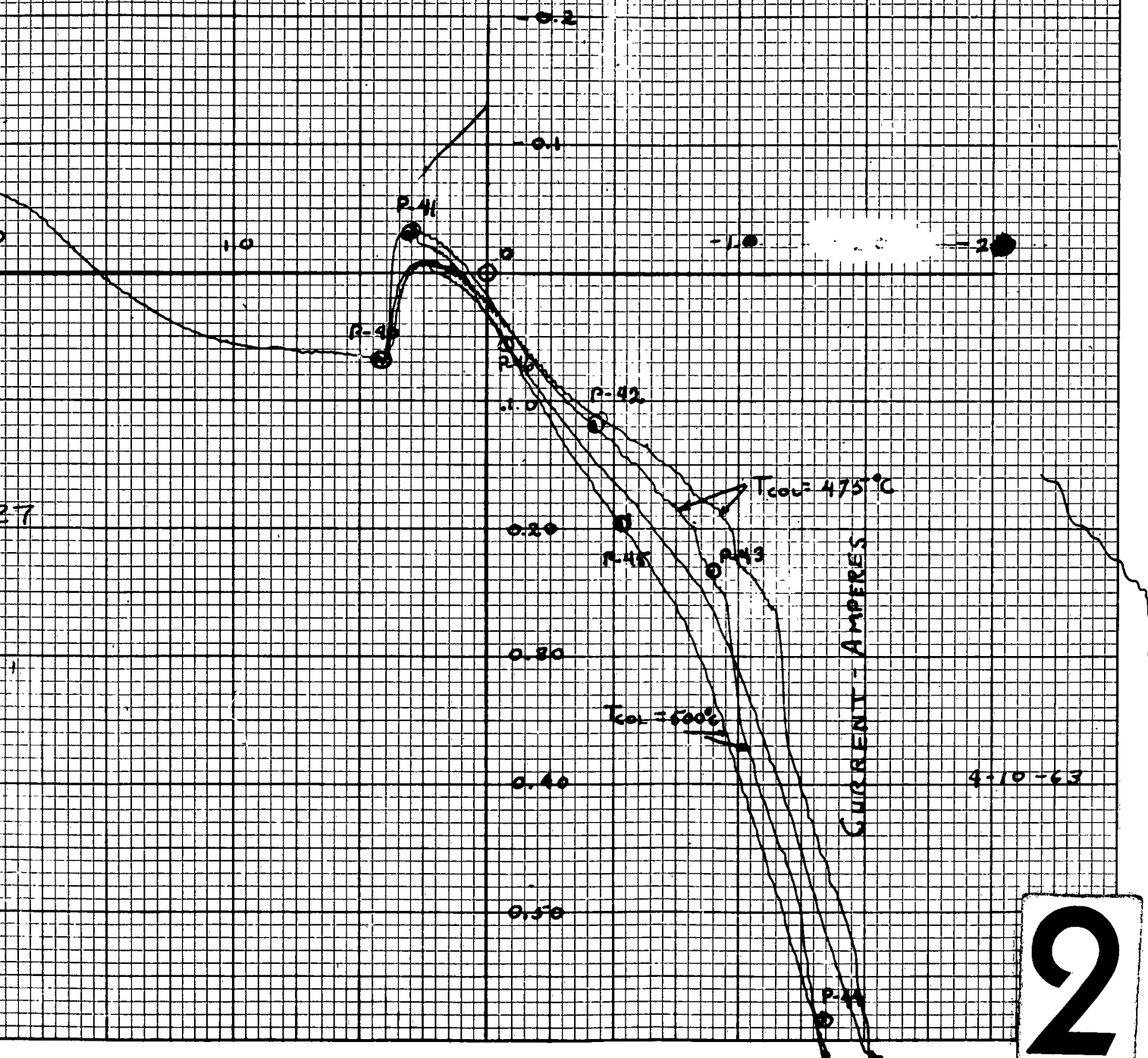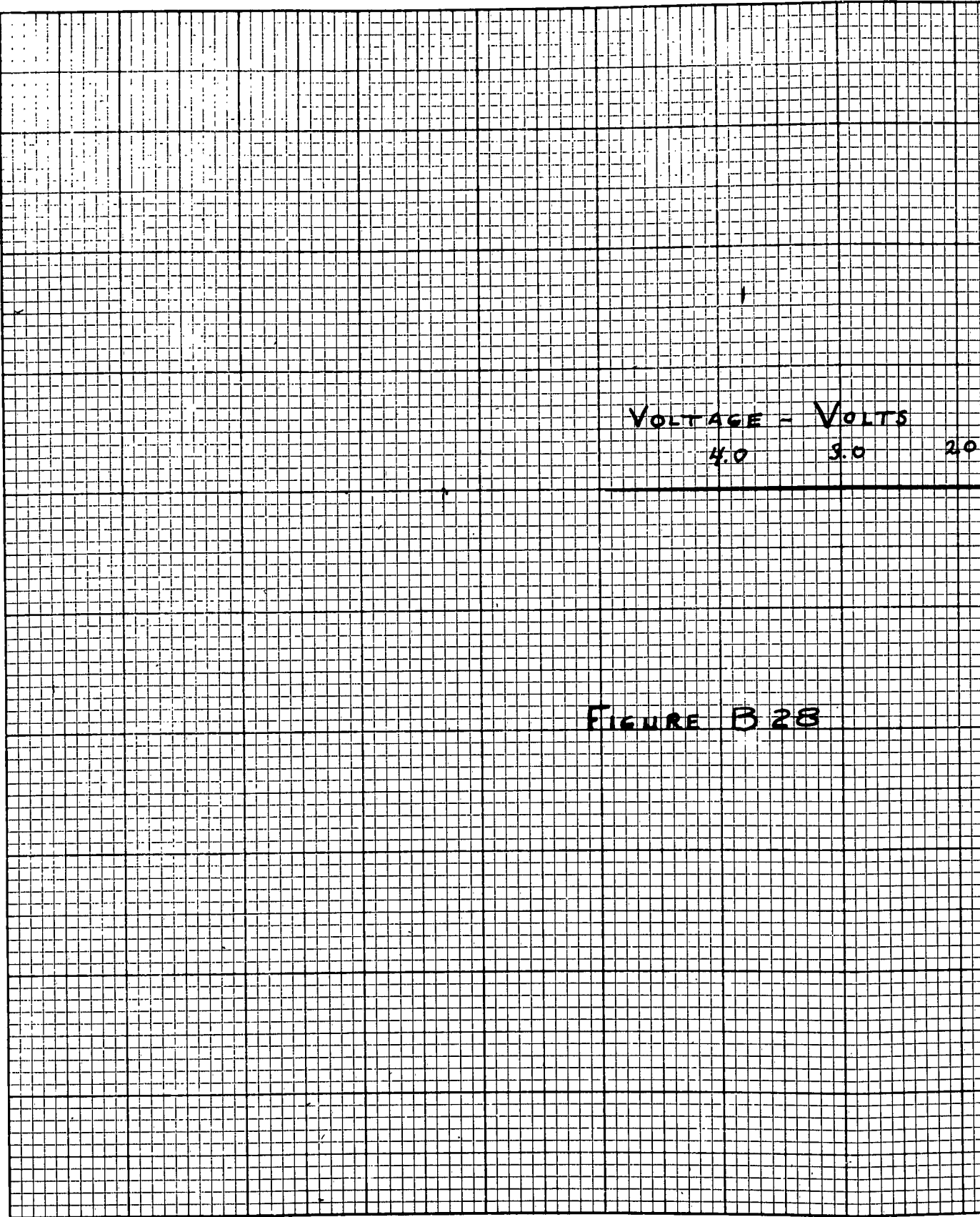
		Y	R	Te	Tcs	
N°	axis	axis		°K	°C	
	v/in	mv/in				
201	1.0	25	0.01	1600	300	2.0
209	1.0	25	0.01	1800	300	2.0

-5.0

-2.5

E ~ VOLTS

3.0   2.0   1.0   0   -1.0   -2.0   -3.0

P-47

P-51 P-53

0

0.2.5

P-48

P-55   P-52

0.5.0

CURRENT - AMPERES

0.75   P-49

P-57   P-01

1600°K

1.0

1800°K

1.25

28

4-10-63

P-50

P-58   P-54

2
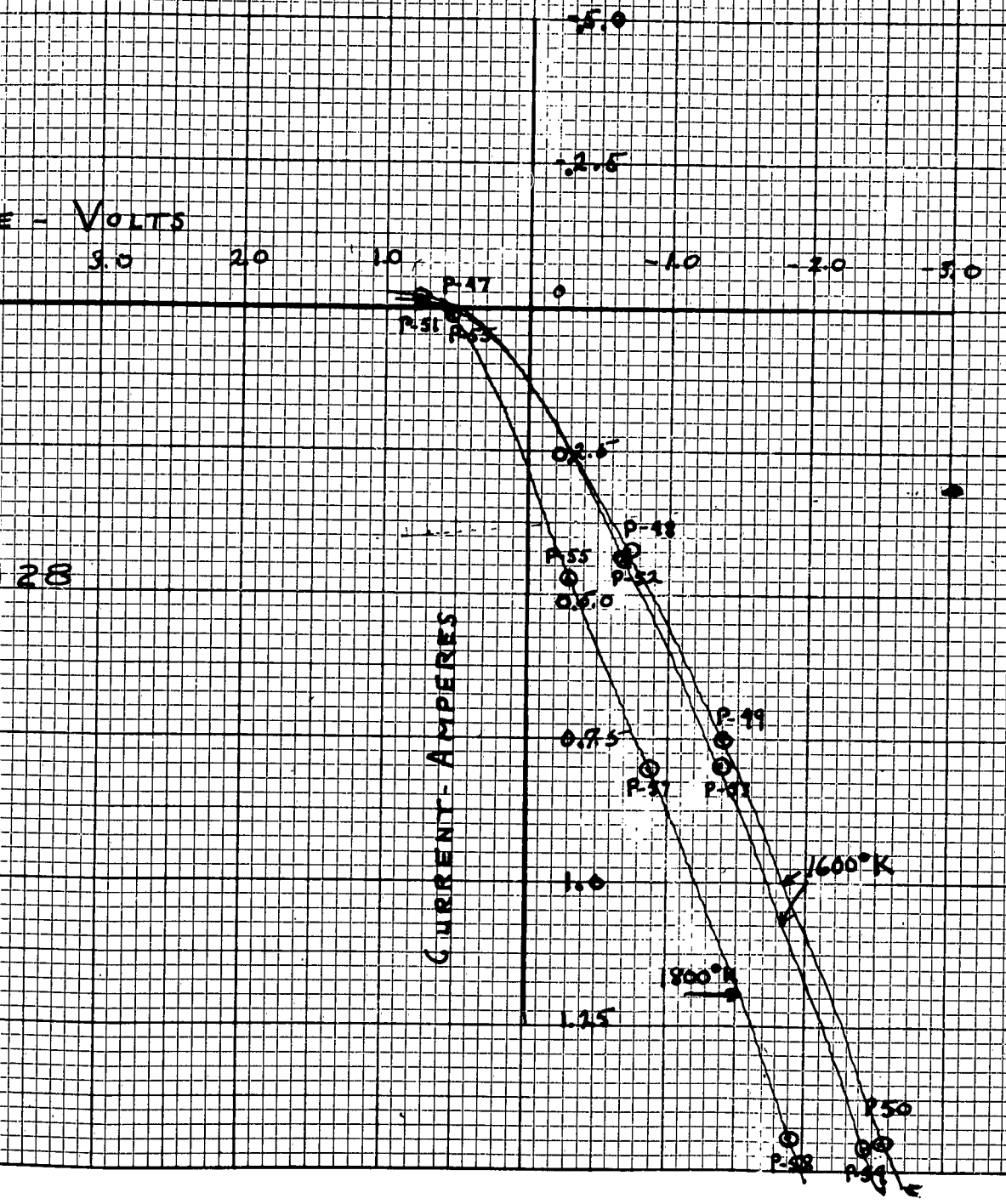
VOLTAGE - VOLTS

3.0   2.5   2.0   1.5

P-59

FIGURE B 29

1

Run X Y R Te Tcs v
No axis axis K C °"
v/in mv/in 1800
213 0.5 50 0.1 ● 300 2.0

1.0

0.5

1.5 1.0 0.5 -0.5 -1.0 -1.5 -2.0

-0.5

0

Q
P-60

0.5

Q
P-61

CURRENT - AMPERES

1.0

B 29

PK2
1.5 Q

2

VOLTAGE - VOLTS

3.3   2.5   2.0   1.5   P-6

P-63

P-64

P-65

FIGURE B39

1
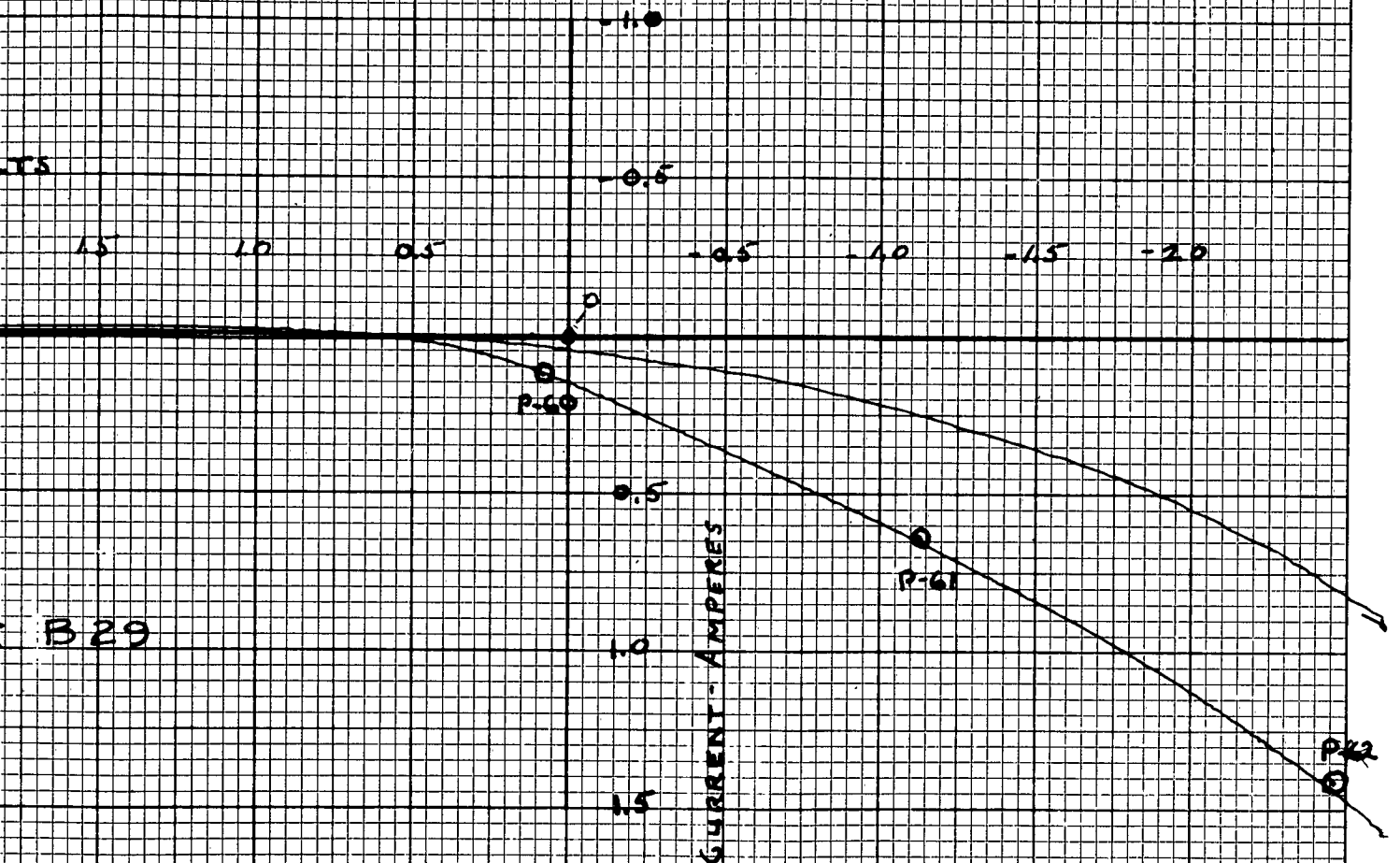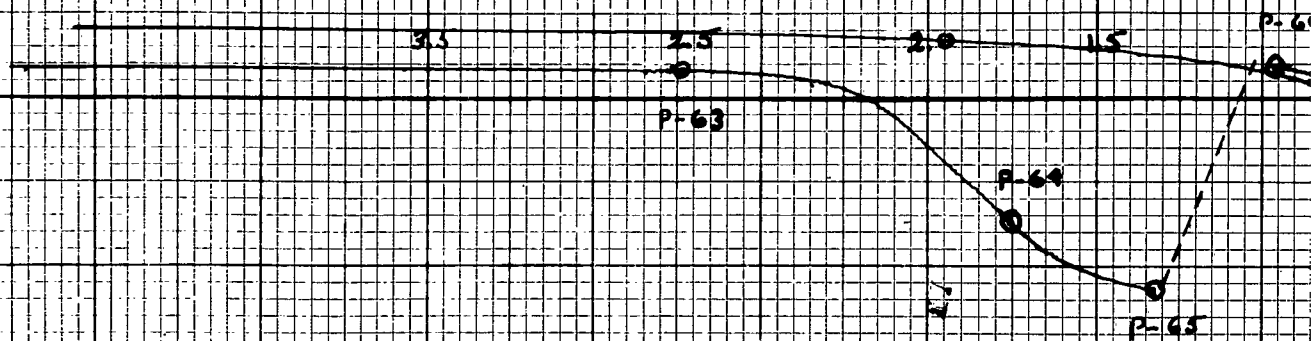
Run   X   Y   R   Te Tcs
No   axis axis   °K   °C
     v/in mv/in

217   0.5   2.5   0.01 1800 250
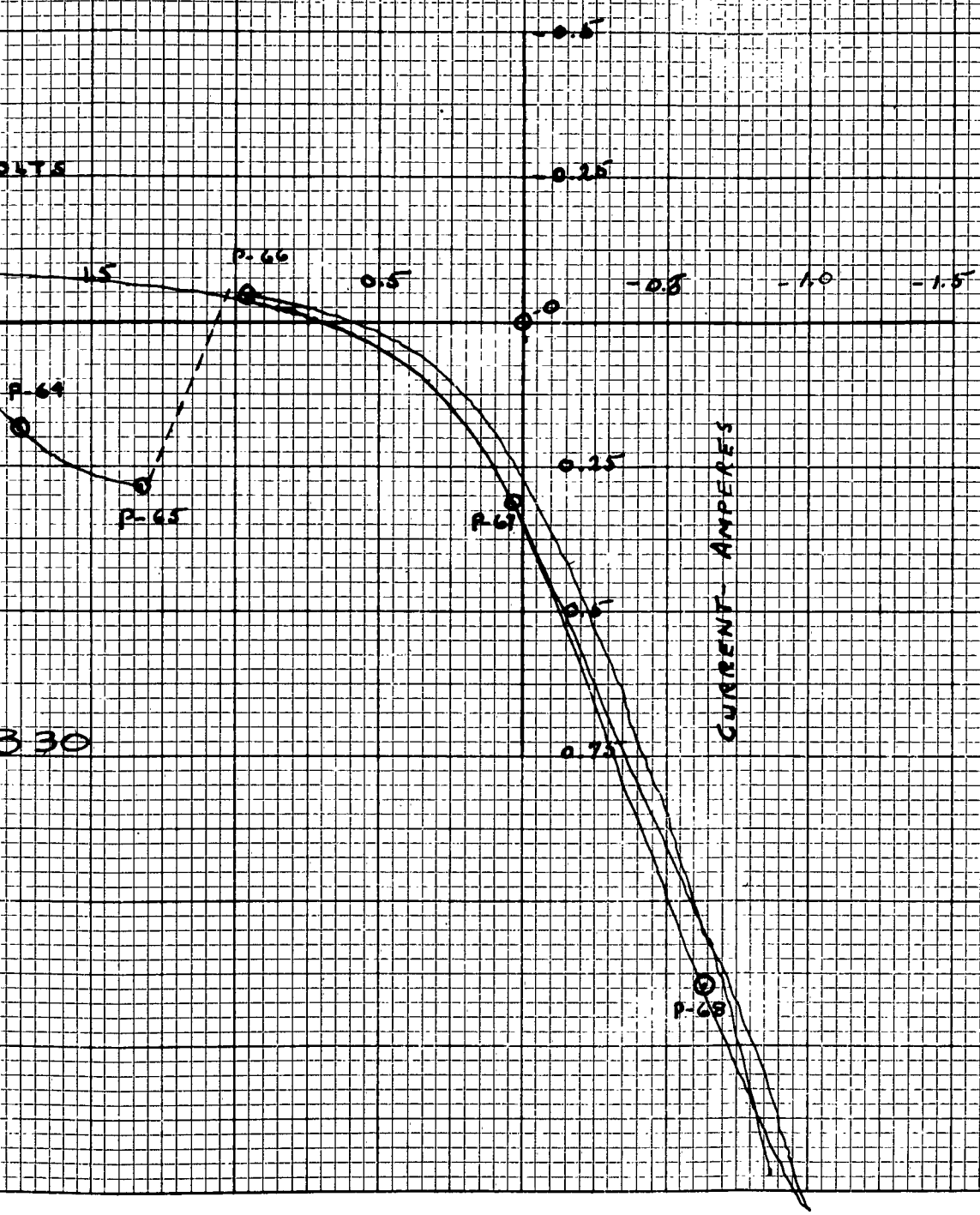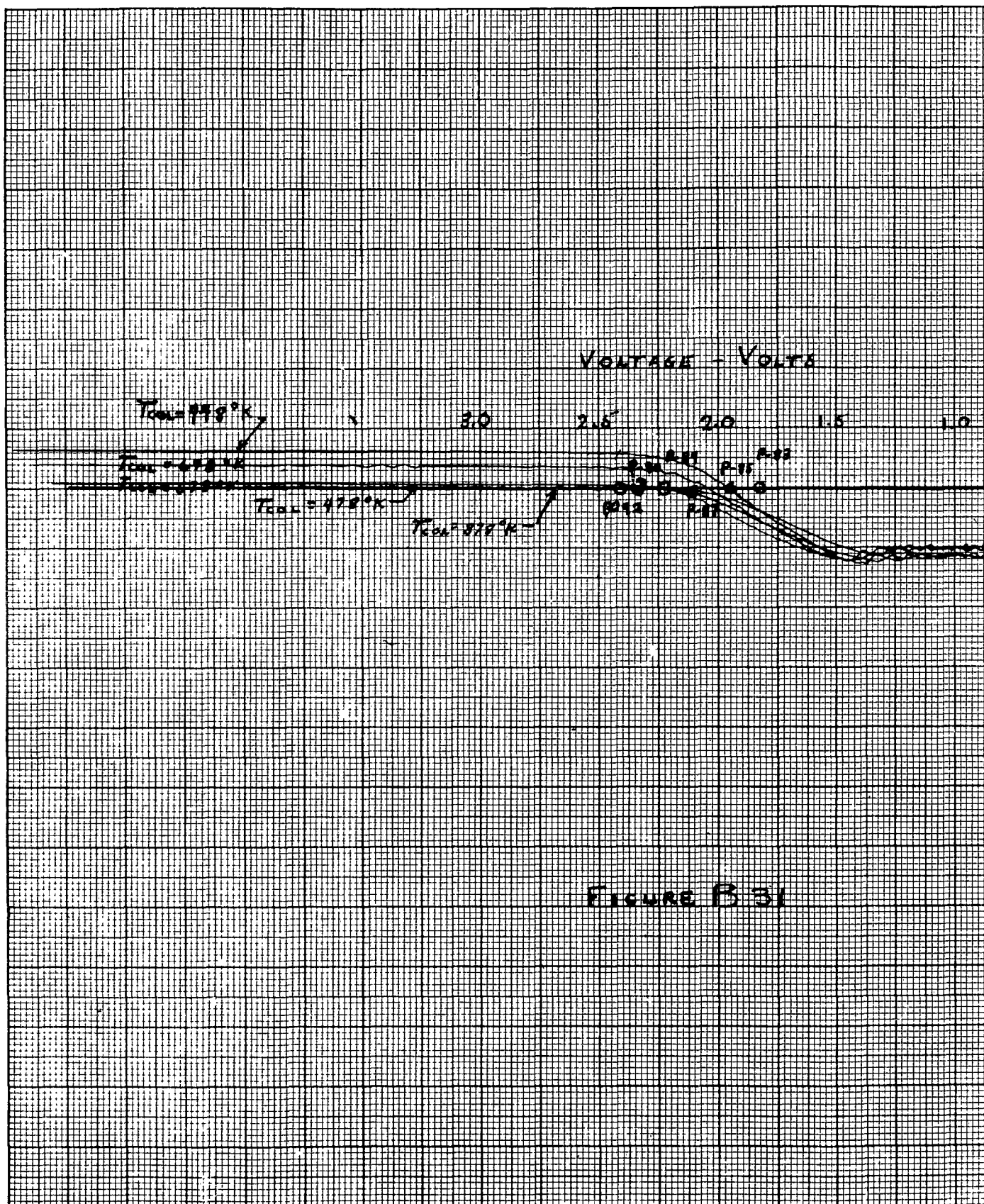
−0.5

0.25

24TS

1.5   P-66   0.5   0.0   −0.5   −1.0   −1.5

P-64

P-65

CURRENT AMPERES

0.25

P-67

0.5

30

0.75

4−11−63

P-68

2

VOLTAGE - VOLTS

$T_{Coll} = 578°K$

$T_{Coll} = 478°K$

$T_{Coll} = 478°K$

$T_{Coll} = 378°K$

FIGURE B-31

Run X Y R Te Tcs
No axis axis K C
v/in mv/ih

227 0.5 1.0 0.01 1600 250

VOLTS

2.0 1.5 1.0 0.5 -0.5 -1.0 -1.5 -2.0

CURRENT-AMPERES

4-30-60

2

Figure B 32

Run X Y R Te Ics
No axis axis K C
v/in mv/in

228 0.5 1.0 0.01 1000 150

-0.2

-0.1

VOLTS

1.5 1.0 0.5 0.0 -0.5 -1.0 -1.5 -2.0
0.95

0.1

0.2

CURRENT — AMPERES

0.3

0.4

4-30-69
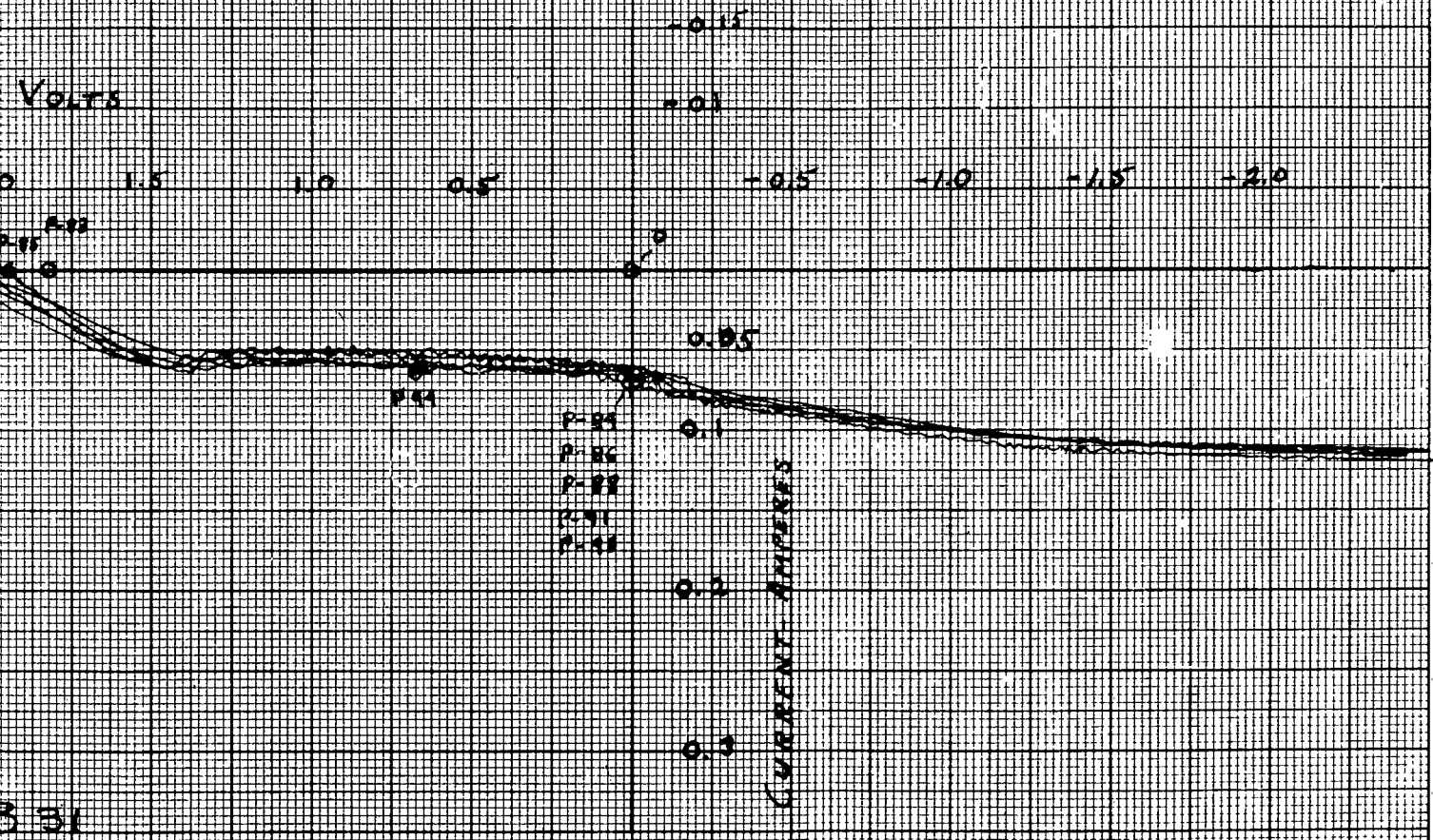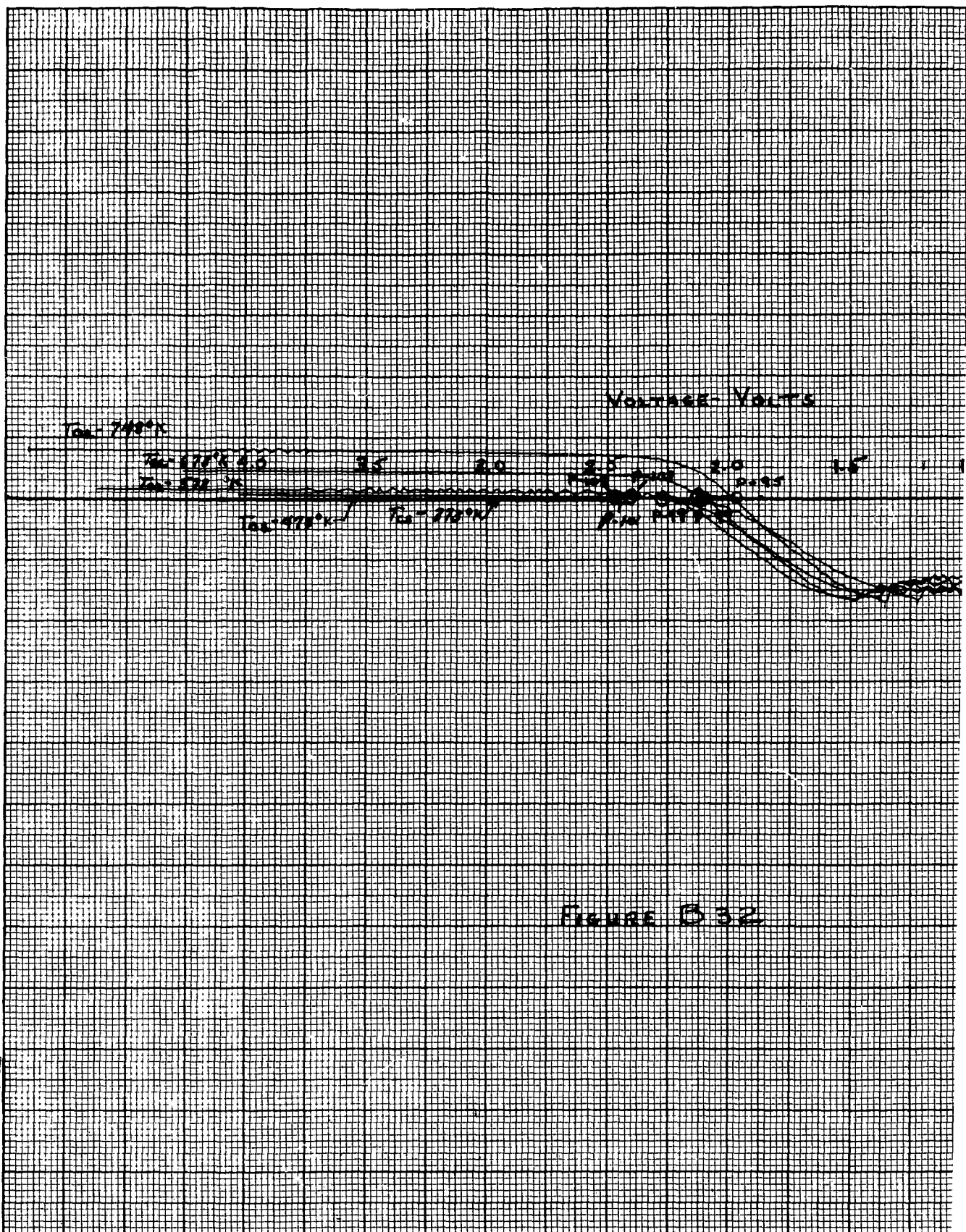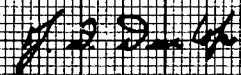
2

DISTRIBUTION LIST

No. of Copies

ACTIVITIES AT WRIGHT-PATTERSON AIR FORCE BASE

ASAPT   1

ASAPR   1

ASRPP   1

ASRPP-20 (G. H. Miller)   3

ASRNE-4   1

OTHER DEPARTMENT OF DEFENSE ACTIVITIES

Office of Naval Research   1
    Code 429
    ATTN: Lt. Cmdr. John J. Connelly
    Washington 25, D. C.

AFORL (CRZAP)   1
    LG Hanscom Fld
    Bedford, Mass.

SSD (SSTRE, Maj. Iller)   1
    AF Unit Post Office
    Los Angeles 45, Calif.

Defense Documentation Center   22
    Arlington Hall Stn
    Arlington 12, Va.

ALISON

	No. of Copies

OTHER U.S. GOVERNMENT AGENCIES

U.S. Atomic Energy Commission   1
    Division of Reactor Development
    ATTN: Lt. Cmdr. J. Prosser
    Washington 25, D.C.

Advanced Research Projects Agency   1
    ATTN: Dr. John Huth
    Washington 25, D.C.

Jet Propulsion Laboratory   1
    Spacecraft Secondary Power Section
    ATTN: Mr. Paul Goldsmith
    4800 Oak Park Drive
    Pasadena, California

Aerospace Corporation   1
    ATTN: Library Technical Document Group
    Post Office Box 95085
    Los Angeles 45, California

U.S. Atomic Energy Commission   1
    San Francisco Operations Office
    ATTN: Reactor Division
    2111 Bancroft Way
    Berkeley 4, California

U.S. Atomic Energy Commission   1
    Office of Technical Information Extension
    P.O. Box 62
    Oak Ridge, Tennessee

	No. of Copies
NASA-Lewis Research Center	1
SEPO	
ATTN: Mr. R. Dennington	
21000 Brookpark Road	
Cleveland 35, Ohio	
NASA-Manned Spacecraft Center	1
SEDD	
ATTN: J. D. Murrell	
Houston, Texas	

Allison Division, General Motors Corporation
FIFTH QUARTERLY TECHNICAL PROGRESS REPORT ON
INVESTIGATION OF THE MONOCAPILLARY THERMIONIC
EMITTER AS A DUAL SOURCE OF IONS AND ELECTRONS.
15 June 1963. 94 p. incl. illus. (Project No. 8173, Task
No. 817305) (Allison EDR 3390) (Contract AF33(616)-8299)

Experimental data is reported on a multicapillary con-
verter, Converter G, which operated for over 300 hours.
Several types of data were obtained including:

1. Current-voltage characteristics for the tem-
   perature range from 1800 to 2100°K
2. High frequency oscillations
3. Ion current measurements
4. Spectroscopic data

It is shown that the data in the temperature range from
1800 to 2100°K agrees with the random current model of
the capillary emitter. For operation at 2000 and 2100°K
the data indicates several competitive advantages over

(over)

1. Theory of Ion Emission
2. Thermionic Emission in
   Cesium Vapor
I. D. L. Dresser
II. J. D. Dunlop
III. R. T. Schneider
IV. Aero-Propulsion Labora-
    tory, ASD
V. Contract AF33(657)-8299

Allison Division, General Motors Corporation
FIFTH QUARTERLY TECHNICAL PROGRESS REPORT ON
INVESTIGATION OF THE MONOCAPILLARY THERMIONIC
EMITTER AS A DUAL SOURCE OF IONS AND ELECTRONS.
15 June 1963. 94 p. incl. illus. (Project No. 8173, Task
No. 817305) (Allison EDR 3390) (Contract AF33(616)-8299)

Experimental data is reported on a multicapillary con-
verter, Converter G, which operated for over 300 hours.
Several types of data were obtained including:

1. Current-voltage characteristics for the tem-
   perature range from 1800 to 2100°K
2. High frequency oscillations
3. Ion current measurements
4. Spectroscopic data

It is shown that the data in the temperature range from
1800 to 2100°K agrees with the random current model of
the capillary emitter. For operation at 2000 and 2100°K
the data indicates several competitive advantages over

(over)

1. Theory of Ion Emission
2. Thermionic Emission in
   Cesium Vapor
I. D. L. Dresser
II. J. D. Dunlop
III. R. T. Schneider
IV. Aero-Propulsion Labora-
    tory, ASD
V. Contract AF33(657)-8299

Allison Division, General Motors Corporation
FIFTH QUARTERLY TECHNICAL PROGRESS REPORT ON
INVESTIGATION OF THE MONOCAPILLARY THERMIONIC
EMITTER AS A DUAL SOURCE OF IONS AND ELECTRONS.
15 June 1963. 94 p. incl. illus. (Project No. 8173, Task
No. 817305) (Allison EDR 3390) (Contract AF33(616)-8299)

Experimental data is reported on a multicapillary con-
verter, Converter G, which operated for over 300 hours.
Several types of data were obtained including:

1. Current-voltage characteristics for the tem-
   perature range from 1800 to 2100°K
2. High frequency oscillations
3. Ion current measurements
4. Spectroscopic data

It is shown that the data in the temperature range from
1800 to 2100°K agrees with the random current model of
the capillary emitter. For operation at 2000 and 2100°K
the data indicates several competitive advantages over

(over)

1. Theory of Ion Emission
2. Thermionic Emission in
   Cesium Vapor
I. D. L. Dresser
II. J. D. Dunlop
III. R. T. Schneider
IV. Aero-Propulsion Labora-
    tory, ASD
V. Contract AF33(657)-8299

Allison Division, General Motors Corporation
FIFTH QUARTERLY TECHNICAL PROGRESS REPORT ON
INVESTIGATION OF THE MONOCAPILLARY THERMIONIC
EMITTER AS A DUAL SOURCE OF IONS AND ELECTRONS.
15 June 1963. 94 p. incl. illus. (Project No. 8173, Task
No. 817305) (Allison EDR 3390) (Contract AF33(616)-8299)

Experimental data is reported on a multicapillary con-
verter, Converter G, which operated for over 300 hours.
Several types of data were obtained including:

1. Current-voltage characteristics for the tem-
   perature range from 1800 to 2100°K
2. High frequency oscillations
3. Ion current measurements
4. Spectroscopic data

It is shown that the data in the temperature range from
1800 to 2100°K agrees with the random current model of
the capillary emitter. For operation at 2000 and 2100°K
the data indicates several competitive advantages over

(over)

1. Theory of Ion Emission
2. Thermionic Emission in
   Cesium Vapor
I. D. L. Dresser
II. J. D. Dunlop
III. R. T. Schneider
IV. Aero-Propulsion Labora-
    tory, ASD
V. Contract AF33(657)-8299

conventional converters, including wider electrode spacings, higher converter voltage, and lower cesium bath temperature. The high frequency oscillation data shows that the peak current-voltage points form an arc mode characteristic. The ion currents at high collector temperature appear to be due to cesium atoms evaporating from the collector and impinging on the emitter surface. Spectrographic data indicates elevated electron temperatures in the arc mode. When high frequency oscillations are present in the passive mode, the line intensities of lower energy excited states are increased.

conventional converters, including wider electrode spacings, higher converter voltage, and lower cesium bath temperature. The high frequency oscillation data shows that the peak current-voltage points form an arc mode characteristic. The ion currents at high collector temperature appear to be due to cesium atoms evaporating from the collector and impinging on the emitter surface. Spectrographic data indicates elevated electron temperatures in the arc mode. When high frequency oscillations are present in the passive mode, the line intensities of lower energy excited states are increased.

conventional converters, including wider electrode spacings, higher converter voltage, and lower cesium bath temperature. The high frequency oscillation data shows that the peak current-voltage points form an arc mode characteristic. The ion currents at high collector temperature appear to be due to cesium atoms evaporating from the collector and impinging on the emitter surface. Spectrographic data indicates elevated electron temperatures in the arc mode. When high frequency oscillations are present in the passive mode, the line intensities of lower energy excited states are increased.

conventional converters, including wider electrode spacings, higher converter voltage, and lower cesium bath temperature. The high frequency oscillation data shows that the peak current-voltage points form an arc mode characteristic. The ion currents at high collector temperature appear to be due to cesium atoms evaporating from the collector and impinging on the emitter surface. Spectrographic data indicates elevated electron temperatures in the arc mode. When high frequency oscillations are present in the passive mode, the line intensities of lower energy excited states are increased.